Mountain permafrost: transient spatial modelling, model verification and the use of remote sensing

Abstract

Permafrost research has a practical relevance for the construction and maintenance of infrastructure as well as for the assessment or prevention of natural hazards in cold-mountain areas. The occurrence and temperature of permafrost are largely controlled by climatic conditions and, therefore, atmospheric warming leads to corresponding warming or thawing of permafrost in most cases. Because it is invisible at the ground surface, the delineation and thermal characterization of permafrost largely depends on numerical models. The design and validation of such models, however, is complicated by the high spatial variability of surface properties and conditions that are characteristic of mountain areas. Three main challenges can be identified for the development of models simulating transient ground temperatures and mountain permafrost: a) to investigate and to model quantitatively, aiming for the transient simulation of three-dimensional temperature fields; b) to investigate surface types such as bedrock or moraines and to expand knowledge on permafrost beyond coarse blocky surfaces; and c) to provide the quantitative spatial input data required by such models.

Several steps in the direction of these challenges were taken and lead to interesting results. A surface energy-balance model partly developed in this dissertation successfully simulates time series of rock surface temperatures in rugged high-mountain terrain. This was validated using the results of a systematic one-year measurement campaign of rock temperatures in the Swiss Alps. Coupled with a one-dimensional ground heat-conduction scheme this validated model was then employed to investigate the evolution and distribution of Alpine rock temperatures in steep terrain using a 22-year forward model run. This combined approach of measurements and modelling was also successful in demonstrating the degradation of permafrost during the hot summer of 2003.

A three-dimensional model of heat-transfer in rock forced with surface temperatures based on measurements and model experiments was used to investigate the effects of topography and variable surface conditions on the temperature distribution at depth. Using this approach, possibilities and caveats of the reconstruction of temperature histories from borehole temperaturedepth profiles could be elaborated.

Straight-forward methods for the delineation of coarse blocky surfaces from aerial photography and airborne laser-scanning were developed and tested. Airborne hyperspectral data was recorded and used to fit BRDF (bidirectional reflectivity distribution function) models and to derive albedo in rugged terrain.

Quantitative transient modelling of mountain permafrost will likely be of increasing importance for research and the assessment of natural or geotechnical hazards in the near future. The methods and results presented in this dissertation contribute to a development into this direction.

Mountain Permafrost: Transient Spatial Modelling, Model Verification and the Use of Remote Sensing.

Dissertation

zur

Erlangung der naturwissenschaftlichen Doktorwürde
(Dr. sc. nat.)

vorgelegt der

Mathematisch-naturwissenschaftlichen Fakultät

der

Universität Zürich

von

Stephan Gruber
aus Deutschland

Promotionskomitee
Prof. Dr. Wilfried Haeberli (Vorsitz)
Prof. Dr. Klaus Itten
Dr. Martin Hölzle
Dr. Daniel Schläpfer

Zürich, 2005

Summary

Permafrost research has a practical relevance for the construction and maintenance of infrastructure as well as for the assessment or prevention of natural hazards in cold-mountain areas. The occurrence and temperature of permafrost are largely controlled by climatic conditions and, therefore, atmospheric warming leads to corresponding warming or thawing of permafrost in most cases. Because it is invisible at the ground surface, the delineation and thermal characterization of permafrost largely depends on numerical models. The design and validation of such models, however, is complicated by the high spatial variability of surface properties and conditions that are characteristic of mountain areas. Three main challenges can be identified for the development of models simulating transient ground temperatures and mountain permafrost: a) to investigate and to model quantitatively, aiming for the transient simulation of three-dimensional temperature fields; b) to investigate surface types such as bedrock or moraines and to expand knowledge on permafrost beyond coarse blocky surfaces; and c) to provide the quantitative spatial input data required by such models.

Several steps in the direction of these challenges were taken and lead to interesting results. A surface energy-balance model partly developed in this dissertation successfully simulates time series of rock surface temperatures in rugged high-mountain terrain. This was validated using the results of a systematic one-year measurement campaign of rock temperatures in the Swiss Alps. Coupled with a one-dimensional ground heat-conduction scheme this validated model was then employed to investigate the evolution and distribution of Alpine rock temperatures in steep terrain using a 22-year forward model run. This combined approach of measurements and modelling was also successful in demonstrating the degradation of permafrost during the hot summer of 2003.

A three-dimensional model of heat-transfer in rock forced with surface temperatures based on measurements and model experiments was used to investigate the effects of topography and variable surface conditions on the temperature distribution at depth. Using this approach, possibilities and caveats of the reconstruction of temperature histories from borehole temperature-depth profiles could be elaborated.

Straight-forward methods for the delineation of coarse blocky surfaces from aerial photography and airborne laser-scanning were developed and tested. Airborne hyperspectral data was recorded and used to fit BRDF (bidirectional reflectivity distribution function) models and to derive albedo in rugged terrain.

Quantitative transient modelling of mountain permafrost will likely be of increasing importance for research and the assessment of natural or geotechnical hazards in the near future. The methods and results presented in this dissertation contribute to a development into this direction.

Zusammenfassung

Permafrost ist relevant für den Bau und Unterhalt von Infrastruktur sowie für die Beurteilung und Prävention von Naturgefahren in kalten Gebirgsregionen. Das Vorkommen und die Temperatur von Permafrost werden hauptsächlich von klimatischen Bedingungen bestimmt und, als Folge davon, führt eine atmosphärische Erwärmung in den meisten Fällen zu einer entsprechenden Erwärmung oder zum Schmelzen des Permafrostes. Weil er an der Oberfläche unsichtbar ist, ist die Abgrenzung und thermische Charakterisierung von Permafrost weitgehend von numerischen Modellen abhängig. Die Entwicklung und Validierung solcher Modelle ist allerdings durch die für Gebirge typische hohe räumliche Variabilität von Oberflächen-Eigenschaften und –Bedingungen erschwert. Für die Entwicklung von Modellen, die transiente Boden-Temperaturen simulieren, können drei große Herausforderungen identifiziert werden: a) quantitative Untersuchungen und Modelle, die eine transiente Simulation von drei-dimensionalen Temperaturfeldern anstreben; b) die Untersuchung von Oberflächentypen wie z.B. anstehendem Fels oder Moränen und das Ausdehnen von Wissen über Bodentemperaturen und Permafrost über grobe Blockoberflächen hinaus; und c) die Erhebung von quantitativen, räumlichen Daten wie sie für solche Modelle benötigt werden.

Mehrere Schritte in Richtung dieser Herausforderungen wurden unternommen und führten zu interessanten Resultaten. Ein Modell der Oberflächen-Energiebilanz, das teilweise in dieser Dissertation entwickelt wurde, simuliert erfolgreich Zeitreihen von Fels-Oberflächentemperaturen im Hochgebirge. Dies wurde mit Felstemperatur-Daten einer einjährigen, systematischen Meßkampagne in den schweizer Alpen validiert. Dieses Modell wurde an ein ein-dimensionales Bodenwärmeleitungs-Modell gekoppelt und für die Untersuchung von Felstemperaturen sowie ihrer räumlichen Verteilung und zeitlichen Entwicklung verwendet. Für diese Untersuchung in steilem Gelände wurde eine Vorwärtsrechnung über 22 Jahre hinweg verwendet. Diese Kombination von Messung und Modellierung wurde auch verwendet um die Permafrost-Degradation im heißen Sommer 2003 zu demonstrieren und zu untersuchen.

Der Effekt, den Topographie und variable Oberflächenbedingungen auf die Temperaturverteilung im Untergrund haben wurde mit einem drei-dimensionalen Wärmeleitungsmodell untersucht. Es wurden Oberflächentemperaturen basierend auf Messungen und Modellrechnungen verwendet. Mit diesem Ansatz wurden die Möglichkeiten und Schwierigkeiten der Rekonstruktion von Temperatur-Zeitreihen aus der Vergangenheit basierend auf Bohrloch-Temperaturmessungen im Gebirgspermafrost aufgezeigt.

Einfache Methoden für die Ausscheidung von Blockoberflächen basierend auf Laserscanner-Daten und Luftbildern wurden entwickelt und getestet. Hyperspektral-Daten wurden in einer Flugkampagne aufgezeichnet und für die Anpassung von BRDF-Modellen (bidirectional reflectivity distribution function) und die Berechnung der Albedo in komplexem Gelände verwendet.

Quantitative, transiente Permafrost-Modelle werden sehr wahrscheinlich in der Zukunft für die Forschung und die Beurteilung von Natur- und geotechnischen Gefahren an Bedeutung gewinnen. Die in dieser Dissertation präsentierten Methoden und Ergebnisse liefern einen Beitrag zur Entwicklung in dieser Richtung.

Structure

This dissertation consists of three different but complementary parts:

Part A: Scientific setting

The scientific work carried out within this dissertation is introduced, briefly described and put into a larger scientific context. The publications that constitute part of this dissertation are discussed within a wider scope and identified clearly (e.g. Gruber et al., 2003a [*Publication 1*]) when quotet in the text. Some unpublished results are included.

Part B: Publications

The six publications that constitute part of this dissertation as discussed in Part A are included here. For each publication the main findings are listed.

Part C: Appendix

A complete list of publications by the candidate, a curriculum vitae and acknowledgements are provided.

Table of contents

Part A: Scientific setting

Part B: Publications

Part C: Appendix

Acronyms

BRDF	bidirectional reflectivity distribution function
BTS	bottom temperature of the snow pack in late winter
FE	finite element
GIS	geographic information system
HDRF	hemispherical-directional reflectance factor
JERS-1	Japanese earth resource satellite 1
LIDAR	light detection and ranging
MAAT	mean annual air temperature
MAGST	mean annual ground surface temperature
MGLD	mean grey level difference
SAR	synthetic aperture radar
TIR	thermal infrared
TTOP	temperature at the top of permafrost

Part A: Scientific setting

1 Introduction

1.1 The definition of permafrost

Permafrost or perennially frozen ground is defined as ground (soil or rock and included ice and organic material) that remains at or below 0 °C for at least two years, for natural climatic reasons (cf. Brown and Péwé, 1973; van Everdingen, 1998). It is thus defined purely on the basis of temperature and time. The word is derived from PERMAnent and FROST and it is evident that the above definition of ground that always has sub-zero temperatures during a whole summer season does not precisely fit the notion of permanence. A discussion as well as schematics illustrating the most important terms relating to permafrost are provided by French (1996, pages 52/53). As permafrost is a subsurface phenomenon it is invisible, making the determination of its presence/absence a field of research of its own (Hauck, 2001; Scott et al., 1979).

The majority of permafrost research has taken place at high-latitudes in Siberia and the Canadian/Alaskan Arctic (see: French, 1996 for a short history). This research has been motivated by the expansion of infrastructure e.g. mining, petroleum exploration, pipelines or military installations. Due to the considerable financial interest involved, a broad range of basic and engineering research has been undertaken on high-latitude permafrost. Only in the 1970, mainly geomorphologists began systematic research on mountain permafrost in Europe (Barsch, 1969; Barsch, 1971; Haeberli, 1975), triggered by interest in rock glaciers, and since then research on mountain permafrost has become a discipline of its own dealing with its specific problems and phenomena. The section “Characteristics of mountain permafrost and its response to a changing climate” describes in more detail the special aspect of mountain permafrost and, where appropriate, makes reference or comparison with high-latitude permafrost features or research.

1.2 The relevance of mountain permafrost

Most permafrost contains water in different quantities and phase states. Much of the importance of mountain permafrost is due to three effects that ice inclusions or their thaw in rock or sediments can have: 1) bonding of fractured rock or sediments; 2) facilitation of creep in ice super-saturated sediments; and 3) prevention of the movement of liquid water.

The economic and scientific relevance of mountain permafrost relates to:

- **Special construction practices**
  Construction in permafrost requires special adaptation and mostly causes additional cost. Possible problems include: the freezing of water pipes or waste water; settling of foundations due to thaw, lateral loading or movement of structures due to creep, permafrost degradation due to changed patterns of snow accumulation or the requirement for special types of concrete. Although often intensified by a changing climate, the problems are mostly created by the interaction of infrastructure and permafrost (Haeberli, 1992a).
- **Rockfall**
  Ice in cracks and crevices can stabilize perennially frozen rock walls. Their geometry may have adapted to this ice-enhanced stability over long time spans, accordingly.

When the ice in the crevices is warmed or thawed the stability of the rock slope may be reduced (Davies et al., 2001; Dramis et al., 1995; Haeberli et al., 1997), leading to rockfall (e.g.: Gruber et al., 2004a [*Publication 1*]; Haeberli et al., 2003; Noetzli et al., 2003)

- **Instability of unconsolidated sediments and debris flows**
  The presence of permafrost usually bonds unconsolidated sediments by ice and thus restricts the amount of material available for erosion and subsequent transport as a debris flow. Changes to the temperature regime will result in thaw and alter the availability of material for erosion. Furthermore, a perched water table in the active layer may quickly lead to saturation, especially at the down-slope limit of the permafrost body. Slope failures may be caused by thaw consolidation in ice super-saturated fine-grained sediments (Harris et al., 2001b). Changes in the frequency and magnitude of debris flows can be the consequence of permafrost degradation but the description of the net effect and processes remains speculative in most respects (cf. Haeberli and Burn, 2002; Zimmermann and Haeberli, 1992; Zimmermann et al., 1997). In special locations, creeping permafrost provides a constant re-supply of debris that is removed by debris flows through steep channels (Rebetez et al., 1997).

- **Hanging glaciers and ice faces**
  Even though they are not considered permafrost themselves, hanging glaciers and ice faces are indicative of permafrost. They would not be stable if their base (the ice-rock interface) were temperate or above freezing. Alterations in the thermal regime of these forms can induce drastic changes to the underlying permafrost body in rock and possibly affect its stability. Investigations concerning hanging glaciers (Alean, 1985; Haeberli et al., 1999; Haeberli et al., 1997; Lüthi and Funk, 1997) and alpine ice faces are still (to date) very rare.

- **Water supply**
  Many central Asian mountains pastures as well as forests are often underlain by perennially frozen ground that facilitates perched water tables and higher soil moisture during summer and thus is a vital element for the vegetation at the surface (cf. Etzelmüller et al., 2002; Goulden et al., 2003). In some arid mountain areas such as the eastern Andes much of the base flow in rivers during summer is derived from thaw in the active layer of large rock glaciers and frozen bodies of debris (Barsch, 1996; Corte, 1976; Gardaz, 1998; Schrott, 1994).

Mainly scientific relevance of mountain permafrost relates to:

- **Creeping mountain permafrost**
  Rock glaciers and ice cored moraines are distinct geomorphic forms caused by the creep of ice-supersaturated perennially frozen debris. They are thus indicative of permafrost – or past permafrost in the case of inactive or fossil forms. Rock glaciers are an abundant and often fascinating landscape element of the periglacial belt in many mountain areas and a wealth of literature exists on the topic (e.g. Barsch, 1996; Frauenfelder, 2004; Haeberli, 1985)

- **Climate archive**
  Heat diffusion into the ground under transient conditions leads to a temperature-depth profile that is characteristic of the temperature history at the upper boundary. In

mountain permafrost, the absence of advection of heat by liquid water and the common absence of a vegetation cover make the observation or inversion of temperature signals from temperature profiles recorded in boreholes (Harris and Haeberli, 2003; Isaksen et al., 2000b; Kohl and Gruber, 2003) an attractive but at the same time difficult (Gruber et al., 2004c [*Publication 4*]; Ludwig, 2003) source of information.

Given the present and projected climatic change, especially the evolution of mountain permafrost over time is of interest, because it will affect many of the above phenomena. For natural hazards such as slope instabilities, permafrost thaw may constitute a transient stability factor that changes rapidly. Much of the traditional hazard assessment, however, is based on historical observation that does not account for these developments. In cold-mountains, steep slopes and large differences in elevation often further amplify and complicate the consequences of individual natural hazards by complex chains of interactions (Huggel, 2004; Huggel et al., 2004).

Based on its scientific and economic relevance knowledge on the distribution and transient behavior of mountain permafrost is important.

1.3 Modelling mountain permafrost

The influence of topography on ground temperatures and permafrost distribution is the most important characteristic of mountain permafrost. As a consequence, models of mountain permafrost must be able to resolve this topographic differentiation and be formulated at an appropriate scale. Hemispheric- or continental-scale models (e.g. Anisimov et al., 1997; Oelke et al., 2003) may be roughly interpreted in terms of continental patterns of mountain permafrost distribution but do not resolve topography and the relevant processes satisfactorily. Models of mountain permafrost should be formulated at spatial resolutions between few hundreds and tens of meters (Etzelmüller et al., 2001). Below about 10 m the spatial resolution slowly approaches the thickness of the active layer and, therefore, its useful lower limit.

Several models of mountain permafrost distribution are described and available today (Hoelzle et al., 2001). They provide a rule or a map indicating different probability classes for the presence of permafrost. Due to the complex patterns and strong variability of permafrost distribution in mountains, as well as the difficulties involved in prospection of permafrost occurrence these models have become valuable tools for research. Most of the models used today have been designed and evaluated based on the distribution of rock glaciers or on BTS (bottom temperature of the snow cover in late winter, Haeberli, 1973) measurements that serve as a proxy for the existence of permafrost.

The first widely known model was a set of rules (Haeberli, 1975), that predicted the presence of permafrost as a function of elevation, slope and aspect. These rules contain factors to account for the effect of different surface types and for topologies influencing avalanches. They rules were partly implemented in the GIS application PERMAKART (Keller, 1992). The later-developped GIS model PERMAMAP (Hoelzle and Haeberli, 1995) uses a statistical relation to predict permafrost based on air temperature and potential direct short-wave solar radiation during summer. A wealth of slightly different models and modelling studies based on the same concepts have followed (e.g. Etzelmüller et al., 1998; Frauenfelder et al., 1998; Gruber and Hoelzle, 2001; Imhof, 1996; Jensen, 1999; Keller and Hoelzle, 1998; King and Kalisch, 1998; Kneisel, 1998; Lewkowicz and Ednie, 2004; Lieb, 1998; Mustafa et al., 2003).

These models largely neglect the influence of different surface types such as moraines, bare rock or coarse debris. They only roughly represent physical processes as they model approximate probability classes instead of real temperatures. For these reasons they are difficult to validate and test and not well suited for spatial or temporal extrapolation. Such models are important and valuable for first-order mapping of permafrost distribution but, additionally, more physics-based approaches are needed in the future. The energy-balance (e.g. Oke, 1987; Pal Arya, 2001) model PERMEBAL (Mittaz et al., 2002; Stocker-Mittaz et al., 2002) has been a step into this direction and, at the same time an important base for the research in this dissertation.

1.4 Challenges in mountain permafrost research

As the consequences of climate change more and more dominate research in mountain permafrost and a larger body of data becomes available, knowledge and numerical models need to be more quantitative. The effects that different surface characteristics as well as snow cover and complex geometries have on ground temperatures need to be considered.

There are three major challenges for the understanding of the complex and dynamic phenomenon of mountain permafrost:

- **To go beyond the traditional realm of the rock glacier**
  and to investigate other surface types. To model or parameterize heat transfer under different surfaces and in different active layer types.
- **To investigate and to model quantitatively**
  in terms of a transient three-dimensional temperature field. This provides the opportunity for validation, sensitivity studies, hypothesis testing and investigations on permafrost changes at depth.
- **To provide quantitative input data**
  for spatial models. Many surface and sub-surface characteristics need to be provided for every point of a spatial model.

This dissertation seeks to demonstrate first steps into these directions and to elucidate corresponding findings and future perspectives.

1.5 Overview of subsequent chapters

Chapter 2 “Characteristics of mountain permafrost and its response to a changing climate” provides a background on the characteristics of mountain permafrost. The main processes governing ground temperatures and their reaction to climate forcing are discussed.

Chapter 3 “Transient modelling of mountain permafrost” outlines the importance of modelling in mountain permafrost research. The model used in this dissertation is presented together with a review of existing other models and parameterizations.

Chapters 4 to 7 present the content of the six publications that constitute the main body of this dissertation structured in a framework of four topics: chapter 4 “Validation of spatial surface energy-balance models in complex terrain” , chapter 5 “Rock wall temperatures”, chapter 6 “Sub-surface temperatures in complex topography”, and chapter 7 “Spatial input data derived by remote sensing”.

Chapter 8 “Synopsis” summarizes the steps that were taken toward the challenges outlined in the introduction and lists the main findings.

Chapter 9 “Open questions and future research” presents research ideas and poses questions that arise from the investigations presented.

Chapter 10 concludes Part A “Scientific setting” of this dissertation and chapter 11 lists the references cited.

2 Characteristics of mountain permafrost and its response to a changing climate

2.1 Factors and processes that influence ground temperatures

Figure 1 provides a conceptual framework of factors and processes that determine ground temperatures in mountains. The distinction of the three domains "Climate", "Topography" and "Ground" helps to understand important differences and individual contributions of the most important influences on ground temperatures. These different domains often correspond to differing model scales, extent of the total area looked at as well as the size and nature of the smallest element that a model statement refers to. For a given task at hand a model may assume one of these domains to be constant or its influence to be negligible and only deal with one or two.

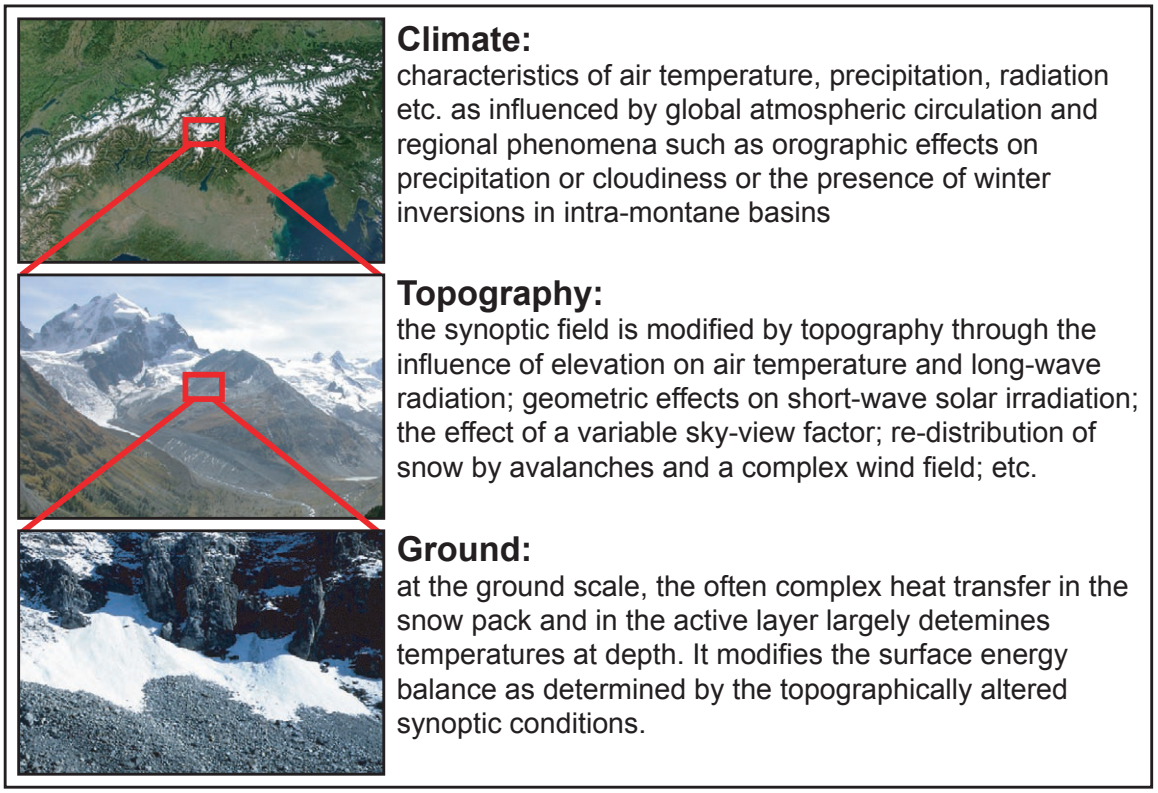

Figure 1 *Hierarchy of domains relating to factors and processes that influence sub-surface temperatures in cold mountains.*

Three experiments of thought illustrate this concept :

Global or continental distribution of mountain permafrost (focus: climatic conditions) The total area looked at is the entire globe or a mountain range such as the Alps. Any statement refers to a smallest element that is many kilometers in size. The factors that determine the distribution patterns are latitudinal position, altitude, global circulation patterns such as the North-Atlantic Current or orographic effects such as the differentiation between the Northern Alps and the Central Alps with their different regimes in cloudiness and solar radiation (cf:

Barry, 1992b). A statement includes all finer detail (topography, ground characteristics, etc.) in the form of an expression of probability i.e. the occurrence of some permafrost in a given element is referred to. Statements on actual ground temperatures or transient 3-dimensional temperature fields are hardly possible.

Regional distribution of mountain permafrost (focus: topography)
The total area looked at has an extension of several tens of kilometers. The smallest element that a statement refers to has an extension in the order of meters to tens of meters. The factors that influence the distribution patterns are mainly elevation and insolation geometry. The climate is assumed to be constant over the area considered. A statement includes the effect of surface types and snow in the form of probability i.e. "permafrost probable" or "permafrost likely". Without prior knowledge on ground heat-transfer, statements on actual ground temperatures or transient 3-dimensional temperature fields are hardly possible. However, e.g. the atmospheric part of the surface energy-balance can be quantified or a proxy for it estimated at each point.

Local sub-surface temperatures (focus: ground heat transfer)
Only one point on the surface and the temperature distribution below it is looked at. Heat transfer through the snow pack, through the active layer and in the permafrost is considered. The factors that influence the temperatures at depth are snow-pack characteristics, ground-material properties, water content and advective processes. At this scale, transient temperatures in a 3-dimensional field can be considered. A statement about the presence of permafrost as well as sound validation of modeled temperatures is possible.

It is important to note that the boundaries between these three domains are not sharp and, that models can include parts of all domains. This hierarchical model of domains does however help to understand the limitations of a chosen modelling approach.

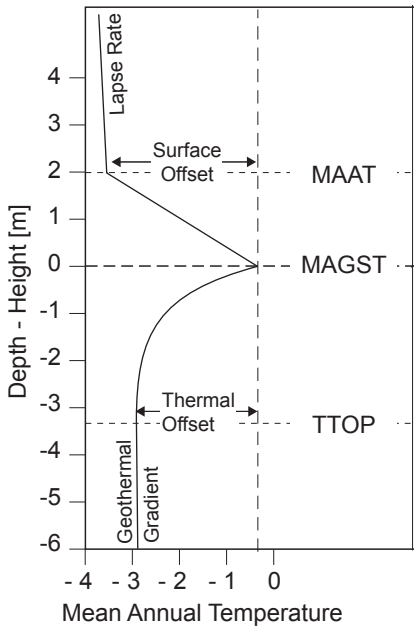

Figure 2 Schematic of the TTOP-model (modified from Smith and Riseborogh (2002)).

A similar conceptual model has been developed in the Arctic (Smith and Riseborough, 1996;

Smith and Riseborough, 2002). It relates the temperature at the top of permafrost (TTOP) to the mean annual ground surface temperature (MAGST) and mean annual air temperature (MAAT). In contrast to most of the Arctic, a large part of the spatial variation in alpine surface offset (MAGST-MAAT, Figure 2) is caused by solar radiation. The surface offset is the equivalent to the *topography* domain in Figure 1 and the thermal offset (MAGST-TTOP, Figure 2) takes place in the *ground* domain mainly by ground heat transfer. In Alpine areas, the surface offset has a range of about 1-10 °C (based on: Gruber et al., 2004b [*Publication 3*]; Gruber et al., 2003a [*Publication 2*]) and the thermal offset can be estimated to range from 0 and 9 °C (Ludwig, 2003).

2.2 The influence of topography

High-mountain topography introduces strong spatial variability into ground surface temperatures that relate mainly to differences in solar radiation input and air temperature. Strong differences in elevation influence the surface energy-balance largely through the effect that air temperature has on sensible heat flux and down-welling long-wave radiation. Most of the spatial variability introduced by solar radiation is due to the highly-variable insolation geometry in mountains. In the Alps, the northern side of an East-West trending ridge can be 6-8 °C colder (annual mean) than the southern side. Equally, an elevation difference of 1000 to 1200 m can cause the same difference of 6-8 °C between two locations that are otherwise similar. Both effects contribute to the high spatial variability of alpine ground temperatures. For comparison: A difference of 6-8 °C in mean annual ground temperatures would be roughly equivalent to that caused by a latitudinal change from Texas to Montana in the United States.

2.3 Surface cover types

Different surface types have a strong influence on ground temperatures at depth also through a number of processes occurring in the active layer. The net effect of these processes is often quantified as the difference between the MAGST and the TTOP and termed “thermal offset” following a study describing “higher mean annual temperatures in the upper portion of the active layer than in permafrost” (Burn and Smith, 1988; cf. also: Romanovsky and Osterkamp, 1995). Figure 3 displays schematics of energy fluxes at and below A) a steep rock surface and B) a coarse blocky surface. The term surface type refers to a surface cover in the geomorphological sense and, therefore includes an inherent statement about the sub-surface. The effect of vegetation is not mentioned in this context although in areas outside the Alps this may be of great importance. The most important surface types in mountain permafrost are:

Bedrock is the most straight-forward surface type (Figure 3A). It has a clearly defined interface with the atmosphere and a great proportion of heat is transferred by conduction alone. However, a considerable moisture content can be present in pores as well as in cracks and crevices. This can lead to the usual effects of latent heat during freezing and thawing and, additionally, to differences in bulk thermo-physical properties between frozen and unfrozen rock as well as between dry rock and rock with considerable water content. Little is known about the spatio-temporal distribution of moisture in rock and the 3-dimensional effects of latent heat caused by eg. ice-filled fissures.

Coarse blocky surfaces such as they occur on scree slopes and rock glaciers are characterized by very coarse clasts having large voids that enable the circulation of air to considerable depths (Figure 3B). At different depths they usually contain differing proportions of coarse clasts, fine

material, air, liquid water and ice. As a consequence, heat transfer is a complex interaction of advection, convection and effects of latent heat. Lateral air circulation along elevational gradients in steep slopes as well as variable air circulation through the snow pack add to the inherently high spatio-temporal heterogeneity in the relevant physical processes complicating the interpretation of measurements and the formulation of valid models. A number of individual investigations of processes in coarse blocky layers and their effect on ground temperatures exist (Goering, 2003; Hanson and Hoelzle, 2003; Hanson and Hoelzle, 2004; Harris, 1996; Harris and Pedersen, 1998; Herz et al., 2003a; Herz et al., 2003b; Hoelzle et al., 1999; Mittaz et al., 2000; Sawada et al., 2003; Wenbing Yu, 2004). Generally, the thermal offset for alpine coarse blocky surfaces can be estimated to be about 5-8 °C (Ludwig, 2003).

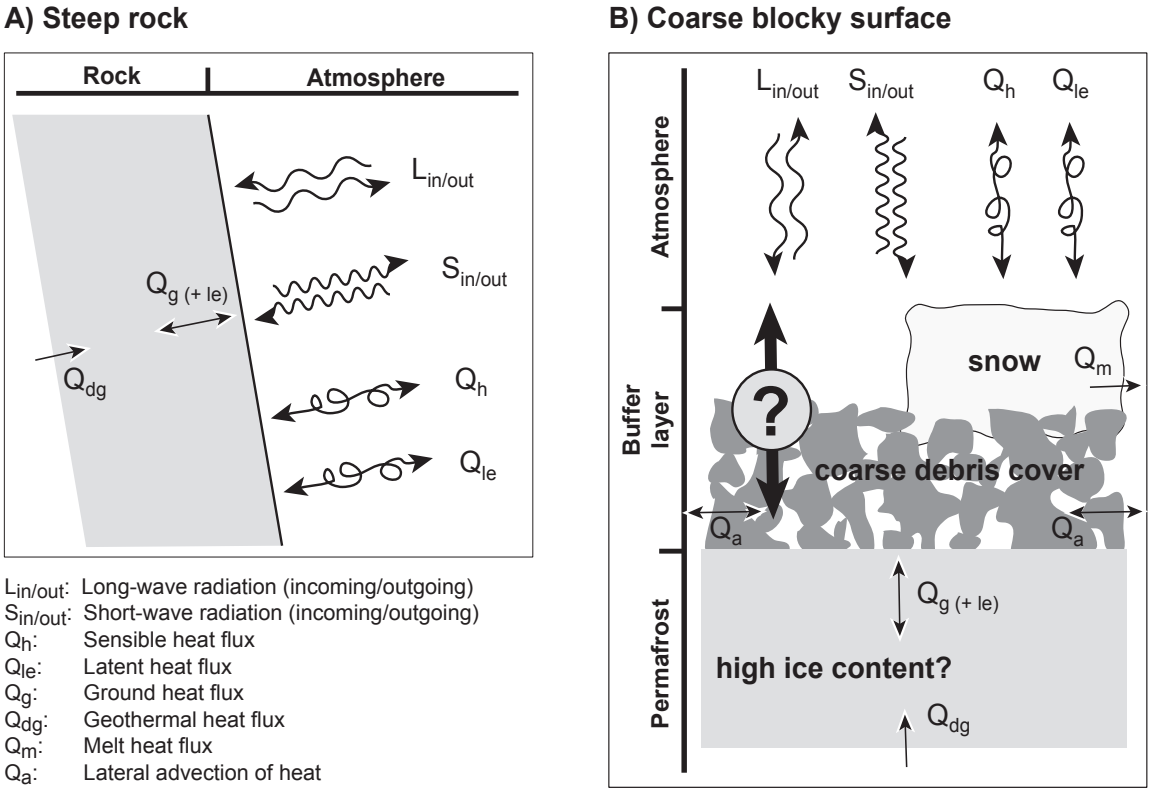

Figure 3 Energy fluxes at and below the surface for steep rock and coarse debris covers.

Moraine surfaces are often distinctly different from coarse blocky surfaces because they have a considerable fraction of fine material even at the surface. This has two results: (1) no large voids that would permit circulation of air as in coarse talus surfaces; and (2) a possibly high and variable water content resulting in temporally differing thermo-physical properties that could also lead to effects of thermal offset.

Ice faces and hanging glaciers are diagnostic features of mountain permafrost as both require areas of cold ice at their base in order to be stable. Rock temperatures can be expected to change considerably (Haeberli et al., 1997; Wegmann et al., 1998) after the disappearance of ice faces or hanging glaciers due to large changes in surface albedo as well as the missing uptake of summer heating by ice melt.

For steep mountain slopes it is evident that talus and bedrock form two end-members that

bracket real situations. As most rock faces have a slope angle somewhere between 37° and 90°, many transitional situations can occur where debris accumulates in parts of slopes or where deeply weathered rock remains in place, forming a surface cover similar to coarse talus slopes. Consequently the thermal properties of the active layer in rock slopes can vary between that of coarse debris and that of bedrock. Equally, there is neither a strict definition nor reliable data that clearly distinguishes coarse blocky surfaces from other surfaces in terms of their characteristics and their thermal offset.

For the impact of climate change on permafrost, different surface and subsurface characteristics are of great importance. The "thermal filter" of coarse blocky layers, for instance, may more readily transmit the cold of autumn and winter than summer warmth. Furthermore, a high ice content in rock glaciers as compared with rock walls significantly retards their warming through effects of latent heat. Owing to the range of thermal offsets and other effects caused by different surfaces it is necessary to distinguish them in models of permafrost distribution.

The importance of the different surface types and their characteristics for sub-surface temperatures brings with it the need for their mapping and characterization in order to provide spatial input data for corresponding models.

2.4 Snow cover

Snow has two main effects on ground temperatures: (1) increase of albedo; (2) insulation of the ground from low and high atmospheric temperatures. The relative weight and the net effect of these influences are determined by the duration, timing (Zhang et al., 2001), thickness and vertical distribution of thermo-physical properties (Zhang et al., 1996) of the snow pack (cf. also: Bernhard et al., 1998; Ishikawa, 2003; Keller and Gubler, 1993; Luetschg et al., 2003). In alpine topography, snow is redistributed by avalanches as well as wind drift. Together with melt that is driven by the spatially highly-variable energy-balance this results in heterogeneous snow pack characteristics in mountains that are difficult to measure or model accurately in the spatial domain.

2.5 Ice content

Ice content in permafrost has implications for its thermo-physical and thermo-mechanical properties. Especially the degradation of permafrost is slowed considerably by a high ice content due to the uptake of energy by the latent heat required for ice melt. Active rock glaciers usually have ice contents of over 30% with an average between 40% and 60% (Barsch, 1996; Elconin and LaChapelle, 1997; Vonder Mühll and Klingelé, 1994; Zhijiu, 1993) and often contain individual layers consisting almost entirely of ice (Arenson, 2002; Isaksen et al., 2000a). Most bedrock has a porosity of 5–25% (Schopper, 1982) that can be occupied by water or by ice and, additionally cracks and crevices can contain significant quantities of almost pure ice. The ice content is a sub-surface phenomenon and in the spatial domain can only be approximately inferred from surface information.

2.6 Depth, time and 3-dimensional effects

The temperature distribution at depth in permafrost is determined by heat diffusion and a transient boundary condition at the permafrost table, as well as subsurface thermo-physical properties (assuming no transport of heat by liquid water and a constant geothermal heat

flow). A change in the temperature at the permafrost table (which can be caused by changing climatic conditions) is dampened and delayed with increasing depth. This is important for the understanding the scales of time and depth involved in the degradation of a permafrost body (Delisle, 1998; Delisle et al., 2003; Lunardini, 1996). Inversely, a temperature-depth profile (so called T(z) profile) from boreholes in permafrost can be used to infer (for a review of one-dimensional inversion techniques see: Wang, 1992) changes in boundary conditions that can be interpreted as climate signals (e.g. Isaksen et al., 2000b; Lachenbruch and Marshall, 1986). 3-dimensional effects such as a spatially heterogeneous upper boundary condition (juxtaposition of e.g. lakes, tundra, forest, buildings, ocean) or variable sub-surface thermo-physical properties have been investigated for arctic permafrost (for a review of early work see: Gold and Lachenbruch, 1973). In mountain permafrost, the problem of 3-dimensionality is complicated further by the often complex geometry and by a strong spatial heterogeneity of the surface conditions and temperatures. Transient effects and heat transfer below complex topography are described by Kohl (1999) along with a review of previous work. Two- or three-dimensional effects on permafrost degradation are likely to be of great importance in steep mountain topography but have received little attention (Haeberli et al., 1997; Wegmann et al., 1998) so far. The derivation of climate signals from T(z) profiles is complicated by 3-dimensional effects in complex topography (Gruber et al., 2004c [*Publication 4*]; Kohl and Gruber, 2003; Ludwig, 2003).

3 Transient modelling of mountain permafrost

3.1 Definition and rationale

A model is a conceptual or mathematical representation of a phenomenon or system. It provides an idealized framework for logical reasoning, mathematical or computational evaluation as well as hypothesis testing. It is idealized in the sense that it may make explicit assumptions or simplifications as long as it serves its purpose with satisfactory accuracy. The process of testing this is called validation.

In this dissertation, the term modelling (of mountain permafrost) refers to computer models describing the thermal state of the (sub-)surface. The design and use of such models generally has two types of objectives:

System research
Models are used as a quantitative formulation of system understanding. They can be used to test hypotheses, to better interpret measurements or to perform numerical experiments (e.g. calculation of idealized case studies or sensitivity studies) that provide insight into the system under investigation.

Predictive simulation
Models are used to simulate and predict a phenomenon for a purpose at hand. Not their formulation but their result is important. They provide a means to make certain aspects of knowledge on a complex system available to other researchers or otherwise interested persons.

The combination of measurements and models is important in quantitative research on mountain permafrost as illustrated by the schematic in Figure 4. The turning arrow in that figure indicates an iterative process. This iteration can take place on sub-systems if the entire system of interest is complex. Finding appropriate combinations of sub-systems is important.

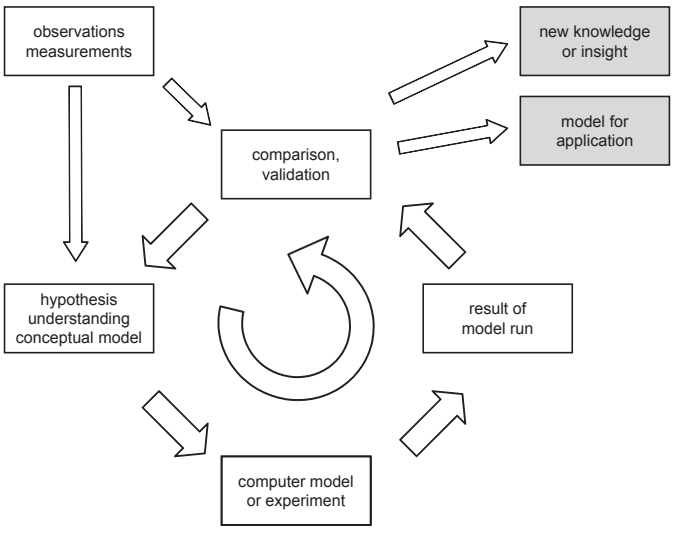

Figure 4 *Schematic illustrating the role of quantitative modelling and measurements in research.*

3.2 The model TEBAL

The model TEBAL (Topography and Energy-Balance) extrapolates meteorological variables from one point over complex topography and simulates the surface energy-balance for each point on the used surface grid. Apart from surface temperatures it calculates the build-up and melt-out of the snow pack. It is based on the model PERMEBAL (Mittaz et al., 2002; Stocker-Mittaz, 2002; Stocker-Mittaz et al., 2002).

TEBAL/PERMEBAL contain algorithms for the mountain-specific extrapolation and parameterization of meteorologic variables and energy fluxes: Wind speed and direction (Plüss, 1997; Purves et al., 1998; Ryan, 1977), potential short-wave solar irradiation (Corripio, 2003; Dozier et al., 1981; Iqbal, 1983), diffuse and direct short-wave radiation (Collares-Pereira and Rabl, 1979), snow albedo (Kondo and Yamazawa, 1990), long-wave radiation (Brutsaert, 1975; Konzelmann et al., 1994; Plüss and Ohmura, 1997) and snow drift (Purves et al., 1998). Other fluxes and parameters are determined using standard procedures such as the bulk-method for the estimation of latent and sensible heat fluxes or elevation gradients for temperature and precipitation.

The model has been further developed as a tool to be used in the context of this dissertation and is programmed in the fourth-generation language IDL (RSI, 2004b). Where necessary, the papers submitted with this dissertation describe individual aspects of the model. However, a brief overview of TEBAL is given here since an entire software that is meanwhile also used by other researchers has resulted from this constant development. Apart from minor alterations and corrections, several changes have been made to the model formulation:

- **converging surface temperature**
  turbulent fluxes, melt energy, ground heat flux as well as long-wave radiation from the surrounding terrain require an initial estimate of surface temperatures. A secant iteration procedure has been introduced that converges the initial estimate and the final model result on surface temperature. The large fluctuations and errors previously observed in PERMEBAL could be reduced and stable temperatures suitable for validation and numerical experimentation were obtained.
- **heat conduction**
  a one-dimensional finite-difference Crank-Nikolson scheme for the conduction of heat has been added that treats latent heat. The latter is treated as apparent heat capacity between 0.5 and 0 °C. This permits the calculation of sub-surface temperatures and more realistic ground heat fluxes. The effect of snow is not included.
- **solar radiation algorithms**
  algorithms (Corripio, 2003) and a code (that was kindly provided by Javier Corripio) for the calculation of terrain shading and solar geometry were included in TEBAL.
- **neighborhood effects for incoming short- and long-wave radiation**
  the calculation of diffuse irradiance as well as the long-wave irradiation from surrounding terrain requires information on albedo and temperature, respectively. These quantities are now determined from a distance-weighted neighborhood instead from the centre pixel alone.

These changes have been published briefly where necessary in the context of their application (Gruber et al., 2004b [*Publication 3*]). A detailed article including a sensitivity analysis will

be forthcoming. Further changes to the model that have improved its usefulness as a research tool include:

- **complete re-programming**
  the model has been rewritten in order to 1) collect all relevant information and variables in a central structure and allow manipulation of all variables through an input parameter file; 2) have a logical structure of subroutines, avoiding redundant code; 3) make optimal use of IDLs array-handling capabilities and pass data by-reference to increase speed; and 4) provide easy handling through a graphical user interface (in collaboration with Dr. Daniel Schläpfer).
- **output choices**
  three types of output can be chosen: *1) integration*: one map of mean surface temperatures, snow cover and days with snow cover for the calculation period is generated; *2) spatial fluxes*: data cubes i.e. one image per calculated time step for individual fluxes or quantities such as surface temperature, diffuse irradiation, snow water equivalent etc.; and *3) point time series*: for a given co-ordinate all surface fluxes and other relevant quantities are written to a file in order to facilitate comparison with measured data.
- **visualization: using ENVI file formats**
  due to the high number of data layers involved in the output of spatial fluxes the remote sensing software ENVI (RSI, 2004a) is used for data visualization and exploration. Data cubes can be analyzed and profiles over different dimensions (including time) can be extracted.
- **one-dimensional version**
  a version that calculates individual points only has been designed in order to perform simple validation runs and in order to calculate look-up tables and experiments. It includes simple parameterizations to account for e.g. the sky-view factor and snow redistribution that need to be handled differently than on a 2-dimensional grid. An option to read surrounding horizon elevations from a file is included.

3.3 Existing and envisioned future transient models

A good representation of transient ground temperatures and mountain permafrost requires the coupling of a spatial energy-balance model for complex topography with a snow pack model and 3-dimensional ground heat transfer. Several models exist and have been evaluated for one or several of these three domains:

Spatial surface energy-balance over complex terrain
Apart from the purely geometric effects on direct short-wave solar radiation, especially the work of Plüss and Fierz (Fierz et al., 1997; Plüss, 1997; Plüss and Ohmura, 1997) as well as Konzelmann (Konzelmann et al., 1994) provided a base for the simulation of surface energy balance over snow in complex topography. These approaches were later used and adapted to better include snow-free surfaces in the models PERMEBAL/TEBAL (Gruber et al., 2004b [*Publication 3*]; Mittaz et al., 2002; Stocker-Mittaz et al., 2002) in order to model the spatial permafrost distribution. Further models using similar or identical approaches are described in the literature (Fierz, 2003; Klok and Oerlemans, 2003; Oerlemans, 1992).

Snow pack
Several models of heat transfer and related processes in the snow pack exist today. Models suit-

able for the simulation of an alpine snow pack in the context of permafrost modelling include: CROCUS (Brun et al., 1989), SNTHERM (Jordan, 1991), DAISY (Bader and Weilenmann, 1992) and SNOWPACK (Bartelt and Lehning, 2002; Lehning et al., 2002a; Lehning et al., 2002b). These models include a surface energy balance module and conduction of heat in the ground.

Ground heat conduction
The parameterization of temperature-dependent liquid water content, effects of latent heat and associated thermo-physical changes in the sub-surface material is of great importance for heat transfer in permafrost and active layers. A wealth of literature and numerical models (e.g.: Goodrich, 1978; Goodrich, 1982a; Goodrich, 1982b; Guymon and Hromadka, 1977; Guymon et al., 1984; Hinzman et al., 1998; Inaba, 1983; Ling and Zhang, 2004; Lunardini, 1991; Outcalt and Hinkel, 1996; Romanovsky et al., 1997; Seregina, 1989) exist, especially in the North American and Russian research on high-latitude permafrost. Examples for the numerical treatment of 2- and 3-dimensional conduction of heat in complex topography (Kohl, 1999; Wegmann et al., 1998) usually neglect the complex thermo-physical processes in the active layer.

The list of models provided is not complete but provides an overview of existing work. Due to their greater practical relevance, snow pack and ground heat-transfer models and the required parameterizations are developed and tested at a higher level of sophistication than most flux parameterizations that are used for energy-balance models in complex topography. As a consequence, the errors and caveats of simulating energy fluxes over mountain terrain are less known than those involved in heat transfer in the snow and ground. For this reason, this dissertation focuses largely on the spatial aspects of modelling in order to provide a base for a future coupling or integration of the above three model domains.

3.4 Designing models of reduced complexity

Complex process-based models need to be simplified for large-area permafrost modelling and for the dissemination of models to potential users in e.g. consulting agencies. The number of variables as well as the complexity of the required computations need to be reduced (cf. Smith and Riseborogh, 2002) in order to make the collection of input data, the computation and the interpretation of model results practicable. In this respect, the availability of process-based models constitutes a valuable asset for the design of reduced-complexity models: A validated complex model can be used to run numerical experiments that form the basis for a simple model (cf. Gruber et al., 2004b [*Publication 3*]). In this way, also model sensitivities and inherent errors can be analyzed and robust models of reduced complexity designed. When surface characteristics or transient effects are of interest, this approach to base simple models on validated process-based models is likely more feasible than using measurements alone. In view of the application of research findings, the development of reduced-complexity modelling strategies should accompany the growing sophistication of process models.

4 Validation of spatial surface energy-balance models in complex terrain

This chapter introduces and summarizes Publication 2 (Gruber et al., 2003a) and Publication 3 (Gruber et al., 2004b), constituting part of this dissertation.

4.1 Terminology

The concept of validation is of great importance for the design and application of models, but, at the same time it is often used with different or even contradicting definitions as pointed out in a review of existing literature by Rykiel (1995). He puts forward a definition that can also be applied to the modelling of ground temperatures in mountains: *Validation* is a demonstration that a model within its domain of applicability possesses a satisfactory range of accuracy consistent with the intended application of the model. It cannot demonstrate the logical validity of the scientific content of the model. It is a yes/no statement about the fulfillment of performance criteria. *Qualification* is aimed at discovering the domain over which a validated model may properly be used and amounts to the revalidation of a model for new cases. The rationale of modelling and validation has been outlined in Section 3 “Transient modelling of mountain permafrost”.

4.2 Previous work

Based on input data for one location, spatial energy-balance models are intended to parameterize the spatial distribution of energy-fluxes at the ground or snow surface over a certain area that is discretized into individual cells. The most common approach is to compare the modelled energy-fluxes that are driven by one meteorological time series to data measured by an independent micro-meteorological station somewhere in the model area (e.g.: Fierz et al., 1997; Fierz, 2003; Stocker-Mittaz, 2002; Stocker-Mittaz et al., 2002). This approach has the great advantage of providing an individual and quantitative assessment of the individual fluxes compared. However, many aspects that are crucially important to modelling in complex topography are not or only partly covered. E.g. sensors for long- and short-wave radiation are usually mounted horizontally (for tilted sensors see: Fierz, 2003). Usually, only few such validation points are available because micro-meteorological measurement in mountain regions entail high cost and effort.

Comparing modelled with observed patterns of snow melt provides a method for assessing the success in the spatial representation of processes. Such an approach has been applied using sequential aerial photography classified for the presence of snow cover (Mittaz et al., 2002; Stocker-Mittaz, 2002). This demonstration of model performance accumulates errors over the entire winter and they cannot be attributed to one of their possible causes such as: erroneous terms in the energy-balance during melt, snow drift, erroneous parameterization of snow fall, or the thresholds used for classification of the imagery used for validation.

Using the presence or absence of permafrost determined by geophysics or rock glacier mapping has only explorational value because strong thermal alterations occurs in the active layer that are not accounted for in the model and, because this would require long-term model runs over several decades or centuries in the past. For rock glaciers, their dynamic behavior (Frauenfelder, 2004) would need to be taken into account, additionally. BTS (Haeberli, 1973)

measurements provide no means for model evaluation because their nature as a proxy variable and their strong inter-annual fluctuations (cf. Hoelzle et al., 2003; Keller, 1994) do not match the accuracy of the energy-balance model. Furthermore, the BTS is to a great degree governed by heat conduction in the ground and snow pack that is not included in simple surface energy-balance models.

4.3 Validation strategy for complex terrain

Measurements in extreme topographic situations (i.e. steep slopes) are necessary in order to test the ability of the model to parameterize surface temperatures via the energy-balance in mountain topography (i.e. only the effects of the "topographic" layer from Figure 1). The main dimensions of variation for the dominating fluxes are elevation (long-wave radiation and sensible heat flux are strongly influenced by air temperature) as well as aspect (short-wave radiation). Measurements for validation should be sampled along these dimensions. Surface temperatures are the desired result of the energy-balance calculation and, their measurement provides a cost-effective and robust means for model evaluation. Several tens of miniature data loggers can be employed at the cost of one micro-meteorological station and, these can measure unattended for one year. Because the measurement of actual surface temperatures is technically difficult and subject to high-frequency fluctuations, temperatures at a depth of 10 cm are measured (Gruber et al., 2003a [*Publication 2*]) and considered a valid surrogate for the rock surface. Locations with a minimal influence of surface characteristics and snow should be chosen in order to establish a clean relation between the measurements and the model. Near-vertical rock walls (cf. Figure 3A) provide a clearly-defined surface, maximum snow-free conditions, maximum topographic differentiation and minimal effects of the heat transfer in the active layer. This new strategy tries to successively validate models of increasing complexity. The system is broken-down into the layers that are conceptionally depicted in Figures 1 and 2. Each new model contains the old model as a sub-system for which the validation has already been performed. As a consequence, our ability to learn from the validation procedure (as the cause of misrepresentation can be attributed better) increases. Rock glaciers, the traditional focus (and beginning) of research on mountain permafrost are the last element of this chain of increasing complexity: 1) topography only (steep rock); 2) topography and snow (horizontal rock); and 3) topography, snow and active layer processes (coarse blocky surfaces).

The first campaign for the collection of data in steep rock (Gruber et al., 2003a [*Publication 2*]) has been successful and the results have been employed for model validation (Gruber et al., 2004b [*Publication 3*]). Based on this validated model, a numerical study of permafrost thaw in steep rock walls during the hot summer of 2003 could be conducted with confidence (Gruber et al., 2004a [*Publication 1*]).

In the validation campaign, a surface-only model version and one with a numerical ground heat-conduction scheme were employed and compared on daily data. All verification runs have been performed using standard values for rock albedo and emissivity. Scaling issues arise from the validation of a model that uses a cell size of tens of meters with measurements that are representative of a surface area with a radius of approximately 20 cm. The scaling issue lies in the misrepresentation of the small area measured by the logger at the coarse grid scale of the model as well as in the failure of a gridded digital elevation model to represent vertical slopes. Factors that influence the measurement but that are not resolved in the grid-based model need to be accounted for are: (1) slope, aspect and elevation need to be measured at the logger and

cannot be taken from the digital elevation model; (2) local horizon shading by small features in the rock wall - these can be measured using a calibrated fish-eye camera on a specialized mount (Gruber et al., 2003a [*Publication 2*]). Subsequently, model validation is performed with one-dimensional model runs using the measured site characteristics instead of data taken from the digital elevation model or a two-dimensional run.

4.4 Conclusion

The presented validation strategy is an ideal complement to the validation using meteorological measurements or, an inexpensive and straight-forward way to perform a qualification study when a validated model is applied in a new area. The measurement strategy put forward here is now part of the Swiss National Permafrost Monitoring System PERMOS where 36 loggers are placed in three areas in Switzerland, covering steep as well as horizontal rock. Furthermore, the results presented in the following Section 5 rely on the confidence resulting from this validation campaign

5 Rock wall temperatures

This chapter introduces and summarizes Publication 1 (Gruber et al., 2004a), Publication 2 (Gruber et al., 2003a) and Publication 3 (Gruber et al., 2004b), constituting part of this dissertation.

5.1 Rationale

Knowledge on the distribution of permafrost and temperatures in steep rock is limited (for a review see: Gruber et al., 2003a [*Publication 2*]) and systematic measurements of their topographic controls and regional distribution were previously missing altogether. The recent rise in atmospheric temperatures (Beniston et al., 1997; Böhm et al., 2001; Diaz and Bradley, 1997; Haeberli and Beniston, 1998; Houghton et al., 2001) is hypothesized (Haeberli, 1992b; Haeberli and Beniston, 1998) and has been demonstrated (Harris et al., 2003) to warm and degrade alpine permafrost. A reduction of the stability during warming and thaw of frozen rock walls is likely to occur (Haeberli et al., 1997) and has been demonstrated by geotechnical experiments (Davies et al., 2001). This can lead to a climate-driven shift in zones of natural hazards that is beyond the historical variability that builds the basis for the mostly experience-derived hazard assessment and zonation procedures (Haeberli et al., 1997; Huggel, 2004). The resulting necessity to investigate and quantitatively model rock temperatures is underscored by the projected rise in atmospheric temperatures (Houghton et al., 2001), even for the coming decades (Knutti et al., 2002; Stott and Kettleborough, 2002; Zwiers, 2002). This effect is exacerbated by the fact that a much stronger rise in temperatures is expected for mountain regions than the global or hemispheric average (Barry, 1990; Barry, 1992a; Beniston et al., 1997; Diaz and Bradley, 1997; Haeberli and Beniston, 1998).

5.2 Method and results

An investigation that uses field measurements and modelling has been carried-out in order to investigate the distribution and evolution of rock temperatures and permafrost. The combination of modelling and measurements has been necessary because: 1) information on locations that were not measured is needed; 2) the inter-annual variability of surface temperatures is so high that one year of data does not suffice; 3) modelling studies provide a chance to explore complex systems; 4) no information on the temperatures at depth were available; and 5) measurements are needed for model validation. It is assumed that the major controlling factor of the spatial and topographic differentiation of rock temperatures is their surface energy-balance. Standard approaches on heat conduction in rock were used to investigate the associated sub-surface effects. Therefore, the model results were not accurate predictions of the sub-surface temperature at a specific location but patterns representing and highlighting regional and topographic controls on temperatures in an idealized framework. These investigations have for the first time provided an insight into the distribution of Alpine permafrost under rock surfaces. Generally, the lower limit of permafrost is a few hundred meters higher in rock than below rock glaciers. The difference between North and South can be as large as 1000 m vertical. The inter-annual variability of the elevation of the 0 °C MAGST line is in the order of 500 m vertical, underscoring the need for the combination of measurement and modelling. Climatic controls on MAGST were demonstrated. The difference between the Northern Alps (Jungfrau Region) and the Central Alps (Corvatsch) is greatest in southern aspects and at high elevation, due to the larger weight of short-wave radiation in these locations. The strong thermal effect of the hot summer 2003 could be modeled (see Section 6) for the surface and sub-surface.

5.3 Conclusion

This first application of a forward, quantitative model of alpine permafrost has been successful on the most straight-forward surface: steep rock. For real alpine rock faces it should be kept in mind that this represents one end-member in a continuum of different topographic and surface conditions. More gently inclined rock faces can accumulate debris and snow and thus partly be governed by processes associated with coarse debris covers. Open questions also remain as to the water and ice content of rock. The contents of liquid water, ice and air in the pore space and crevices of the active layer in bedrock likely undergo changes due to variations in temperature and surface conditions. These changes can theoretically cause considerable thermal offset, even in bedrock.

6 Sub-surface temperatures in complex topography

This chapter introduces and summarizes Publication 4 (Gruber et al., 2004c) and Publication 1 (Gruber et al., 2004a), constituting part of this dissertation.

6.1 Rationale

Quantitative research on permafrost always has a dimension of depth and time to it because a temperature signal is progressively attenuated and delayed with increasing distance from the surface (Carslaw and Jaeger, 1959; Williams and Smith, 1989). At greater depth, the time over which the contained temperature signal was averaged as well as its age increase. In mountain topography, the temperature field at depth is characterized by a complex geometry as well as a highly-variable temperature boundary condition at the surface. As a consequence, investigations of permafrost degradation or the interpretation of borehole temperatures in terms of temperature histories are more complex than the usual one-dimensional case that assumes a semi-infinite homogenous medium. A transect of eight 100 m deep boreholes in mountain permafrost has recently been established in the EU-project PACE (Harris et al., 2001a). This transect is intended for the monitoring of changes in permafrost temperatures and associated regional trends as well as for the interpretation in terms of past climate signals (cf. Harris et al., 2003; Isaksen et al., 2001; Isaksen et al., 2000b).

6.2 Method and results

Three studies (Gruber et al., 2004c [*Publication 4*]; Kohl and Gruber, 2003; Ludwig, 2003) were performed in order to investigate sub-surface temperatures below complex topography.

Depth of thaw and the depth of annual freeze-thaw cycles

Using the validated surface energy-balance model together with a 1-dimensional heat conduction scheme (Gruber et al., 2004a [*Publication 1*]; Gruber et al., 2004b [*Publication 3*]) the effects of the hot summer of 2003 were investigated using model experiments from 1982 to 2003. It was demonstrated that the thaw during 2003 likely exceeded the thaw of previous decades or centuries. This underscored the hypothesis that the extreme frequency of rockfall during 2003 was related to the thaw of permafrost. The spatial/topographic distribution of annual freeze-thaw cycles and thus approximate depths for the detachment of rockfall due to active layer thickening was derived from the model experiments. Furthermore it was shown that the majority of events took place before the time of maximum thaw that was simulated for homogeneous rock. Questions on the influence of ice-filled discontinuities on the depth and timing of thaw arise from this.

Temperature histories and 2- or 3-dimensional temperature fields

The three-dimensional temperature field (or two-dimensional sections) has been numerically simulated using the finite-element (FE) code FRACTure (Kohl and Hopkirk, 1995). The temperature boundary conditions were derived based on a measurement campaign (Gruber et al., 2003a [*Publication 2*]), statistical (Gruber and Hoelzle, 2001) and process-based (Gruber et al., 2004b [*Publication 3*]) model experiments as well as existing literature. Model experiments (assuming homogenous surface characteristics) and comparison with data from the Stockhorn borehole showed that even under steady-state conditions, negative gradients and curved tem-

perature profiles can exist in homogenous material. Furthermore, the temperature and curvature of the profile are very sensitive to the location of the borehole. These effects (i.e. noise) are in the magnitude of several °C and therefore a major obstacle in the interpretation of temperature trends using standard approaches (for a review see: Wang, 1992). Figure 5 is compiled from Ludwig (2003). It shows the additional uncertainty introduced by variations in surface conditions to amount to several °C as well. Keeping in mind that these are 2-dimensional model cases that have a regular geometry and homogenous areas of surface characteristics it is easily understood that real geometry and surface characteristics can be a major obstacle to the inversion of temperature histories. Kohl and Gruber (2003) demonstrate a method for the inversion of 2- or 3-dimensional cases using a forward FE-scheme and a parameter estimation program. The upper boundary condition for the heat-conduction domain is the TTOP. Due to the many unknowns in the processes of heat transfer in alpine active layers as well as the problems of measuring or modelling precise data fields of snow cover, subsurface properties etc. the inversion of temperature histories will remain highly uncertain. However, if atmospheric temperatures rise and research on mountain permafrost continues, the signal-to-noise ratio in this type of investigations also increases.

6.3 Conclusion

These results highlight the importance and practical relevance of 1-, 2- and 3-dimensional investigations that include the sub-surface transfer of heat for mountain permafrost research. Especially, questions of the fast degradation in steep rock need to be addressed in this way.

Figure 5 *The influence of topography, variable surface temperatures and variable surface types on the temperature distribution at depth. The left panel shows a cross-section of a hypothetical mountain. The right panels show temperature profiles extracted from the hypothetical boreholes labeled a, b, c in the cross-section. Based on Ludwig, 2003.*

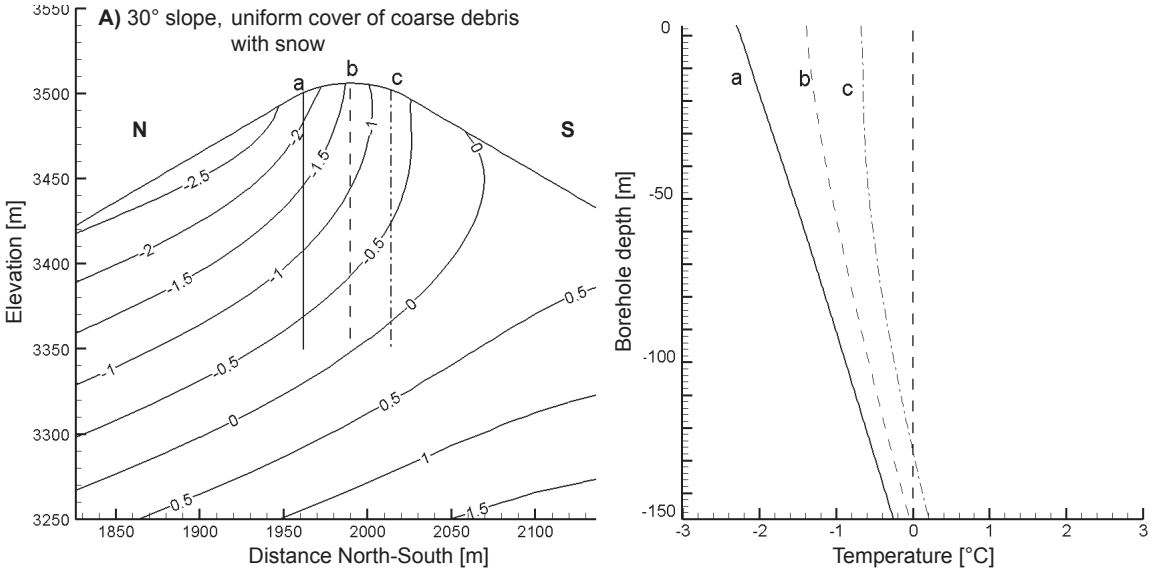
A) 30° slope, uniform cover of coarse debris with snow
N
S
a
b
c
Elevation [m]
Distance North-South [m]
Borehole depth [m]
Temperature [°C]

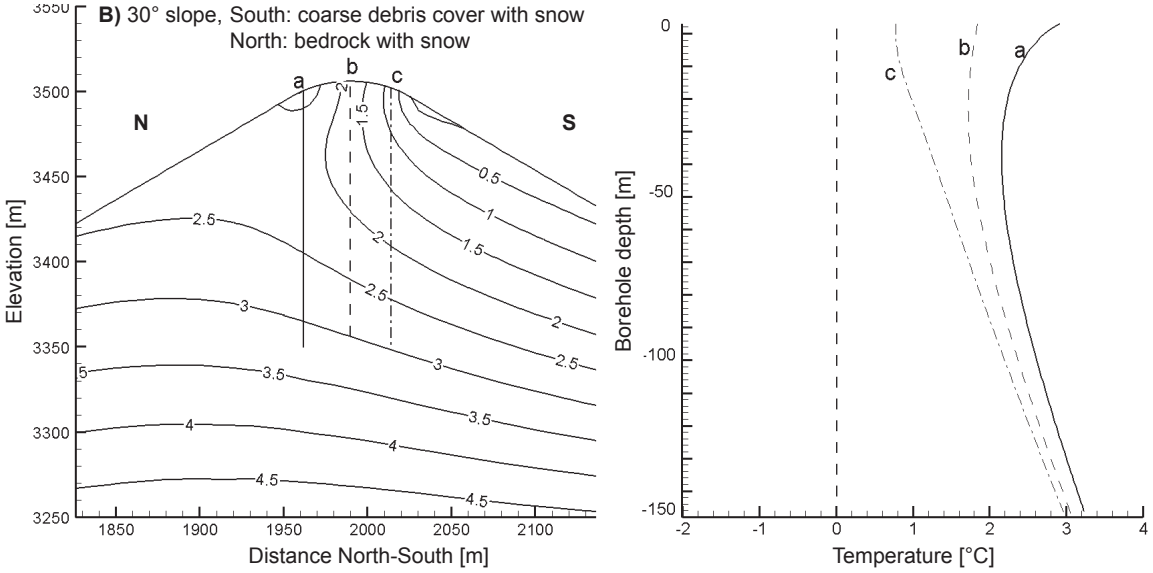
B) 30° slope, South: coarse debris cover with snow
North: bedrock with snow
N
S
a
b
c
Elevation [m]
Distance North-South [m]
Borehole depth [m]
Temperature [°C]

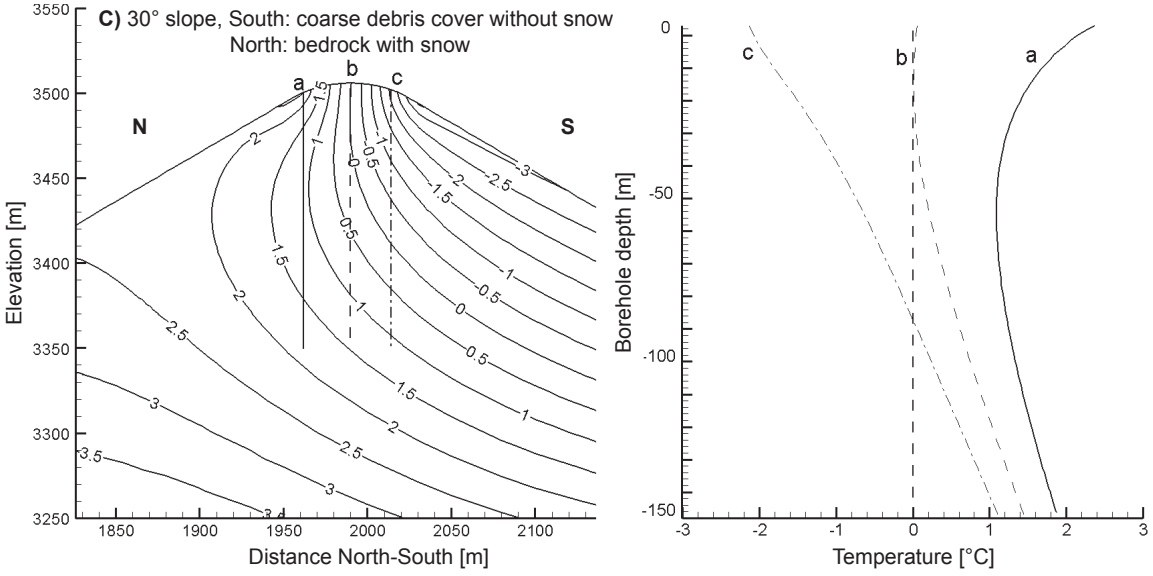
C) 30° slope, South: coarse debris cover without snow
North: bedrock with snow
N
S
a
b
c
Elevation [m]
Distance North-South [m]
Borehole depth [m]
Temperature [°C]

7 Spatial input data derived by remote sensing

This chapter introduces and summarizes Publication 5 (Gruber et al., 2003b) and Publication 6 (Gruber et al., 2004, submitted), constituting part of this dissertation.

7.1 Rationale

Quantitative models of ground temperatures require quantitative information on surface characteristics as these influence the energy-exchange processes. Sub-surface material properties are of interest, because quantitative models require a parameterization or numerical treatment of heat transfer in the ground. The spatial application of quantitative models thus requires quantitative spatial data fields describing these properties. For surface parameters, direct remote sensing as well as the designation of standard values based on surface classes derived from other sources are viable options. Sub-surface properties can only be inferred from spatial surface information combined with a priori knowledge of the sub-surface or information derived by e.g. geophysics or drilling at individual locations.

The delineation of block fields is of great importance for spatial permafrost models due to the large possible thermal offset. Albedo and emissivity are factors in the short- and long-wave radiation balance that mostly dominates the surface energy-balance and, therefore, are likely to have a strong influence on surface temperatures. Based on the above reasoning, the delineation of block fields that have a high surface roughness as well as the remote measurement of albedo and emissivity are regarded to be of high priority.

7.2 Surface roughness / delineation of coarse debris cover

The results of this section are taken from Heiner, 2003.

Three sources of information were evaluated:

JERS-1 SAR (Satellite-based Synthetic Aperture Radar)
SAR data contains information on surface roughness and in mountain areas, the correction and treatment of geometric effects such as layover and foreshortening can be time consuming if continuous spatial coverage is desired. Unfortunately however, no useable results could be obtained from the JERS-1 data due to the low ground resolution and the relatively low positional accuracy.

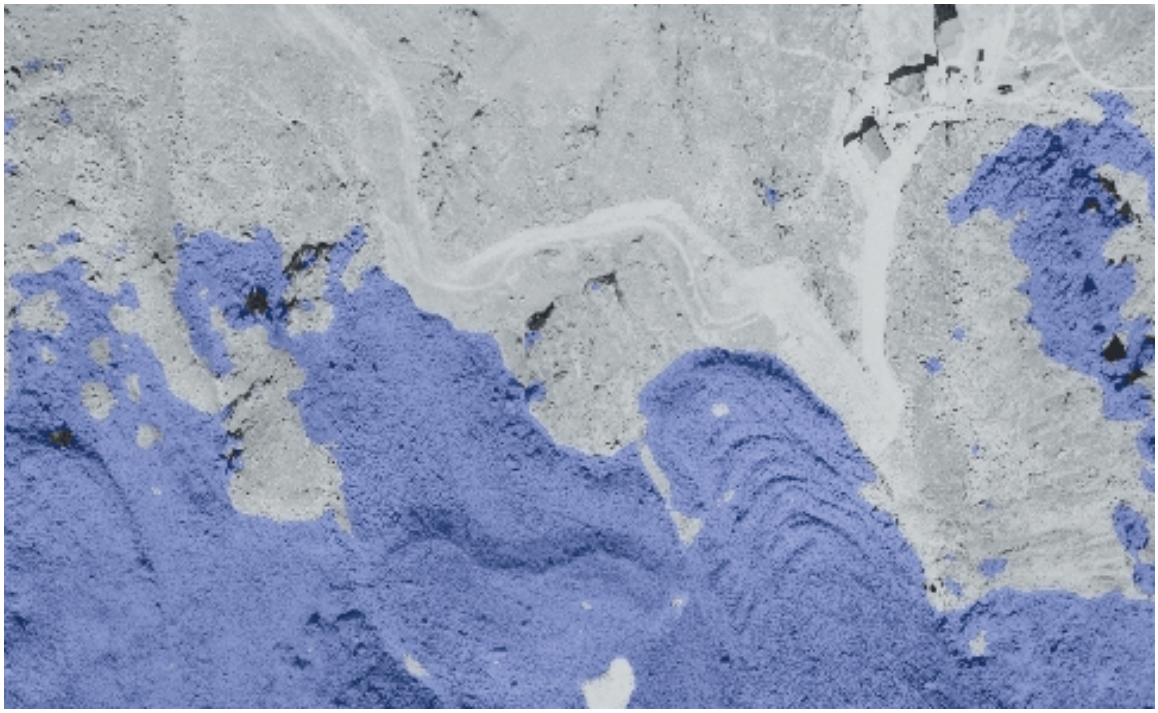

Figure 6 *Delineation of coarse blocky surfaces (blue) overlaid on aerial photograph. The rock glacier Murtèl is visible in the lower right.*

Aerial photography (black and white, ortho-referenced)
Classes of different surface roughness could be derived based on the mean grey level difference (MGLD) and the successful delineation of block fields has been demonstrated visually (cf. Figure 6). The extracted classes are not directly related to physical meaningful values of roughness. The method is straight-forward and inexpensive to apply.

Airborne LIDAR (laser scanning, Falcon/TopoSys)
A helicopter-borne LIDAR campaign has been conducted in the summer of 2003. A simple indicator, the surface-to-base ratio that is a physically meaningful measure of roughness was extracted from the high-accuracy data provided by the LIDAR and the successful delineation of block fields has been demonstrated visually. The high-accuracy LIDAR data can be used to attach ranges of physical values to the classes derived from MGLD. A large future potential exists because statistics of the vertical distribution of measured points can be used to discriminate between coarse surfaces that have deep voids (and produce a strong thermal offset) and those where the voids are filled by fine material (e.g. moraine).

7.3 Albedo

In micro-meteorology albedo is mostly treated as a scalar value (e.g. Oke, 1987; Pal Arya, 2001) and most energy-balance models (including TEBAL) use scalar input. However, the albedo of natural surfaces is spectrally and angularly variable. For the remote sensing of albedo, the hyperspectral sensor DAIS7915 (Chang et al., 1993) was chosen in order to have a good coverage of the spectrum of irradiant short-wave solar radiation. After ortho-rectification and topo-atmospheric correction the resulting image of HDRFs (Hemispherical-directional reflectance factor, see: Martonchik et al., 2000) showed strong artifacts due to angular anisotropy of

the surface reflectance. Empirical functions for their compensation can be employed (Richter and Schläpfer, 2002) and a method for their optimization in mountain terrain has been developed (Gruber et al., 2003c). However, the physical basis of the measurement is lost during empirical correction.

To overcome this limitation, a parameterization of BRDF (Bidirectional Reflectance Distribution Function, Nicodemus et al., 1977) using kernel-based models was performed in order to: 1) correct the angular effects in the topo-atmospherically corrected (HDRF) image and derive values of albedo; and 2) investigate the angular dimension of albedo and its influence on the surface energy-balance in mountain areas. A new method for the derivation of BRDF-parameters from single flight lines was designed and applied on coarse blocky surfaces because no suitable multi-angle observations were available. Standard procedures for narrow-to-broadband conversion were employed. The sensitivity of surface temperatures to snow-free albedo was investigated using TEBAL model experiments. The sensitivity to angular anisotropy was investigated by coupling of TEBAL with a parameterization scheme for albedo using kernel-based BRDF models.

The approximate error for the determination of broadband albedo from the DAIS7915 hyperspectral data in the presented campaign is ±16% relative or about 0.035 absolute. Based on the sensitivity study this corresponds to an error in mean annual surface temperature of less than ±0.2°C for most topographic situations. The treatment of albedo as a constant value (white-sky albedo) amounts to an error of less than ±5% relative to a full angular parameterization for most of the test area. As a consequence, the correction of BRDF effects is necessary for the derivation of albedo from imagery or ground-based measurements over rugged mountain terrain. However, for the block surfaces investigated an angular parameterization of albedo during energy-balance calculation is not required as the error involved is comparably small.

The mean sensitivity (based on a simulation over 40,000 cells) of mean annual groung surface temperatures to the total range (0.05 - 0.40) of likely snow-free albedo is in the order of ±0.5 °C. However, most natural surfaces will have an albedo variation in a much smaller range and, as a consequence, the corresponding error in temperature will be considerably smaller than ±0.5 °C for most topographic situations. Validation in steep topography (Gruber et al., 2004b [*Publication 3*]) indicates the total model error to be in the range of ±1.3 °C for the mean annual ground surface temperature. For this validation campaign, albedo was estimated and assumed to be equal for all validation sites. Therefore, the error of ±1.3 °C contains the error due to inaccurate albedo estimation.

Model errors from other sources are likely more important than the effect of inaccurate albedo at the present state. However, the sensitivity of modeled ground surface temperatures to albedo indicates the usefulness of albedo measurements to constrain model errors. Given the high cost, effort and error involved in the remote sensing of albedo, ground measurements that are applied to surface classes in a GIS appear to be a cost-effective alternative to obtain spatial data field on summer albedo.

7.4 Emissivity

In analogy to albedo, also emissivity is mostly treated as a scalar value in micro-meteorology (e.g. Oke, 1987; Pal Arya, 2001) and most energy-balance models (including TEBAL) use scalar input. However, the emissivity of natural surfaces is spectrally and angularly variable.

The sensitivity of surface temperatures to emissivity has been evaluated in a sensitivity study using TEBAL (Figure 7). As most surfaces are expected to have a broadband emissivity of 0.93-0.99 the sensitivity is about ±0.5°C or considerably less due to snow cover that was not included in the study. This is approximately the same sensitivity as that of albedo (but with inverse slope).

Several aspects make the accurate derivation, use and evaluation of broadband emissivity difficult:

- **Underdetermined system**
  An underdetermined set of equations having n+1 unknowns must be solved if n spectral channels with thermal infrared measurements are available for derivation of emissivity AND temperature. Therefore, certain assumptions (increasing the uncertainty of the result) have to be made in order to further constrain the system.
- **Remote sensing focus on temperature derivation and geology**
  Most publications dealing with temperature-emissivity separation from thermal infrared (TIR) data have the purpose of deriving narrow-band emissivity, only. Few publications address the issue of broad-band emissivity derivation (e.g. Ogawa et al., 2002).
- **Poor spectral coverage of Planck-curve**
  The spectral bands of sensors covering the 8-14 μm atmospheric window are near the peak of the black-body radiation curve but, only 1/4 to 1/3 of the total energy is eradiated in that waveband. As a consequence, inferring broad-band emissivity from a remote measurement in the 8-12 μm window is inherently unsound. For a limited number of processed laboratory spectra (5-30 μm) a root mean square (RMS) difference of 0.02 and a bias of 0.012 due to the smaller spectral coverage of remote sensors was found (Ogawa et al., 2002).
- **Emissivity = absorptivity**
  In the energy balance model the emissivity is used as a factor for the emitted and the absorbed long-wave radiation. However, while the spectral distribution of potentially emitted energy is defined by the Planck curve, the spectral characteristics of the downwelling atmospheric radiation is spectrally highly variable, especially between overcast and clear-sky conditions. As a consequence, even a very precise value for broadband emissivity at a certain temperature will introduce an error due to its simultaneous use as absorptivity.
- **Bi-directional effects**
  Many measurements of emissivity assume perfectly diffuse background radiation and perfectly diffuse reflective/emittive behaviour of the surface. However, effects of BRDF can cause errors as large as 0.1-0.2 absolute, and even near the surface normal direction errors about 0.02 (Kribus et al., 2003).

While the sensitivity of emissivity is similar to that of albedo in the energy-balance model, the above list of constraints demonstrates that its accurate derivation and use is more difficult. It is assumed, that the errors in the derivation of broad-band emissivity from DAIS7915 data will be greater than those inherent in the derivation of albedo. An error that is markedly larger than 0.035 absolute does not compare well to the total estimated range of 0.06 (0.93-0.99) for emissivity. Most likely, systematic errors relating to solar illumination, viewing angle and angular effects will dominate the derived data product. Using surface classes derived on vis-

ible/near infrared remote sensing, terrain analysis, map interpretation or aerial photography as a base for assigning values of emissivity appears to be more promising.

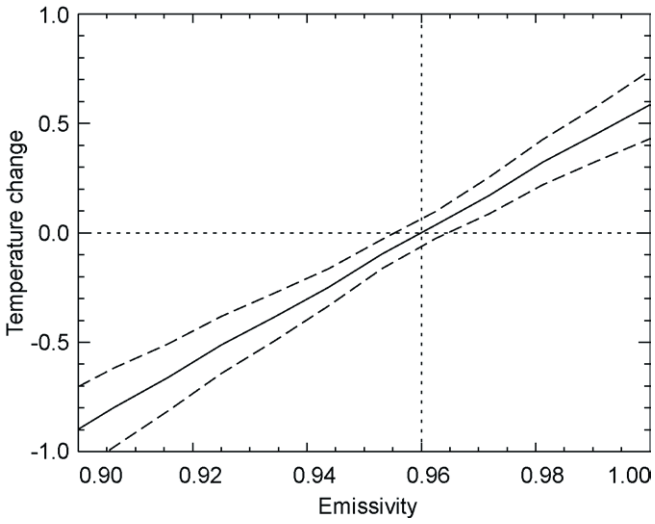

Figure 7 *Sensitivity of surface temperatures to changes in broadband emissivity based on TEBAL experiments.*

7.5 Conclusion

The delineation procedure for coarse blocky surfaces can directly be used for statistical as well as physically-based permafrost models. Because of the strong cooling effect of block surfaces this represents a major improvement of a models ability to delineate permafrost. The application of LIDAR for surface characterization is very promising, especially in the distinction of coarse block surfaces and moraines. The DAIS7915 campaign demonstrated the use of hyperspectral imagery for the derivation of albedo and, later possibly other parameters in complex mountains. As quantitative spatial research continues in mountain areas, this will likely be a key technology for the characterization of the very heterogeneous alpine surfaces.

8 Synopsis

8.1 Main progress

A brief synopsis of the work is given in the light of the three challenges that were identified in the introduction: 1) To go beyond the traditional realm of the rock glacier; 2) To investigate and to model quantitatively, and 3) To provide quantitative spatial input data.

Several steps into these directions were taken and yielded promising results:

- A conceptual hierarchy of model scales has been defined that helps to understand the different dimensions of variation of ground temperatures as well as the ranges of variability in those dimensions.
- A method for validating models in the spatial domain, along with a corresponding strategy for the measurement of near-surface rock temperatures has been designed and successfully applied.
- An energy-balance model has been adapted and validated in order to simulate transient rock temperatures at the surface and sub-surface in complex topography.
- A systematic measurement campaign of rock temperatures was performed. In combination with a 22-year forward-model run an investigation of rock temperature distribution and evolution was performed that overcame many of the limits inherent in research based on measurements only.
- The validated energy-balance model TEBAL has been used to perform sensitivity studies and numerical experiments.
- Surface temperatures derived from modelling and measurements were used to drive a model of 3-dimensional heat flow in rock.
- Aerial photographs and LIDAR were used to design methods for the reproducible and semi-automatic delineation of coarse block fields.
- A BRDF-model was derived from hyperspectral imagery; this allowed the investigation of angular anisotropy of albedo and the derivation of quantitative spatial data fields of albedo.
- A first example of using energy-balance model runs as the basis for a model of reduced complexity has been demonstrated.

8.2 Main findings

Several important findings resulted from the application of these methods and the approach to quantitatively investigate bedrock surfaces. The most important of these findings are:

- The inter-annual and diurnal variability of temperatures in the South is greater than in the North because two signal contribute (air temperature, solar radiation).
- The difference between Northern and Central Alps is greatest in southern aspects and at high elevation due the importance of short-wave radiation.
- The North-South differentiation of rock temperatures is almost 1000 m vertical.

- T(z) profiles from permafrost boreholes in complex topography are strongly influenced by variable surface conditions as well as topography.
- The depth of thaw in Alpine permafrost during the extreme summer of 2003 likely exceeded previous maxima by decades or even centuries – possibly millennia.
- Thaw of permafrost is the most plausible cause to explain the strong rockfall activity during the summer 2003
- Rockfall due to active layer thickening is a direct reaction to extremely hot summers and has an approximate depth range in the order of 1-10 m.
- The lower limit of permafrost in rock walls is likely a few hundred meters higher than that in debris-covered slopes.
- Spatial distribution patterns of rock-surface temperatures as well as their inter-annual variations are described.
- Mean temperatures as well as gradients and T(z) profile curvature can vary strongly depending on the borehole location (within tens of meters horizontal) even in steady state.
- Temperature histories from T(z) profiles in mountains can only be inverted successfully using special techniques for 3-dimensional conditions.
- The noise introduced to the profile by topography and variable surface conditions is likely in the same magnitude or greater than atmospheric warming during the 20th century. Derived temperature histories need to be interpreted with care.
- Angular anisotropy of the albedo of a surface results in actual differences for the surface energy balance. A different albedo for north- and south-facing slopes can result from identical surfaces.
- Approximation of angularly-dependent albedo with the constant white-sky albedo results in an error below ±5% for most coarse blocky surfaces in the test area.
- The correction of BRDF-effects is needed for the derivation of albedo from imagery in complex topography but the inclusion of an angular parameterization scheme for albedo into the energy-balance model is of minor importance for alpine block surfaces.

9 Future research and open questions

A number of perspectives and challenges for future research as well as open questions arise from this dissertation. Many parts of the research presented could be taken further or performed in a better way with the knowledge gained during its course. It would for instance be interesting to measure and use the rock albedo at the places where the data loggers for model validation (Chapter 4) have been installed. Naturally, many of these ideas for the continuation or improvement of current research exist at the end of a dissertation. Additionally and more important, however, several new research questions have evolved as a basis for possible future investigations:

- **Mechanisms of thermal offset in bedrock**
  Variable proportions of water, ice and air in bedrock can lead to different thermal conductivities in frozen and thawed state and, as a consequence induce a thermal offset. Equally, fractures in the active layer could have a much higher thermal conductivity during winter when ice filled than during drained summer conditions. Both effects could favor permafrost in much lower elevations than calculated from surface temperatures and standard heat conduction approaches. This effect could be investigated in a modelling study and, later on be measured in a borehole with several temperature sensors.

- **Snow in rock walls**
  Steep rock can successfully be modeled now. However, most rock faces have a slope angle between about 37° and 70°. How much snow remains in which part steep rock walls and what is the thermal influence that is has? Model experiments and temperature data loggers could highlight the sensitivity as well as the magnitude of the thermal effect. Quantitative techniques for the determination of snow cover in rock walls would have to be employed to gain a more quantitative insight. One perspective would be the recently developed ground-based LIDAR-systems for automatic monitoring of avalanche slopes.

- **Surface characteristics in non-vertical rock walls**
  For the same reason as above, coarse debris as well as highly-fractured zones of bedrock are often present in non-vertical rock walls. A campaign using oblique aerial photography, ground-based or airborne LIDAR could be conducted in order to gain an insight into the surface characteristics of large rock walls (e.g. Eiger). The importance of debris cover could then, in a first step be investigated in a model study.

- **Time and depth scales of permafrost degradation**
  The degradation of permafrost is a thermal process at depth. How long does it take before a 20 m thick body of permafrost disappears? How long for thaw at the base, how long at the permafrost table? What is the influence of massive ice in large crevices? Hypothetical model cases of mountain topography such as ridges, spurs, the lower limit of a permafrost body etc. should be investigated numerically. At these places, faster than usual degradation may result from lateral heat fluxes. But also the degradation in large rock walls will have different time scales than that on horizontal terrain due to the altered heat flow inside mountain topography.

- **A proxy variable of the thaw-related increase in rockfall hazard**
  Many rockfall events are hypothesized to be linked to the degradation of permafrost. However, when these are mapped, what thermal variable are they compared with (on a 2-dimensional map) in order to make a statement? What variable could be used to express additional, thaw-related hazard? It should by a variable that contains a statement in the form of "volume of thawed bedrock multiplied by the overburden thickness". The volume of thawed material is proportional to the chance of thawing a critical discontinuity. The amount of overburden is proportional to the size of the event caused at that point. Thawing of an ice-filled crevice will alter the total volume thawed due to laten heat. Should the variable then be additional to the heat flux? At which depth? It is evident that a lot of work and experimentation is needed to make this concept solid. But, it is also evident that there is a need for such a concept.
- **Quantification of the melt-related increase in rockfall hazard**
  Having a proxy-variable of thaw-related increase in rock fall hazard, it is be desirable to relate it to an actual probability of rockfall. This connection is important (because it is necessary for the estimation of e.g. financial consequences), and, at the same time hard to make. An inventory of the events of 2003, approximate knowledge of normal frequencies for rockfall of this magnitude and, a map of the approximate thaw (expressed in terms of the above proxy variable) in 2003 could be used for a probabilistic assessment in one area. The results will only be an order of magnitude, but, a better signal that the summer of 2003 is not available. This would also provide a basis for projections based on future scenarios for which the thaw-proxy could be calculated.
- **Consequences of disappearing ice faces and hanging glaciers**
  A transient model that includes ice faces and hanging glaciers could be used to investigate the thermal consequences of their warming or disappearance. A strong change in surface and sub-surface temperatures is expected.
- **Sensitivity and accuracy of a fully-coupled model**
  A fully coupled model for the surface energy-balance, heat conduction in the snow and heat conduction in the ground should be evaluated. Error propagation can be achieved using Monte-Carlo techniques and then compared to validation performed using field measurements. Priorities for future development should be investigated in this way and, by conducting specific sensitivity studies. A forward model can also be tested in locations where deep (tens to hundred of meters) boreholes exist.

10 Conclusion

Permafrost in mountains is relevant for natural hazards as well as the construction and maintenance of infrastructure. Especially its degradation resulting from present and projected atmospheric warming raises interest in quantitative understanding and validated, quantitative models that help to understand its transient response. In this dissertation, several steps were successfully taken toward more quantitative modelling and knowledge of mountain permafrost and resulted in a number of new findings. For the near future, the likely most urgent research questions relate to temperatures and temperature changes in steep mountain sides as their thermal response and potential energy available for natural hazards is highest. Here, the need for quantitative research and the investigation of bedrock and ice-covered surfaces that have previously received very little research constitute exciting future challenges.

11 References

Alean, J. 1985. Ice avalanche activity and mass balance of high-altitude hanging glaciers in the Swiss Alps. *Annals of Glaciology*, 6: 248-249.

Anisimov, O.A., Shiklamonov, N.I. and Nelson, F.E. 1997. Global warming and active-layer thickness: results from transient general circulation models. *Global and Planetary Change*, 15: 61-77.

Arenson, L.U., 2002. Unstable alpine permafrost: a potentially important natural hazard. Variations of Geotechnical behaviour with time and temperature. PhD Thesis, ETH Zürich, Zürich, 271 pp.

Bader, H.P. and Weilenmann, P. 1992. Modeling temperature distribution, energy and mass flow in a (phase changing) snowpack. I Model and case studies. *Cold Regions Science and Technology*, 20(2): 157-181.

Barry, R.G. 1990. Changes in mountain climate and glacio-hydrological responses. *Mountain Research and Development*, 10(2): 161-170.

Barry, R.G. 1992a. Mountain Climatology and Past and Potential Future Climatic Changes in Mountain Regions - a Review. *Mountain Research and Development*, 12(1): 71-86.

Barry, R.G., 1992b. Mountain Weather and Climate. Chapman and Hall, New York.

Barsch, D. 1969. Studien und Messungen an Blockgletschern in Macun, Unterengadin. *Zeitschrift für Gletscherkunde und Glazialgeologie*, 8: 11-30.

Barsch, D. 1971. Rockglacier and ice-cored moraines. *Geografiska Annaler*, 53(3-4): 203-206.

Barsch, D., 1996. Rockglaciers. Indicators for the present and former geoecology in high mountain environments. Springer, Berlin, 331 pp.

Bartelt, P.B. and Lehning, M. 2002. A physical SNOWPACK model for Avalanche Warning Services. Part I: Numerical Model. *Cold Reg. Sci. Technol.*(35): 123-145.

Beniston, M., Diaz, H.F. and Bradley, R.S. 1997. Climatic change at high elevation sites: an overview. *Climatic Change*, 36: 233-251.

Bernhard, L., Sutter, F., Haeberli, W. and Keller, F., 1998. Processes of snow/permafrost-interactions at a high-mountain site, Murtèl/Corvatsch, Eastern Swiss Alps. In: A.G. Lewkowicz and M. Allard (Editors), 7th International Conference on Permafrost. Proceedings. Collection Nordicana. Centre d'Etudes Nordiques, Université Laval, Yellowknife, Canada, pp. 35-41.

Böhm, R., Auer, I., Brunetti, M., Maugeri, M., Nanni, T. and Schöner, W. 2001. Regional temperature variability in the European Alps 1760–1998 from homogenised instrumental time series. *International Journal of Climatology*, 21: 1779– 1801.

Brown, R.J.E. and Péwé, T.L., 1973. Distribution of permafrost in North America and its relationship to the environment, a review 1963 - 1973. In: F.J. Sanger and P.J. Hyde (Editors), 2nd International Conference on Permafrost. Proceedings. National Academy of Sciences, Washington D.C., Yakutsk, USSR, pp. 71-100.

Brun, E., Martin, E., Simon, V., Gendre, C. and Coleou, C. 1989. An energy and mass model

of snow cover suitable for operational avalanche forecasting. *J. of Glaciol.*, 35(121): 333-342.

Brutsaert, W. 1975. On a derivable formula for long-wave radiation from clear skies. *Water Resources Research*, 11(5): 742-744.

Burn, C.R. and Smith, C.A.S. 1988. Observations of the 'thermal offset' in near-surface mean annual ground temperatures at several sites near Mayo, Yukon Territory Canada. *Arctic*, 41: 99-104.

Carslaw, H.S. and Jaeger, J.C., 1959. Conduction of heat in solids, Oxford Science Publications. Clarendon Press, Oxford, pp. 510.

Chang, S.-H., Westfield, M.J., Lehmann, F., Oertel, D. and Richter, R. 1993. 79-Channel Airborne Imaging Spectrometer. *Im. Spec. of the Terr. Env.*, SPIE Vol. 1937: 164-172.

Collares-Pereira, M. and Rabl, A. 1979. The average distribution of solar radiation correlations between diffuse and hemispherical and between daily and hourly insolation values. *Solar Energy*, 22: 155-164.

Corripio, J.G. 2003. Vectorial algebra algorithms for calculating terrain parameters from DEMs and the position of the sun for solar radiation modelling in mountainous terrain. *International Journal of Geographical Information Science*, 17(1): 1-23.

Corte, A.E. 1976. The hydrological significance of rock glaciers. *Journal of Glaciology*, 17: 157-158.

Davies, M.C.R., Hamza, O. and Harris, C. 2001. The effect of rise in mean annual temperature on the stability of rock slopes containing ice-filled discontinuities. *Permafrost and Periglacial Processes*, 12(1): 137-144.

Delisle, G. 1998. Numerical simulation of permafrost growth and decay. *Journal of Quaternary Science*, 13(4): 325-333.

Delisle, G., Caspers, G. and Frend, H., 2003. Permafrost in north-central Europe during the Weichselian: how deep? In: M. Phillips, S. Springman and L. Arenson (Editors), 8th International Conference on Permafrost, Proceedings. Swets & Zeitlinger, Lisse, Zürich, pp. 187-192.

Diaz, H.F. and Bradley, R.S. 1997. Temperature variations during the last century at high elevation sites. *Climatic Change*, 36(3): 253-279.

Dozier, J., Bruno, J. and Downey, P. 1981. A faster solution to the horizon problem. *Computer & Geosciences*, 7(2): 145-151.

Dramis, F., Govi, M., Guglielmin, M. and Mortara, G., 1995. Mountain permafrost and slope instability in the Italian Alps: the Val Pola landslide, Permafrost and Periglacial Processes. John Wiley & Sons, Ltd., pp. 73-82.

Elconin, R.F. and LaChapelle, E.R. 1997. Flow and internal structure of a rock glacier. *Journal of Glaciology*, 43(144): 238-244.

Etzelmüller, B., Berthling, I. and Sollid, J.L., 1998. The distribution of permafrost in southern Norway - a GIS approach. In: A.G. Lewkowicz and M. Allard (Editors), 7th International Conference on Permafrost. Proceedings. Collection Nordicana. Centre d'Etudes Nordiques, Université Laval, Yellowknife, Canada, pp. 251-257.

Etzelmüller, B., Heggem, E.S.F., Frauenfelder, R., Sharkhuu, N., Jambaljav, Y., Tumentsetseg, S., Romanovsky, V. and Kääb, A., 2002. Permafrost mapping and distribution modelling at the eastern shore of Lake Hövsgöl, northern Mongolia. Report from the field campaign in summer 2002.

Etzelmüller, B., Hoelzle, M., Heggem, E.S.F., Isaksen, K., Mittaz, C., Vonder Mühll, D., Ødegård, R.S., Haeberli, W. and Sollid, J.L. 2001. Mapping and modelling the occurrence and distribution of mountain permafrost. *Norwegian Journal of Geography*, 55(4): 186 -194.

Fierz, C., Plüss, C. and Martin, E. 1997. Modelling the snow cover in a complex Alpine topography. *Annals of Glaciology*, 25: 312-316.

Fierz, C., Riber, C., Adams, E.E., Curran, A.R., Föhn, P.M.B., Lehning, M., Plüss, C. 2003. Evaluation of snow-surface energy balance models in alpine terrain. *J. Hydrol.*: 76-94.

Frauenfelder, R., 2004. Regional-scale modelling of the occurrence and dynamics of rockglaciers and the distribution of paleopermafrost. PhD-Thesis Thesis, University of Zürich.

Frauenfelder, R., Allgöwer, B., Haeberli, W. and Hoelzle, M., 1998. Permafrost investigations with GIS - a case study in the Fletschhorn area, Wallis, Swiss Alps. In: A.G. Lewkowicz and M. Allard (Editors), 7th International Conference on Permafrost. Proceedings. Collection Nordicana. Centre d'Etudes Nordiques, Université Laval, Yellowknife, Canada, pp. 291-295.

French, H.M., 1996. The periglacial environment. Longman, Essex, 341 pp.

Gardaz, J.-M., 1998. Permafrost prospecting, periglacial and rock glacier hydrology in mountain areas. Case studies in the Valais Alps, Switzerland. PhD Thesis, University of Fribourg, Fribourg, 184 pp.

Goering, D.J., 2003. thermal response of air convection embankments to ambient temperature fluctuations. In: M. Phillips, S. Springman and L. Arenson (Editors), 8th International Conference on Permafrost, Proceedings. Swets & Zeitlinger, Lisse, Zürich, pp. 291-296.

Gold, L.W. and Lachenbruch, A.H., 1973. Thermal conditions in permafrost - a review of North American literature. In: F.J. Sanger and P.J. Hyde (Editors), 2nd International Conference on Permafrost. Proceedings. National Academy of Sciences, Washington D.C., Yakutsk, USSR, pp. 3-25.

Goodrich, L.E. 1978. Efficient Numerical Technique for One-Dimensional Thermal Problems with Phase-Change. *International Journal of Heat and Mass Transfer*, 21(5): 615-621.

Goodrich, L.E. 1982a. The influence of snow cover on the ground thermal regime. *Canadian Geotechnical Journal*, 19: 421-432.

Goodrich, L.E., 1982b. An introductory review of numerical methods for ground thermal regime calculations. 1061, Division of Building Research, National Research Council of Canada, Ottawa, Canada.

Goulden, C., Sharkhuu, N., Jambaljav, Y., Etzelmüller, B., Heggem, E.S.F., Romanovsky, V., Frauenfelder, R., Kääb, A., Ariuntsetseg, L., Saruul, N. and Tumentsetseg, S., 2003. New permafrost studies at Lake Hövsgöl, North-central Mongolia., 8th International Conference on Permafrost, Zurich, pp. 45–46.

Gruber, S., Dangel, S., Schläpfer, D. and Itten, K. 2004, to be submitted. Estimating BRDF

and albedo od coarse debris surfaces from hyperspectral imagery in rugged topography using single flight lines.

Gruber, S. and Hoelzle, M. 2001. Statistical modelling of mountain permafrost distribution: local calibration and incorporation of remotely sensed data. *Permafrost and Periglacial Processes*, 12(1): 69-77.

Gruber, S., Hoelzle, M. and Haeberli, W. 2004a. Permafrost thaw and destabilization of Alpine rock walls in the hot summer of 2003. *Geophys. Res. Lett.*, 31.

Gruber, S., Hoelzle, M. and Haeberli, W. 2004b. Rock wall temperatures in the Alps: Modelling their Topographic Distribution and Regional Differences. *Permafrost and Periglacial Processes*, 15(3): 299-307.

Gruber, S., King, L., Kohl, T., Herz, T., Haeberli, W. and Hoelzle, M. 2004c. Interpretation of geothermal profiles perturbed by topography: the Alpine permafrost boreholes at Stockhorn Plateau, Switzerland. *Permafrost and Periglacial Processes*, 15(4): 349-357.

Gruber, S., Peter, M., Hoelzle, M., Woodhatch, I. and Haeberli, W., 2003a. Surface temperatures in steep alpine rock faces – A strategy for regional-scale measurement and modelling. In: L. Arenson (Editor), 8th International Conference on Permafrost, Proceedings. Swets & Zeitlinger, Lisse, Zürich, pp. 325-330.

Gruber, S., Schläpfer, D. and Hoelzle, M., 2003b. Imaging spectrometry in high-alpine topography: the derivation of accurate broadband albedo. In: M. Habermeyer (Editor), 3rd Intl. Workshop on Imaging Spectroscopy. EARSeL, Herrsching, Germany, pp. 196-205.

Gruber, S., Schläpfer, D. and Hoelzle, M., 2003c. Snow-free albedo derived from DAIS 7915 hyperspectral imagery for energy balance modeling in high-alpine topography. In: D. Brandova (Editor), 8th International Conference on Permafrost, Extended Abstracts. University of Zurich, Zürich, pp. 47-48.

Guymon, G.L. and Hromadka, T.V., 1977. Finite element model of transient heat conduction with isothermal phase change (two and three dimensional). 77-38, Corps of Engineers, U.S. Army., Hanover, NH, USA.

Guymon, G.L., Hromadka, T.V. and Berg, R.L. 1984. Two-Dimensional Model of Coupled Heat and Moisture Transport in Frost-Heaving Soils. *Journal of Energy Resources Technology-Transactions of the Asme*, 106(3): 336-343.

Haeberli, W., 1973. Die Basis-Temperatur der winterlichen Schneedecke als möglicher Indikator für die Verbreitung von Permafrost in den Alpen, Zeitschrift für Gletscherkunde und Glazialgeologie. Universitätsverlag Wagner - Innsbruck, pp. 221-227.

Haeberli, W., 1975. Untersuchungen zur Verbreitung von Permafrost zwischen Flüelapass und Piz Grialetsch (Graubünden). Mitteilungen der Versuchsanstalt für Wasserbau, Hydrologie und Glaziologie der ETH Zürich, 17. ETH Zürich, Zürich, 221 pp.

Haeberli, W., 1985. Creep of mountain permafrost. Internal structure and flow of alpine rock glaciers. Mitteilungen der VAW-ETH Zürich, 77, Zürich, 142 pp.

Haeberli, W. 1992a. Construction, Environmental Problems and Natural Hazards in Periglacial Mountain Belts. *Permafrost and Periglacial Processes*, 3(2): 111-124.

Haeberli, W., 1992b. Possible effects of climatic change on the evolution of Alpine permafrost.

In: M. Boer and E. Koster (Editors), Greenhouse-impact on cold-climate ecosystems and landscapes. Catena Supplement, pp. 23-35.

Haeberli, W. and Beniston, M., 1998. Climate change and its impacts on glaciers and permafrost in the Alps. In: A. Rapp and E. Kessler (Editors), AMBIO - A Journal of the Human Environment. The Royal Swedish Academy of Sciences, pp. 258-265.

Haeberli, W. and Burn, C.R., 2002. Natural hazards in forests: glacier and permafrost effects as related to climate change. In: R.C. Sidle (Editor), Environmental Change and Geomorphic Hazards in Forests. IUFRO Research Series. CABI Publishing, Wallingford/New York, pp. 167-202.

Haeberli, W., Huggel, C., Kääb, A., Polkvoj, A., Zotikov, I. and Osokin, N., 2003. Permafrost conditions in the starting zone of the Kolka-Karmadon rock/ice slide of 20 September 2002 in North Osetia (Russian Caucasus). In: W. Haeberli and D. Brandova (Editors), 8th International Conference on Permafrost, Extended Abstracts. University of Zurich, Zürich, pp. 49-50.

Haeberli, W., Kääb, A., Hoelzle, M., Bösch, H., Funk, M., Vonder Mühll, D. and Keller, F., 1999. Eisschwund und Naturkatastrophen im Hochgebirge. Schlussbericht NFP31. vdf Hochschulverlag an der ETH Zürich, Zürich, 190 pp.

Haeberli, W., Wegmann, M. and Vonder Mühll, D. 1997. Slope stability problems related to glacier shrinkage and permafrost degradation in the Alps. *Eclogae geol. Helv.*, 90: 407-414.

Hanson, S. and Hoelzle, M., 2003. The thermal regime of the coarse blocky active layer at the Murtèl rock glacier in the Swiss Alps. In: W. Haeberli and D. Brandova (Editors), 8th International Conference on Permafrost, Extended Abstracts. University of Zurich, Zürich, pp. 51-52.

Hanson, S. and Hoelzle, M. 2004. The thermal regime of the active layer at the murtèl rock glacier based on data from 2002. *Permafrost and Periglacial Processes*, 15(3): 273-282.

Harris, C. and Haeberli, W., 2003. Warming permafrost in the mountains of Europe, World Meteorological Organization Bulletin, pp. 1-6.

Harris, C., Haeberli, W., Vonder Mühll, D. and King, L. 2001a. Permafrost monitoring in the high mountains of Europe: the PACE project in its global context. *Permfrost and Periglacial Processes*, 12(1): 3-11.

Harris, C., Rea, B. and Davies, M. 2001b. Scaled physical modelling of mass movement processes on thawing slopes. *Permafrost and Periglacial Processes*, 12(1): 125-135.

Harris, C., Vonder Mühll, D., Isaksen, K., Haeberli, W., Sollid, J.L., King, L., Holmlund, P., Dramis, F., Guglielmin, M. and Palacios, D. 2003. Warming permafrost in European mountains. *Global and Planetary Change*, 39: 215-225.

Harris, S.A., 1996. Lower mean annual ground temperature beneath a block stream in the Kunlun Pass, Qinghai Province, China., 5th Chinese Permafrost Conference, Lanzhou, China, pp. 227-237.

Harris, S.A. and Pedersen, D.E. 1998. Thermal regimes beneath coarse blocky material. *Permafrost and Periglacial Processes*, 9: 107-120.

Hauck, C., 2001. Geophysical methods for detecting permafrost in high mountains. PhD Thesis, ETH-Zürich, Zürich, 204 pp.

Heiner, S., 2003. Surface roughness discrimination in alpine areas using advanced remote sensing technologies., University of Zurich, Zurich, 93 pp.

Herz, T., King, L. and Gubler, H., 2003a. Microclimate within coarse debris of talus slopes in the alpine periglacial belt and its effect on permafrost. In: M. Phillips, S. Springman and L. Arenson (Editors), 8th International Conference on Permafrost, Proceedings. Swets & Zeitlinger, Lisse, Zürich, pp. 383-387.

Herz, T., King, L. and Gubler, H., 2003b. Thermal regime of coarse debris layers in the Ritigraben catchment, Matter valley, Swiss Alps. In: W. Haeberli and D. Brandova (Editors), 8th International Conference on Permafrost, Extended Abstracts. University of Zurich, Zürich.

Hinzman, L.D., Goering, D.J. and Kane, D.L. 1998. A distributed thermal model for calculating soil temperature profiles and depth of thaw in permafrost regions. *Journal of Geophysical Research-Atmospheres*, 103(D22): 28975-28991.

Hoelzle, M. and Haeberli, W. 1995. Simulating the effects of mean annual air temperature changes on permafrost distribution and glacier size. An example from the Upper Engadin, Swiss Alps. *Annals of Glaciology*, 21: 400-405.

Hoelzle, M., Haeberli, W. and Stocker-Mittaz, C., 2003. Miniature ground temperature data logger measurements 2000-2002 in the Murtèl-Corvatsch area. In: M. Phillips, S. Springman and L. Arenson (Editors), 8th International Conference on Permafrost, Proceedings. Swets & Zeitlinger, Lisse, Zürich, pp. 419-424.

Hoelzle, M., Mittaz, C., Etzelmüller, B. and Haeberli, W. 2001. Surface energy fluxes and distribution models of permafrost in European mountain areas: an overview of current developments. *Permafrost and Periglacial Processes*, 12(1): 53-68.

Hoelzle, M., Wegmann, M. and Krummenacher, B. 1999. Miniature temperature dataloggers for mapping and monitoring of permafrost in high mountain areas: First experience from the Swiss Alps. *Permafrost and Periglacial Processes*, 10(2): 113-124.

Houghton, J.T., Ding, Y., Briggs, D.G., Noguer, M., van der Linden, P.J., Dai, X., Mastell, K. and Johnson, C.A.e., 2001. Climate Change 2001: The Scientific Basis. Third Assessment. Cambridge Univ. Press: Cambridge., Intergovernmental Panel on Climate Change (IPCC).

Huggel, C., 2004. Assessment of glacial hazards based on remote sensing and GIS modelling. PHD-thesis Thesis, University of Zürich, Zurich, Switzerland.

Huggel, C., Kääb, A. and Salzmann, N. 2004. GIS-based modeling of glacial hazards and their interactions using Landsat-TM and IKONOS imagery. *Norwegian Journal of Geography*(58): 61-73.

Imhof, M. 1996. Modelling and verification of the permafrost distribution in the Bernese Alps (Western Switzerland). *Permafrost and Periglacial Processes*, 7: 267-280.

Inaba, H. 1983. Heat-Transfer Behavior of Frozen Soils. *Journal of Heat Transfer-Transactions of the Asme*, 105(3): 680-683.

Iqbal, M., 1983. An introduction to solar radiation. Academic Press, Toronto, 390 pp.

Isaksen, K., Holmlund, P., Sollid, J.L. and Harris, C. 2001. Three deep alpine-permafrost boreholes in Svalbard and Scandinavia. *Permafrost and Periglacial Processes*, 12(1): 13-25.

Isaksen, K., Ødegård, R.S., Eiken, T. and Sollid, J.L. 2000a. Composition, flow and development of two tongue-shaped rock glaciers in the permafrost of Svalbard. *Permafrost and Periglacial Processes*, 11: 241-257.

Isaksen, K., Vonder Mühll, D., Gubler, H., Kohl, T. and Sollid, J.L. 2000b. Ground surface temperature reconstruction based on data from a deep borehole in permafrost at Janssonhaugen, Svalbard. *Annals of Glaciology*, 31: 287-294.

Ishikawa, M. 2003. Thermal response at the snow-ground interface and their implications for permafrost investigation. *Geomorphology*, 52: 105-120.

Jensen, J., 1999. An analysis of permafrost distribution on Plateau Mountain, Alberta using the Geographic Information System ARC/INFO, University of Calgary, Calgary, 32 pp.

Jordan, R., 1991. A one-dimensional temperature model for a snow cover: Technical documentation for SNTHERM.89. Special report 91-16, US Army Cold Regions Research and Engineering Laboratory, Hanover, NH, USA.

Keller, F. 1992. Automated mapping of mountain permafrost using the program PERMAKART within the Geographical Information System ARC/INFO. *Permafrost and Periglacial Processes*, 3(2): 133-138.

Keller, F., 1994. Interaktionen zwischen Schnee und Permafrost - Eine Grundlagenstudie im Oberengadin. Dissertation Thesis, ETH Zürich, Zürich, 145 pp.

Keller, F. and Gubler, H.U., 1993. Interaction between snow cover and high mountain permafrost, Murtèl-Corvatsch, Swiss Alps. In: C. Guodong (Editor), 6th International Conference on Permafrost. Proceedings. South China University of Technology Press, Beijng, China, pp. 332-337.

Keller, F. and Hoelzle, M., 1998. PERMAKART und PERMAMAP. In: W. Haeberli and M. Hoelzle (Editors), Simulation der Permafrostverbreitung in den Alpen mit geographisachen Informationssystemen. vdf-Hochschulverlag, Zürich, pp. 36-46.

King, L. and Kalisch, A., 1998. Permafrost distribution and implications for construction in the Zermatt area, Swiss Alps. In: A.G. Lewkowicz and M. Allard (Editors), 7th International Conference on Permafrost. Proceedings. Collection Nordicana. Centre d'Etudes Nordiques, Université Laval, Yellowknife, Canada, pp. 569-574.

Klok, E.J. and Oerlemans, J. 2003. Model study of the spatial distribution of the energy and mass balance of Morteratschgletscher, Switzerland. *Journal of Glaciology*, 48(163): 505-518.

Kneisel, C., 1998. Occurrence of surface ice and ground ice/permafrost in recently deglaciated glacier forefields, St. Moritz area, Eastern Swiss Alps. In: A.G. Lewkowicz and M. Allard (Editors), 7th International Conference on Permafrost. Proceedings. Collection Nordicana. Centre d'Etudes Nordiques, Université Laval, Yellowknife, Canada, pp. 575-581.

Knutti, R., Stocker, T.F., Joos, F. and Plattner, G.K. 2002. Constraints on radiative forcing and future climate change from observations and climate model ensembles. *Nature*, 416:

719-723.

Kohl, T. 1999. Transient thermal effects at complex topographies. *Tectonophysics*, 306: 311-324.

Kohl, T. and Gruber, S., 2003. Evidence of paleaotemperature signals in mountain permafrost areas. In: W. Haeberli and D. Brandova (Editors), 8th International Conference on Permafrost, Extended Abstracts. University of Zurich, Zürich, pp. 83-84.

Kohl, T. and Hopkirk, R. 1995. "FRACTure" a simulation code for forced fluid flow and transport in fractured porous rock. *Geothermics*, 24(3): 345-359.

Kondo, J. and Yamazawa, H. 1990. A prediction model for snowmelt, snow surface temperature and freezing depth using a heat balance method. *Jounal of Applied Meteorology*, 29: 375-384.

Konzelmann, T., Van de Wal, R.S.W., Greuell, W., Binanja, R., Henneken, E.A.C. and Abe-Ouchi, A. 1994. Parameterization of global and longwave incoming radiation for the Greenland Ice Sheet. *Global and Planetary Change*, 9: 143-164.

Kribus, A., Vishnevetsky, I., Rotenberg, E. and Yakir, D. 2003. Systematic errors in the measurement of emissivity caused by directional effects. *Applied Optics*, 42(10): 1839-1846.

Lachenbruch, A.H. and Marshall, B.V. 1986. Changing climate: geothermal evidence from permafrost in the Alaskan Arctic. *Science*, 234: 689-696.

Lehning, M., Bartelt, P.B., Brown, R.L., Fierz, C. and Satyawali, P. 2002a. A physical SNOWPACK model for the Swiss Avalanche Warning Services. Part III: Meteorological Boundary Conditions, Thin Layer Formation and Evaluation. *Cold Reg. Sci. Technol.*, 35: 169-184.

Lehning, M., Bartelt, P.B., Brown, R.L., Fierz C. and P., S. 2002b. A physical SNOWPACK model for the Swiss Avalanche Warning Services. Part II: Snow Microstructure. *Cold Reg. Sci. Technol.*, 35: 147-167.

Lewkowicz, A.G. and Ednie, M. 2004. Probility mapping of mountain permafrost using the BTS method, wolf Creek, Yukon Territory, Canada. *Permafrost and Periglacial Processes*, 15(1): 67-80.

Lieb, G.K., 1998. High-mountain permafrost in the Austrian Alps (Europe). In: A.G. Lewkowicz and M. Allard (Editors), 7th International Conference on Permafrost. Proceedings. Collection Nordicana. Centre d'Etudes Nordiques, Université Laval, Yellowknife, Canada, pp. 663-668.

Ling, F. and Zhang, T.J. 2004. A numerical model for surface energy balance and thermal regime of the active layer and permafrost containing unfrozen water. *Cold Regions Science and Technology*, 38(1): 1-15.

Ludwig, F., 2003. Variable Oberflächenbedingungen als Ursache der Temperaturverteilung im Untergrund alpiner Permafrostgebiete - Limitationen der Klimarekonstruktion aus Bohrlochtemperaturprofilen im Permafrost. Masters thesis Thesis, Justus-Liebig-University, Giessen, Germany, 62 pp.

Luetschg, M., Bartelt, P., Lehning, M., Stoeckli, V. and Haeberli, W., 2003. Numerical simulation of the interaction processes between snow cover and alpine permafrost. In: M. Phillips, S. Springman and L. Arenson (Editors), 8th International Conference on Permafrost,

Proceedings. Swets & Zeitlinger, Lisse, Zürich, pp. 697-702.

Lunardini, V.J., 1991. Heat Transfer with Freezing and Thawing. 65, CRREL, U.S. Army Corps of Engineers, Hanover, NH, USA.

Lunardini, V.J. 1996. Climatic warming and the degradation of warm permafrost. *Permafrost and Periglacial Processes*, 7: 311-320.

Lüthi, M. and Funk, M. 1997. Wie stabil ist der Hängegletscher am Eiger? *Spektrum der Wissenschaft*, 97(5).

Martonchik, J.V., Bruegge, C.J. and Strahler, A.H. 2000. A Review of Reflectance Nomenclature Used in Remote Sensing. *Remote Sensing Reviews*, 19: 9-20.

Mittaz, C., Hoelzle, M. and Haeberli, W. 2000. First results and interpretation of energy-flux measurements of Alpine permafrost. *Annals of Glaciology*, 31: 275-280.

Mittaz, C., Imhof, M., Hoelzle, M. and Haeberli, W. 2002. Snowmelt evolution mapping using an energy balance approach over an alpine terrain. *Arctic, Antarctic and Alpine Research*, 34(3): 264-281.

Mustafa, O., Gude, M. and Hoelzle, M., 2003. Modeling permafrost distribution in the northern Alps using global radiation. In: W. Haeberli and D. Brandova (Editors), 8th International Conference on Permafrost, Extended Abstracts. University of Zurich, Zürich, pp. 111-112.

Nicodemus, F.E., Richmond, J.C., Ginsberg, I.W. and Limperis, T., 1977. Geometrical Considerations and Nomenclature for Reflectance. National Bureau of Standards, US. Department of Commerce, pp. 52.

Noetzli, J., Hoelzle, M. and Haeberli, W., 2003. Mountain permafrost and recent Alpine rockfall events: a GIS-based approach to determine critical factors. In: M. Phillips, S. Springman and L. Arenson (Editors), 8th International Conference on Permafrost, Proceedings. Swets & Zeitlinger, Lisse, Zürich, pp. 827-832.

Oelke, C., Zhang, T., Serreze, M.C. and Armstrong, R.L. 2003. Regional-scale modeling of soil freeze/thaw over the Arctic drainage basin. *J. Geophys. Res. (D10)*, 108: 4314.

Oerlemans, J. 1992. A model for the surface balance of ice masses: part I. Alpine Glaciers. *Zeitschrift für Gletscherkunde und Glazialgeologie*, 27/28: 63-83.

Ogawa, K., Schmugge, T., Jacob, F. and French, A. 2002. Estimation of broadband land surface emissivity from multi-spectral thermal infrared remote sensing. *Agronomie*, 22: 19-20.

Oke, T.R., 1987. Boundary layer climates. Cambridge University Press, 435 pp.

Outcalt, S.I. and Hinkel, K.M. 1996. The response of near-surface permafrost to seasonal regime transitions in tundra terrain. *Arctic and Alpine Research*, 28(3): 274-283.

Pal Arya, S., 2001. Micrometeorology. International Geophysics Series, 79. Academic Press, New York, 417 pp.

Plüss, C., 1997. The Energy Balance Over an Alpine Snowcover, Point Measurements and Areal Distribution. Zürcher Geographische Schriften, 65. Department of Geography, University of Zürich, Zürich, 115 pp.

Plüss, C. and Ohmura, A. 1997. Longwave radiation on snow-covered mountainous surfaces.

Journal of Applied Meteorology, 36(6): 818-824.

Purves, R.S., Barton, J.S., Mackaness, W.A. and Sugden, D.E. 1998. The development of a rule-based spatial model of windtransport and deposition of snow. *Annals of Glaciology*, 26: 197-202.

Rebetez, M., Lugon, R. and Baeriswyl, P.A. 1997. Climatic change and debris flows in high mountain regions: the case study of the Ritigraben Torrent (Swiss Alps). *Climatic Change*, 36: 371-389.

Richter, R. and Schläpfer, D. 2002. Geo-atmospheric processing of airborne imaging spectrometry data. Part 2: Atmospheric/Topographic Correction. *International Journal of Remote Sensing*, 23(13): 2631-2649.

Romanovsky, V.E. and Osterkamp, T.E. 1995. Interannual variations of the thermal regime of the active layer and near surface permafrost in northern Alaska. *Permafrost and Periglacial Processes*, 6: 313-335.

Romanovsky, V.E., Osterkamp, T.E. and Duxbury, N.S. 1997. An evaluation of three numerical models used in simulations of the active layer and permafrost temperature regimes. *Cold Regions Science and Technology*, 26(3): 195-203.

RSI, 2004a. ENVI User's Guide v4.0. http://www.rsinc.com/training/docsets.asp (accessed 1. October 2004).

RSI, 2004b. Using IDL v6.0. http://www.rsinc.com/training/docsets.asp (accessed 1. October 2004).

Ryan, B.C. 1977. A mathematical model for diagnosis and prediction of surface winds in mountainous terrain. *Journal of Applied Meteorology*, 16: 571-584.

Rykiel, E.J. 1995. Testing ecological models: the meaning of validation. *Ecological modelling*, 90: 229-224.

Sawada, Y., Ishikawa, M. and Ono, Y. 2003. Thermal regime of sporadic permafrost in a block slope on Mt. Nishi-Nupukaushinupuri, Hokkaido Island, Northern Japan. *Geomorphology*, 52(1-2): 121-130.

Schopper, J.R., 1982. Porosity and permeability., Landolt-Boernstein. Numerical Data and Functional Relationships in Science and Technology. Group V: Geophysics and Space Research. Springer-Verlag, Inc., pp. 184-303.

Schrott, L., 1994. Die Solarstrahlung als steuernder Faktor im Geosystem der sub-tropischen semiariden Hochanden (Agua Negra, San Juan, Argentinien). PhD Thesis, Geographisches Institut Universität Heidelberg, Heidelberger Geographische Schriften, 199 pp.

Scott, W.J., Sellmann, P.V. and Hunter, J.A., 1979. Geophysics in the study of permafrost. In: R.J.E. Brown (Editor), Third International Conference on Permafrost, Edmonton, Alberta, Canada, pp. 93-115.

Seregina, N.V., 1989. Some of the mathematical models used in Geocryology and methods of their numerical solution (in Russian). Moscow State University, Moscow.

Smith, M.W. and Riseborogh, D.W. 2002. Climate and the limits of permafrost: a zonal analysis. *Permafrost and Periglacial Processes*, 13(1): 1-15.

Smith, M.W. and Riseborough, D.W. 1996. Ground temperature monitoring and detection of climate change. *Permafrost and Periglacial Processes*, 7: 301-310.

Smith, M.W. and Riseborough, D.W. 2002. Climate and the limits of permafrost: A zonal analysis. *Permafrost and Periglacial Processes*, 13(1): 1-15.

Stocker-Mittaz, C., 2002. Permafrost distribution modeling based on energy balance data. PhD Thesis, University of Zurich, Zurich, 122 pp.

Stocker-Mittaz, C., Hoelzle, M. and Haeberli, W. 2002. Permafrost distribution modeling based on energy-balance data: a first step. *Permafrost and Periglacial Processes*, 13(4): 271-282.

Stott, P.A. and Kettleborough, J.A. 2002. Origins and estimates of uncertainty in predictions of twenty-first century temperature rise. *Nature*, 416: 723-726.

van Everdingen, R.O., 1998. Multi-language glossary of permafrost and related ground ice terms. International Permafrost Association.

Vonder Mühll, D. and Klingelé, E. 1994. Gravimetrical investigation of ice rich permafrost within the rock glacier Murtèl-Corvatsch. 5(1): 13-24.

Wang, K.L. 1992. Estimation of Ground Surface Temperatures from Borehole Temperature Data. *Journal of Geophysical Research-Solid Earth*, 97(B2): 2095-2106.

Wegmann, M., Gudmundsson, G.H. and Haeberli, W. 1998. Permafrost changes and the retreat of Alpine glaciers: a thermal modelling approach. *Permafrost and Periglacial Processes*, 9: 23-33.

Wenbing Yu, Y.L., Xuefu Zhang, Shujuan Zhang and Jiangzhang Xiao 2004. Laboratory investigation on cooling effect of coarse rock layer and fine rock layer in permafrost regions. *Cold Regions Science and Technology§*, 38(1): 31-42.

Williams, P.J. and Smith, M.W., 1989. The Frozen Earth. Studies in Polar Research. Cambridge University Press, Cambridge, 306 pp.

Zhang, T., Barry, R.G. and Haeberli, W. 2001. Numerical simulations of the influence of the seasonal snow cover on the occurrence of permafrost at high latitudes. *Norwegian Journal of Geography*, 55(4): 261-266.

Zhang, T., Osterkamp , T.E. and Stamnes, K. 1996. Influence of the depth hoar layer of the seasonal snow cover on the ground thermal regime. *Water Resources Research*, 32(7): 2075-2086.

Zhijiu, C., 1993. An investigation of rock glaciers in the Kunlun Shan, China. In: C. Guodong (Editor), 6th International Conference on Permafrost. Proceedings. South China University Technology Press, Beijing, China, pp. 208-211.

Zimmermann, M. and Haeberli, W. (Ed.), 1992. Climatic change and debris flow activity in high-mountain areas - a case study in the Swiss Alps. Catena Supplement, 22, 59-72 pp.

Zimmermann, M., Mani, P., Gamma, P., Gsteiger, P., Hunziger, P. and Heiniger, O., 1997. Murganggefahr und Klimaänderungen - ein GIS-basierter Ansatz. (in German). Final Report NFP31, 4031-33253. vdf, Hochschulverlag an der ETH, Züruch, Switzerland.

Zwiers, F.W. 2002. The 20-year forecast. *Nature*, 416: 690-691.

Part B: Publications

Publication 1:

Permafrost thaw and destabilization of Alpine rock walls in the hot summer of 2003

Citation:

Gruber, S., M. Hoelzle, and W. Haeberli. 2004. Permafrost thaw and destabilization of Alpine rock walls in the hot summer of 2003. Geophys. Res. Lett. 31, L13504.

Main findings:

- The depth of thaw in Alpine permafrost during the extreme summer of 2003 likely exceeded previous maxima by decades or even centuries – possibly millennia.
- Thaw of permafrost is the most plausible cause to explain the strong rockfall of the summer 2003
- Rockfall due to active layer thickening is a direct reaction to extremely hot summers.
- Increased rockfall is a likely and well-perceptible impact of future climate change. Especially so, given the projected greater frequency of extremely hot summers.
- The topographic control on the depth of seasonal freeze-thaw has been conceptionally shown using a model experiment.

GEOPHYSICAL RESEARCH LETTERS, VOL. 31, L13504, doi:10.1029/2004GL020051, 2004

Permafrost thaw and destabilization of Alpine rock walls in the hot summer of 2003

Stephan Gruber, Martin Hoelzle, and Wilfried Haeberli

Glaciology and Geomorphodynamics Group, Department of Geography, University of Zurich, Zurich, Switzerland

Received 22 March 2004; revised 3 June 2004; accepted 11 June 2004; published 13 July 2004.

[1] Exceptional rockfall occurred throughout the Alps during the unusually hot summer of 2003. It is likely related to the fast thermal reaction of the subsurface of steep rock slopes and a corresponding destabilization of ice-filled discontinuities. This suggests that rockfall may be a direct and unexpectedly fast impact of climate change. Based upon our measurements in Alpine rock faces, we present model simulations illustrating the distribution and degradation of permafrost where the summer of 2003 has resulted in extreme thaw. We argue that hotter summers predicted by climate models for the coming decades will result in reduced stability of many alpine rock walls. *INDEX TERMS:* 1823 Hydrology: Frozen ground; 1625 Global Change: Geomorphology and weathering (1824, 1886); 1630 Global Change: Impact phenomena. **Citation:** Gruber, S., M. Hoelzle, and W. Haeberli (2004), Permafrost thaw and destabilization of Alpine rock walls in the hot summer of 2003, *Geophys. Res. Lett.*, *31*, L13504, doi:10.1029/2004GL020051.

1. Introduction

[2] The summer of 2003 was ~3°C warmer in Switzerland than average 1961–1990 [*Schär et al.*, 2004] and exceptional rockfall activity has been reported [e.g., *Keller*, 2003] throughout the Alps, especially at high elevations and in north-facing slopes. In the absence of unusually strong precipitation or other plausible transient effects on slope stability the fast degradation of mountain permafrost has been hypothesized to be the likely cause for the extreme rockfall and, as a consequence, this topic received much public attention [e.g., *Schiermeier*, 2003].

[3] The temperature distribution and evolution in steep rock was largely unknown until now, even though, permafrost thaw in rock faces maybe equally consequential (in terms of natural hazards and geotechnical consequences for infrastructure) as that in debris-covered slopes. Additionally, the thermal response of rock faces to individual extreme events is fast compared to debris slopes that are often insulated by blocky surfaces [*Harris and Pedersen*, 1998] and have a high ice-content.

[4] During the last century, Alpine permafrost in Europe has warmed by 0.5 to 0.8°C in the upper tens of meters [*Harris et al.*, 2003]. The stability of steep rock slopes can be reduced due to melting of ice-filled crevices and subsequent build-up of hydrostatic pressure [*Haeberli et al.*, 1997]. Even prior to thaw, frozen rock joints have been demonstrated to destabilize with rising temperatures, entering a zone of minimal stability between −1.5 and 0°C [*Davies et al.*, 2001]. The exceptional rockfall activity during the summer 2003 is likely an indication of this rapid destabilization that takes place as an almost immediate reaction to extreme warming. This paper seeks to elucidate the effect that the summer of 2003 had on perennially frozen Alpine rock faces and the role of rockfall as an impact of future climate change.

0094-8276/04/2004GL020051$05.00

2. Measurement and Modeling of Rock Temperatures

[5] In autumn 2002 we recovered 14 data loggers that had recorded one year of near-surface temperatures in steep Alpine rock faces (Figure 1) between the summers of 2001 and 2002 [*Gruber et al.*, 2003]. Measurement sites were chosen between 2600 and 4500 m a.s.l. trying to represent slope expositions evenly (Figure 2). Data were recorded at a depth of 10 cm every two hours. These data were used to verify an energy-balance model [*Gruber et al.*, 2004] simulating daily surface temperatures based on meteorological observations from the standard Swiss observational network operated by MeteoSwiss. The model is based on the algorithms used in PermEbal [*Stocker-Mittaz et al.*, 2002; *Mittaz et al.*, 2002] and simulates the one-dimensional energy balance at the rock surface as well as the subsurface heat conduction using daily time steps. After calculation of the short-wave net radiation and the long-wave irradiance, the turbulent heat flux and upwelling long-wave radiation are parameterized using an estimated surface temperature. The derived ground heat flux is used as upper boundary condition of a heat conduction scheme having 200 nodes, evenly spaced every 10 cm. The initial surface temperature estimate and the calculated temperature are iterated to converge to better than 0.3°C. Latent heat due to freezing/melting of pore water in the rock is included as apparent heat capacity between −0.5 and 0.0°C. The verification runs were based on daily meteorological data of the MeteoSwiss stations Zermatt, Corvatsch or Jungfraujoch. All calculations were based on the same parameters to prevent "fitting" of results: albedo: 0.28; emissivity: 0.96; roughness length: 0.3 mm; environmental lapse rate: -0.006°C m^{-1}; moisture content: 1%; volumetric heat capacity of dry rock: 1.8 10^6 J m^{-3} K^{-1}; thermal conductivity: 2.2 W K^{-1} m^{-1} [based on *Čermák and Rybach*, 1982]. Due to strong topographic [*Kohl*, 1999] and transient [*Harris et al.*, 2003] effects it is unknown whether the geothermal heat flux at the lower boundary is positive or negative and therefore assumed to be zero. With the parameters above, only elevation, slope and aspect were adapted to each measurement site and the appropriate meteorological station was chosen for the

Figure 1. Installation of a rock-face temperature data logger during summer 2001.

driving time series of the verification run. Daily averages of measured temperatures are compared to the model results at all 14 sites. The mean annual near-surface temperature has a mean absolute difference of 1.2°C (9 series were better than 1°C and 5 series between 1.0 and 3.8°C without a bias related to elevation or aspect). The mean R^2 is 0.88 (min: 0.72; max: 0.96). This indicates that the model and the parameterizations used are reliable to simulate the surface energy balance over rock faces in complex terrain. Using this model, rock temperatures for different aspects and elevations were calculated from 1982 to 2003. Daily rock temperatures for a slope of 70°, seven elevations from 2000–5000 m and eight aspects (N, NE, …. W, NW) were simulated based on meteorological data from Jungfraujoch from 01/1982 to 12/2003. Oct.–Dec. 2003 were not yet available at the time of calculation and substituted by 2002 data. Being after the extreme summer and after the time of maximum ground heat flux, this substitution does not influence our results. The temperature profile at depth was initiated using the 1982 mean surface temperature followed by a two-year transient run with 1982 data to ensure a realistic temperature distribution at depth before the start of the 1982–2003 experiment.

3. Results and Discussion

[6] From the simulated daily temperatures, the distribution of mean annual ground surface temperatures (MAGST) for rock faces was calculated (Figure 2) and a mean 0°C isotherm derived. This mean isotherm represents the elevation that limits the presence of permafrost under the climatic conditions used for the 21-year model run. In reality, the lower limit of permafrost within rock walls is assumed to be about 1.0°C or 150 m lower than this line due to 20th century atmospheric warming [*Haeberli and Beniston*, 1998; *IPCC*, 2001; *Böhm et al.*, 2001; *Beniston et al.*, 1997; *Diaz and Bradley*, 1997]. Additionally, three zones are delineated by the two thin dashed lines: a) the zone of seasonal frost (SF-zone, MAGST > 0°C for all years); b) the zone of active permafrost (AP-zone, MAGST

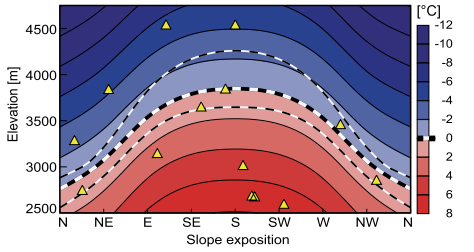

Figure 2. Mean annual surface temperatures and mean 0°C isotherm (thick dashed line) in Alpine rock faces from 1982 to 2002, modeled for the Jungfrau area and 70° slope inclination. The thin dashed lines show the highest and lowest mean annual 0°C isotherm during that period. Yellow triangles indicate the aspect and elevation of the 14 rock-wall temperature data loggers used for model verification.

< 0°C for all years); and c) a transitional zone (T-zone), where only some years have a MAGST < 0°C. The interannual variation of the mean 0°C isotherm elevation is 400–550 m vertical, underscoring the necessity for a combination of measurements and models in determining the distribution of permafrost in rock walls. From the calculated transient subsurface temperature field, the progression of summer thaw or winter freezing can be extracted (Figure 3). The modeled thaw of 2003 exceeds the maximum of all previous years. The associated depth range of this anomaly and of the possible destabilization depends on site characteristics and water content [*Wegmann et al.*, 1998] in the rock but its overall pattern is not affected fundamentally. It is striking that most rock fall took place between June and August when the depth of thaw was not at its maximum but when the heat flux in the ground at somewhat shallower depths was greatest. Figure 4a shows the mean maximum depth of the 0°C isotherm (1982–2002). In the AP-zone, this is the depth of summer thaw, in the SF-zone it is the depth of winter freezing and in the T-zone it can be either one or even a signal from the previous year. In our model, the summer thaw of 2003 is 10–50 cm deeper than the maximum of the 21 previous years throughout the AP-zone (Figure 4b).

[7] In northern slopes, the depth of thaw is mainly controlled by the influence of air temperature (mostly via long-wave radiation) on surface temperatures, whereas

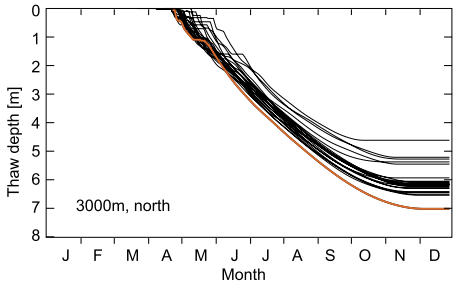

Figure 3. Summer thaw in Alpine permafrost. Depth evolution for individual years 1982–2002 (black) and 2003 (orange).

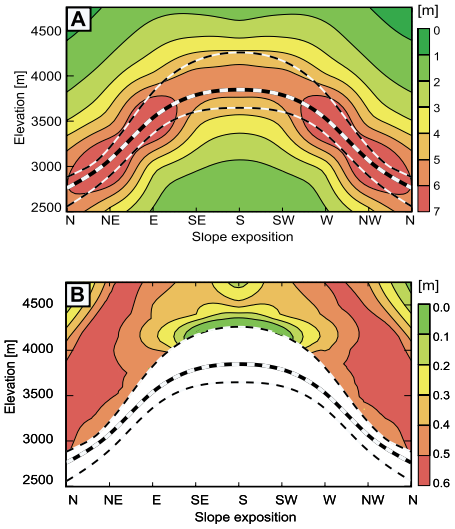

Figure 4. Depth range of freezing or thawing. (a) Average maximum annual depth of the 0°C isotherm in the ground. (b) 2003 permafrost degradation shown as the depth exceeding the 1982–2002 maximum modeled depth of thaw.

southern slopes additionally receive high amounts of shortwave radiation. As a consequence, southern slopes exhibit greater inter-annual variability of thaw depth, larger pre-2003 maxima and, therefore, a smaller 2003 anomaly. In the T-zone, the 2003 signal is less clear and may only be at its maximum in the following year due to the great depth of the active layer. The increased thaw during the summer of 2003 far outweighs the direct effect that gradually rising temperatures have on rock wall stability in the uppermost meters. The extreme frequency of rockfall in the Alps during 2003 [*Keller*, 2003; *Schiermeier*, 2003] corroborates this finding. The observed domination of events in northern slopes can be explained by the strong effect of 2003 (Figure 4b) as well as the greater extent of perennially frozen northern slopes. The 2003 thaw depth is likely to exceed previous maxima even on time scales of centuries, considering the pronounced recent global and hemispheric temperature rise inferred from instrumental records and proxy data [*IPCC*, 2001; *Mann et al.*, 1999] and its influence on Alpine ground temperatures [*Harris et al.*, 2003]. The thermal response of permafrost to atmospheric warming [*Lunardini*, 1996; *Haeberli et al.*, 1997; *Haeberli and Beniston*, 1998] generally takes place at different scales of time and depth which correspond to frequency and magnitude of the expected destabilization. Following increases in temperature, with a delay of only months or years (direct response), the active layer (uppermost meters that are subject to annual freeze/thaw cycles) thickens and thus, new volumes of rock will be subjected to critical temperature ranges. This immediate response has been observed in the summer of 2003. Then (delayed response), the temperature profile within the permafrost becomes disturbed and the lower boundary of the permafrost layer will rise (final response), both possibly causing large and deep-seated instabilities delayed by decades or centuries. Therefore, following the projected rise in mean annual and summer temperatures during the 21st century [*Zwiers*, 2002; *Stott and Kettleborough*, 2002; *Knutti et al.*, 2002; *Ohmura et al.*, 1996; *IPCC*, 2001], the locations, magnitudes and frequencies of rock wall instabilities are likely to develop beyond the ranges of historic variability.

4. Conclusion

[8] Past and modeled future climatic change is likely more pronounced in mountain areas than the global or hemispheric average [*Haeberli and Beniston*, 1998; *Beniston et al.*, 1997; *Diaz and Bradley*, 1997; *Barry*, 1992, 1990]. Thus, coming decades are expected see a well-perceptible transient response of Alpine permafrost to the projected 0.3–1.3°C rise (2020–2030) in global mean temperature [*Zwiers*, 2002; *Stott and Kettleborough*, 2002; *Knutti et al.*, 2002]. In addition to a warming trend of 5°C, a study based on regional climate models [*Schär et al.*, 2004] predicts a 74% increase in the standard deviation of summer temperatures in Switzerland (2070–2099). The extreme summer of 2003 and its impact on mountain permafrost may be seen as a first manifestation of these projections. Wide-spread rockfall and geotechnical problems with human infrastructure are likely to be recurrent consequences of warming permafrost in rock walls due to predicted climatic changes.

[9] **Acknowledgment.** Research was supported by the Swiss National Science Foundation project "Analysis and Spatial Modelling of Permafrost Distribution in Cold-Mountain Areas by Integration of Advanced Remote Sensing Technology".

References

Barry, R. G. (1990), Changes in mountain climate and glacio-hydrological responses, *Mt. Res. Dev.*, *10*(2), 161–170.

Barry, R. G. (1992), Mountain climatology and past and potential future and climatic changes in mountain regions: A review, *Mt. Res. Dev.*, *12*(1), 71–86.

Beniston, M., H. F. Diaz, and R. S. Bradley (1997), Climatic change at high elevation sites: An overview, *Clim. Change*, *36*(3), 233–251.

Böhm, R., I. Auer, M. Brunetti, et al. (2001), Regional temperature variability in the European Alps: 1760–1998 from homogenized instrumental time series, *Int. J. Climatol.*, *21*, 1779–1801.

Čermák, V., and L. Rybach (1982), Thermal conductivity and specific heat of minerals and rocks, in *Landolt-Börnstein Zahlenwerte and Funktionen aus Naturwissenschaften und Technik, Neue Serie, Physikalische Eigenschaften der Gesteine (V/1a)*, edited by G. Angeneister, pp. 305–343, Springer Verlag, New York.

Davies, M. C. R., O. Hamza, and C. Harris (2001), The effect of rise in mean annual temperature on the stability of rock slopes containing ice-filled discontinuities, *Permafrost Periglacial Processes*, *12*(1), 137–144.

Diaz, H. F., and R. S. Bradley (1997), Temperature variations during the last century at high elevation sites, *Clim. Change*, *36*(3), 253–279.

Gruber, S., M. Peter, M. Hoelzle et al. (2003), Surface temperatures in steep Alpine rock faces—A strategy for regional-scale measurement and modelling, *Proc. 8th Int. Conf. Permafrost*, *1*, 325–330.

Gruber, S., M. Hoelzle, and W. Haeberli (2004), Rock wall temperatures in the Alps, *Permafrost Periglacial Processes*, in press.

Haeberli, W., and M. Beniston (1998), Climate change and its impacts on glaciers and permafrost in the Alps, *Ambio*, *27*(4), 258–265.

Haeberli, W., M. Wegmann, and D. Vonder Mühll (1997), Slope stability problems related to glacier shrinkage and permafrost degradation in the Alps, *Eclogae Geol. Helv.*, *90*, 407–414.

Harris, C., D. Vonder Mühll, K. Isaksen et al. (2003), Warming permafrost in European mountains, *Global Planet. Change*, *39*(3–4), 215–225.

Harris, S. A., and D. E. Pedersen (1998), Thermal regimes beneath coarse blocky material, *Permafrost Periglacial Processes*, *9*, 107–120.

Intergovernmental Panel on Climate Change (IPCC) (2001), *Climate Change 2001: The Scientific Basis. Intergovernmental Panel on Climate*

Change (IPCC) Third Assessment, edited by J. T. Houghton et al., Cambridge Univ. Press, New York.
Keller, F. (2003), Kurzbericht über die Steinschlagereignisse im heissen Sommer 2003 im Bergell (Project report on rock fall 2003 to the Kanton Graubünden), report, Inst. für Tourismus und Landschaft Acad. Engiadina, Samedan, Switzerland.
Knutti, R., T. F. Stocker, F. Joos, and G. K. Plattner (2002), Constraints on radiative forcing and future climate change from observations and climate model ensembles, *Nature*, *416*, 719–723.
Kohl, T. (1999), Transient thermal effects below complex topographies, *Tectonophysics*, *306*, 311–324.
Lunardini, V. J. (1996), Climatic warming and the degradation of permafrost, *Permafrost Periglacial Processes*, *7*(4), 311–320.
Mann, M. E., R. S. Bradley, and M. K. Hughes (1999), Northern Hemisphere temperatures during the past millennium: Inferences, uncertainties and limitations, *Geophys. Res. Lett.*, *26*, 759–763.
Mittaz, C., M. Imhof, M. Hoelzle, and W. Haeberli (2002), Snowmelt evolution mapping using an energy balance approach over an alpine terrain, *Arct. Antarct. Alp. Res.*, *34*(3), 274–281.
Ohmura, A., M. Beniston, M. Rotach et al. (1996), Simulation of climate trends over the Alpine region, final scientific report, Swiss Natl. Res. Prog. 31, Zurich, Switzerland.
Schär, C., P. L. Vidale, D. Lüthi et al. (2004), The role of increasing temperature variability in European summer heatwaves, *Nature*, *427*, 332–336.
Schiermeier, Q. (2003), Alpine thaw breaks ice over permafrost's role, *Nature*, *424*, 712.
Stocker-Mittaz, C., M. Hoelzle, and W. Haeberli (2002), Modelling alpine permafrost distribution based on energy-balance data: A first step, *Permafrost Periglacial Processes*, *13*(4), 271–282.
Stott, P. A., and J. A. Kettleborough (2002), Origins and estimates of uncertainty in predictions of twenty-first century temperature rise, *Nature*, *416*, 723–726.
Wegmann, M., H. G. Gudmundsson, and W. Haeberli (1998), Permafrost changes in rock walls and the retreat of alpine glaciers: A thermal modelling approach, *Permafrost Periglacial Processes*, *9*(1), 23–33.
Zwiers, F. W. (2002), The 20-year forecast, *Nature*, *416*, 690–691.

S. Gruber, W. Haeberli, and M. Hoelzle, Glaciology and Geomorphodynamics Group, Department of Geography, University of Zurich, Winterthurerstrasse 190, CH-8057 Zurich, Switzerland. (stgruber@geo.unizh.ch)

Publication 2:

Surface temperatures in steep alpine rock faces – A strategy for regional-scale measurement and modelling

Citation:

Gruber, S., M. Peter, M. Hoelzle, I. Woodhatch, and W. Haeberli. 2003. Surface temperatures in steep alpine rock faces – A strategy for regional-scale measurement and modelling. Pages 325-330 in M. Phillips, S. Springman, and L. Arenson, editors. 8th International Conference on Permafrost, Proceedings. Swets & Zeitlinger, Lisse, Zürich.

Main findings:

- The lower limit of permafrost in rock walls is likely a few hundred meters higher than that in debris-covered slopes.
- The North-South differentiation of mean annual near-surface rock temperatures is almost 1000 m vertical.
- First systematic investigation of the spatial/topographic differentiation of rock temperatures in cold-mountains. A one-year data set of 14 time series recorded every two hours at near-vertical locations between 2500 and 4500 m and all aspects has been provided.
- The shading by local horizons in steep rock faces can be measured using fish-eye photography from a specialized mount.
- A measurement and research strategy for rock temperatures has been described and tested. This methodology is now tested in the pilot phase of the Swiss National Permafrost Monitoring Network PERMOS.
- Near-surface rock temperatures are valuable for the validation of energy-balance models in complex topography.

Permafrost, Phillips, Springman & Arenson (eds)

Surface temperatures in steep alpine rock faces – A strategy for regional-scale measurement and modelling

S. Gruber, M. Peter, M. Hoelzle, I. Woodhatch & W. Haeberli
Department of Geography, University of Zurich, Switzerland

ABSTRACT: A wealth of near-surface rock temperatures have been published, but no systematic study of their spatial distribution is available. A campaign for the spatial characterisation of rock surface temperatures in the Swiss Alps is presented. The four main aspects are: 1) sampling strategy and site selection based on an existing ground temperature model; 2) logger design; 3) logistics of safely and efficiently accessing sites and 4) criteria for the local placement of data loggers. In 2001, more than 20 data loggers were placed at locations between 2000 and 4500 m a.s.l., recording temperatures at a depth of 10 cm every two hours. Sites were selected in order to cover a wide range of temperatures, altitudes and slope aspects. In autumn 2002, 14 complete time series were recovered. First analyses and results are presented.

1 INTRODUCTION

The stability of rock faces with ice-filled discontinuities is strongly influenced by its temperature. In depth ranges from centimetres to many tens of metres temperature-dependent processes are subject to changes on time scales of hours to centuries (cf. Lunardini 1996, Matsuoka et al. 1998). The frequency of larger and potentially hazardous events resulting from degradation of warm permafrost or from a rising permafrost base could potentially increase as a response to a warming climate (Haeberli et al. 1997; cf. also Noetzli et al. 2003, this issue). Such deep-seated events are usually attributed to loss of ice/rock "adhesion" upon the phase change from ice to water, or to elevated water pressure due to the existence of liquid ground water. Additionally, Davies et al. (2001) showed that changing properties of warming ice before the actual phase change may result in failure of rock slopes that would be stable at low temperatures or when ice-free. Where can such thermal conditions be found however and how can present or past events be attributed to them? Which rock faces might become potentially destabilised and require further investigations? To address these questions, quantitative data on the spatial distribution of rock surface temperatures is needed because, to a large degree, the temperature field at depth is determined by surface conditions.

The ability to model and parameterise surface temperatures of rock faces is not only an important asset for the high resolution stage of natural hazard assessment but also for studies of rock weathering in general. Acting on a shorter depth/time scale, an increasing active-layer thickness will subject perennially frozen rock to freeze-thaw cycles and corresponding effects such as joint widening (macrogelivation). Effective frost weathering by granular disintegration and small flaking (microgelivation) is known to occur preferentially in a rather narrow sub-zero temperature range (see Matsuoka 2001 for a summary of typical values for several lithologies). Depending on surface temperatures, corresponding time windows vary strongly at different depths (cf. Anderson 1998). Whereas studies involving sediment traps can easily rely on in-situ measurements, investigations of rock-wall processes and retreat rates could benefit from the possibility of establishing temperature ranges.

The derivation of climate signals from geothermal analysis of borehole temperature profiles in permafrost (e.g. Isaksen et al. 2000) is a promising means of evaluating the integrated effect of climatic change on ground temperatures. Interpretation of borehole temperatures in alpine topography such as those measured along the European PACE transect (Harris et al. 2001) however, require careful corrections of topographically derived distortions that might otherwise be mistaken for climate signals (Kohl 1999). In the mean annual ground-surface temperature field required for the interpretation of permafrost thermal data, rock-wall temperatures constitute one component in a continuum of surface conditions, ranging from snow-free rock-faces to flat ground with a thick winter snow cover and a mixed-media active layer. Parameterisation of rock-wall temperatures involves considerable problems of representative sampling under conditions of difficult access. In this article, a strategy for systematic investigation of near-surface temperatures of Alpine rock faces in a spatial context is presented. The initial data obtained in the measurement campaign between the summers of 2001 and 2002 is briefly examined.

2 BACKGROUND

Several researchers report rock surface or near-surface temperature measurements (e.g. Lewkowicz, 2001,

Table 1. Temperature differences for rock faces of different expositions measured at otherwise comparable sites.

Author	Temperature difference (°C)	Sensor depth (mm)	Elevation (m a.s.l.)	Latitude	Averaging period
Lewkowicz (2001)	0.2	15	270	80N	month (polar night)
Lewkowicz (2001)	1.5	15	270	80N	month (polar day)
Lewkowicz (2001)	>5	15/20	270	80N	month (spring)
Hall (1997)	1.32	?	300	71S	5 days (polar day)
Hall & André (2001)	~8	on surface	30	67S	1 minute (11. Dec)
Matsuoka et al. (1997)	~5 & ~4	100	2850	46N	year
Wegmann (1998)	3.3	centimeters	3560	46N	year
Wegmann (1998)	5.0	?	3600	46N	year
Wegmann (1998)	7.7	centimeters	2730	46N	year

Hall and André, 2001; Matsuoka and Sakai, 1999; Wegmann, 1998; Hall, 1997; Matsuoka et al. 1997 or Coutard and Francou, 1989) but the question of their spatial distribution on a regional scale remains open. Aspect-related differences in temperature as summarised in Table 1 lead to the conclusion that air temperature alone is a bad surrogate for rock surface temperatures. Net short-wave radiation is likely to be the major controlling factor causing this observed lateral variation of several degrees celsius in rugged topography.

Data recorded during Antarctic/Arctic winters by Hall (1997) and Lewkowicz (2001) demonstrate that, in the absence of solar radiation, rock-surface temperatures follow air temperature closely. The influence of rock albedo is evident *a priori* and has been demonstrated semi-quantitatively by Hall (1997) who showed surface temperature averages to differ by 1.1°C for dark and light coloured rocks in otherwise comparable situations for one Antarctic summer. A temperature difference between rock faces of E/W exposition that theoretically should receive a similar input of solar energy can often be observed. This is likely to be due to the influence of diurnal variations in cloud cover such as convective clouds in the afternoon that reduce solar radiation totals on W-slopes.

Snow cover has two important effects on rock surface temperatures: 1) smoothing of radiation-induced lateral differences and of high-frequency fluctuations, by insulation of the ground from the atmosphere 2) increasing ground temperatures by insulation during winter when most energy loss takes place. This is demonstrated by Coutard & Francou (1989), who at 6 cm depth and an interval of 2 hours measured a daily range of 24.6°C without snow and only 1.2°C under snow cover at two almost identical sites (February, south-facing, 3000 m a.s.l., 45N). In the Japanese Alps, Matsuoka & Sakai (1999) measured mean annual ground surface temperatures at a snow-covered site at 3120 m to be 2.4°C warmer than at a comparable snow-free location. For a discussion of the special case of thin snow cover, see Keller & Gubler (1993). Timing and duration of snow cover are treated by Zhang et al. (2001). The almost complete absence of snow cover, combined with the direct coupling of surface and subsurface energy balance (without complex thermal offset in a mixed-media active layer) makes near-vertical rock faces a system that is easier to characterise than ground temperatures on flat terrain. Based on the above reasoning, a lateral variation of mean annual rock-surface temperatures in the order of 5–10°C is expected for sites of similar elevation in the Alps. It is expected that this spatial differentiation is largely related to net short-wave solar radiation. Hoelzle & Haeberli (1995) and Gruber & Hoelzle (2001) demonstrate successful statistical modelling of a ground temperature proxy (BTS – bottom temperature of the winter snow pack cf. Haeberli 1973), that is subject to noise induced by snow cover and a mixed-media active layer. The absence of these sources of error makes statistical parameterisation of rock-wall temperatures a promising task.

3 RESEARCH STRATEGY

3.1 *Sampling strategy and site selection*

The cost and effort involved in installing data loggers in steep rock faces is obvious and their total number must therefore be kept small. At the same time, an even distribution of measurements over the assumed range of surface temperatures is desired. As a first approximation, the model described in Gruber and Hoelzle (2001) has been employed to simulate BTS values as a proxy for MAGST in the test areas. Pixels steeper than 45° derived from a digital elevation model (DEM) with a grid size of 25 m have been used to identify rock faces. Potential sampling areas, together with a temperature proxy could therefore be laid over a topographic map. Aiming at an even distribution of 20 loggers over the BTS range of 0 to −15°C, individual

sites have been pre-selected at altitudes from 2000 to 4500 m covering the entire range of expected permafrost conditions in Alpine rock-walls. As the BTS model is likely to underestimate rock-surface temperature differentiation by solar radiation it has been attempted to cover different slope aspects evenly. For the recovery of realistic daily surface temperatures, the interval of recording and measurement, as well as sensor depth, must be considered. Thermistors are placed at a depth of 10 cm, avoiding the difficult and error-prone direct measurement of rapidly fluctuating surface temperatures. The surface area and time over which the measured signal is integrated by heat diffusion within the rock increases with sensor depth. As a consequence, the alteration of the signal caused by the sensor and its wiring is reduced and high-frequency signals are dampened, allowing for accurate sampling at an interval of two hours.

3.2 *Logger design and installation*

Loggers have to be water-proof, resistant to temperature fluctuation and extremes, tolerant to minor rock-fall and fast to install without many tools. Battery life and storage capacity should exceed 1 year. UTL-1 data loggers (see: Hoelzle et al. 1999) were redesigned for this project as these have been employed successfully before. They have the capacity to store 7944 8-bit measurements in the range between −30 and +40°C, and an accuracy of greater than ±0.25°C is given by the manufacturer. A screw-in metal lid with rubber "O"-rings ensures waterproof sealing of the logger.

Our main alteration was the construction of a water-proof and protective sensor arm that also establishes the logger/sensor geometry. The sensor side of this arm is 10 cm long to ensure placement at equal depths and the logger side has a length of 12 cm in order to keep thermal disturbance at the surface directly above the sensor at a minimum (Fig. 1). After inserting the 8 mm arm into a 10 mm drill hole together with some silicon sealant, the logger is screwed to the rock wall using a clamp and a wall-plug in a second 10 mm hole. The sensor arm is made of PVC and was screwed and glued into the logger housing consisting of DELRIN plastic. Prior to installation, all loggers were equipped with a new lithium battery and a silica gel pack to ensure dry electronics, calibrated in a 0°C ice bath and programmed in the laboratory.

3.3 *Site access, safety and logistics*

The sites finally chosen for instrumentation have to be easily accessible in order to keep the total time used for placement and recovery of data logger small. Generally, sites were chosen that could be reached from the top in one rappel. The equipment carried for logger placement on belay (Fig. 2) included a HILTI drill, bolt plates, screw and wall-plug, a screw driver, a wrench and a hammer, loggers, silicon, a camera, compass and clinometer as well as usual climbing aids.

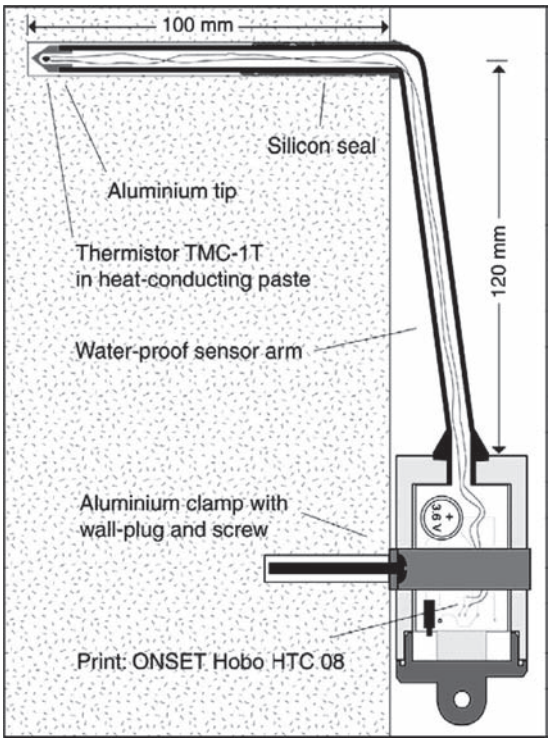

Figure 1. Schematic of modified data logger.

3.4 *Local placement of data loggers*

After selecting a site according to its elevation, exposition and expected temperature, the local placement of data loggers is of great importance. Rock-faces that from afar appear to be exposed in one direction usually exhibit many individual facets of distinctly different steepness, exposition or local shading. The facet chosen for measurement should resemble the general character of the large face as close as possible. Near-vertical situations are preferable due to a minimum snow cover. A vertical distance of several meters should be kept to the flat terrain below in order to avoid coverage by snow piles. Measurements should only be attempted on surfaces that are homogeneous and free of visible fractures or discontinuities within a radius of more than 30 cm.

3.5 *Auxiliary information requirements*

During and after logger installation, several parameters are recorded. The coordinates (usually at the belay

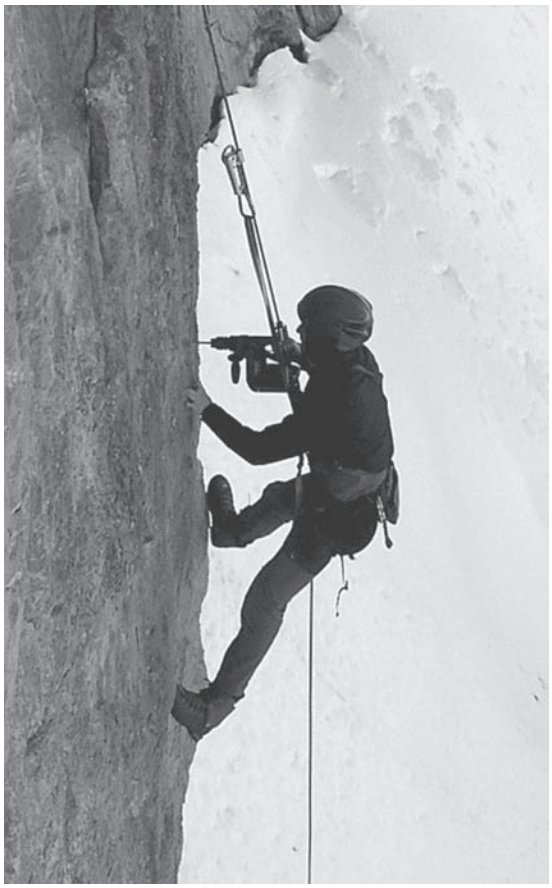

Figure 2. Installation of a data logger.

point) are determined with a hand-held GPS receiver. Slope angle and azimuth at the logger are measured and the elevation is determined using a barometric altimeter.

Because topographic shading has a major effect on solar radiation input in rugged terrain, horizon lines need to be determined for the calculation of solar illumination. Usually, horizon shading is derived from DEMs. In rock walls however, their facet-structure and micro-topography often introduces significant horizons that locally influence temperature measurements, but are not resolved in DEMs. In this campaign, local horizons are therefore recorded using a digital camera (Nikon Coolpix 990) with a fish eye converter (Nikon FC-E8). A device to mount the camera in the remaining hole after removal of the data logger has been constructed (Fig. 3). The camera is installed on a platform held by a ball-joint and equipped with a compass and a sprit level. One image with a vertical camera nadir is taken and the azimuth of a marker in the image is read from the compass. This information allows for subsequent extraction of horizon lines in the office and to calculate more realistic solar radiation.

Figure 3. Camera with fish eye lens mounted in rock wall.

4 SAMPLING PROGRAM

In summer and autumn 2001, 21 data loggers were installed at elevations between 2000 and 4500 m a.s.l. at sites where the transportation infrastructure present at high altitude in the Swiss Alps facilitated quick access. Loggers were placed in the following areas: Gornergrat/Stockhorn, Monte Rosa and Kleinmatterhorn/Gandegg close to Zermatt, Birg/Schilthorn and Jungfraujoch in the Bernese Alps and Corvatsch/Furtschellas close to St. Moritz.

In autumn 2002 all data loggers were reclaimed except for one that could not be reached. Photographs of the hemispheric horizon for later extraction of horizon lines were taken at most sites, but failure of the camera and bad weather made this impossible in some cases. Only one logger had been physically damaged. It had a broken sensor arm and had been filled with ice.

5 FIRST RESULTS AND EXPERIENCES

14 complete time series (see example in Fig. 6) of one year and several shorter ones have been obtained from the measurements. Detailed description and analysis of the dataset will be published elsewhere, but first results indicate that:

- the lower limit of permafrost is somewhat higher than that established on more gentle terrain (e.g. Haeberli, 1975)

- the lower limit of negative mean annual rock temperatures in the south is about 1000 m higher than in the north (Fig. 4)
- diurnal temperature cycles, and therefore the influence of factors such as clouding are discernible in the data (Fig. 5)

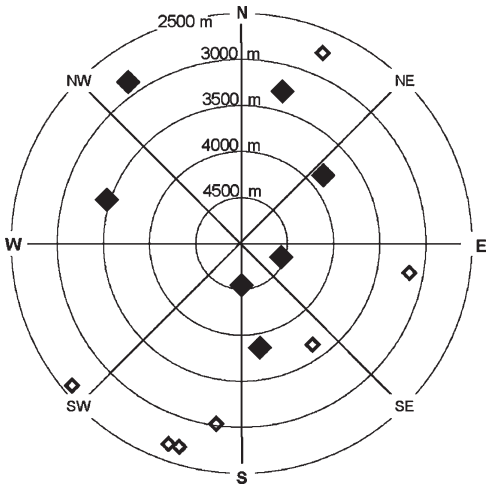

Figure 4. Elevation and exposition of data logger locations. Full diamonds indicate sites with negative mean annual rock temperatures at 10 cm depth.

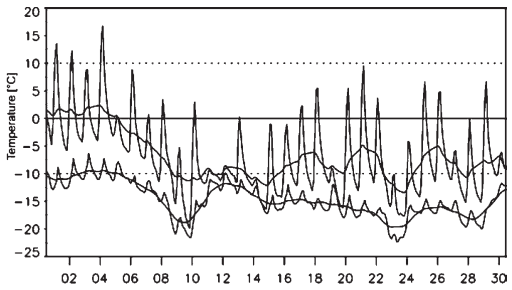

Figure 5. 2-hourly temperatures recorded at 4500 m during November 2001. Lower curve: north-facing (Zumsteinspitze), upper curve: south-facing (Signalkuppe). Smooth lines represent the 2-day running average.

Unfortunately, even at low elevation sites, several data loggers stopped recording after only a few days or weeks. This was probably caused by a batch of spoiled batteries. Individual loggers may have stopped recording due to low temperatures such as one at 4500 m at a north-facing site that experienced a severe temperature drop and stopped below 225°C. On the other hand, a south-facing logger at the same altitude recorded 227°C that night and survived similar conditions of low air-temperatures without problems. This suggests that temperature was not the sole cause of failure. The data registered by all loggers could be read without problems after replacement of the battery. The data logger with the broken sensor arm was completely filled with clear ice but was also readable after drying. The recording of local horizons using a digital camera with a fish eye lens was generally successful. Unfortunately, the required good visibility puts a constraint on possible periods for field work and several sites could not therefore be photographed due to fog or snow fall.

6 CONCLUSION AND OUTLOOK

The data collected during this campaign is of good quality and is suitable as a basis for the intended analysis and modelling of the spatial distribution of Alpine rock-face temperatures. This is expected to provide necessary information for research related to the stability of frozen rock-walls under a warming climate and to be beneficial for investigations of weathering and landform evolution.

The experiences and data collected in the course of this project bring additional benefits for calibration and verification of energy-balance models. The direct coupling between atmospheric and rock temperatures constitutes a unique opportunity for quantitative spatial evaluation of relative and absolute model accuracy. A combination of rock-wall temperature measurements, together with measurements of level (and thus potentially snow-covered) rock surfaces will provide more quantitative data for the analysis and modelling of

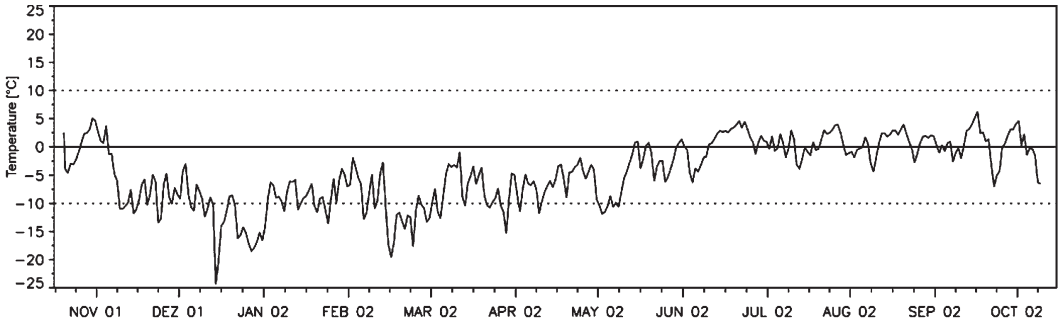

Figure 6. Daily near-surface rock temperatures at Signalkuppe, 4545 m a.s.l., south-exposed.

ground temperature conditions than BTS alone. Corresponding strategies of combined BTS and rock-surface measurement campaigns are currently being developed.

ACKNOWLEDGEMENTS

The authors are grateful for the support given by the International Foundation High Altitude Research Stations Jungfraujoch and Gornergrat (HFSJG), the Gornergrat-Monte Rosa-Bahnen, the Matterhorn-bahnen/Burgergemeinde Zermatt and Prof. Dr. Lorenz King. Two anonymous reviewers gave valuable comments.

REFERENCES

Anderson, R. 1998. Near-surface thermal profiles in alpine bedrock: Implications for the frost weathering of rock. *Arctic and Alpine Research* 30(4): 362–372.

Coutard, J-P. & Francou, B. 1989. Rock temperature measurements in two Alpine environments: Implications for frost shattering. *Arctic and Alpine Research* 8(4): 399–416.

Davies, M.C.R., Hamza, O. & Harris, C. 2001. The effect of rise in mean annual temperature on the stability of rock slopes containing ice-filled discontinuities. *Permafrost and Periglacial Processes* 12(1): 137–144.

Gruber, S. & Hoelzle, M. 2001. Statistical modeling of mountain permafrost distribution: Local calibration and incorporation of remotely sensed data. *Permafrost and Periglacial Processes* 12(1): 69–77.

Haeberli, W. 1973. Die Basistemperatur der winterlichen Schneedecke als möglicher Indikator für die Verbreitung von Permafrost in den Alpen. *Zeitschrift für Gletscherkunde und Glazialgeologie* XI(1–2): 221–227.

Haeberli, W. 1975. Untersuchungen zur Verbreitung von Permafrost zwischen Flüelapass und Piz Grialetsch (Graubünden). *Mitteilungen der Versuchsanstalt für Wasserbau, Hydrologie, Glaziologie, 17, ETH Zürich.*

Haeberli, W., Wegmann, M. & Vonder Mühll, D. 1997. Slope stability problems related to glacier shrinkage and permafrost degradation in the Alps. *Eclogae geol. Helv*. 90: 407–414.

Hall, K. & André, M-F. 2001. New insights into rock weathering from high-frequency rock temperature data: an Antarctic study of weathering by thermal stress. *Geomorphology* 41: 23–35.

Hall, K. 1997. Rock temperatures and implications for cold region weathering. I: New data from Viking Valley, Alexander Island, Antarctica. *Permafrost and Periglacial Processes* 8: 69–90.

Harris, C., Haeberli, W., Vonder Mühll, D. & King, L. 2001. Permafrost monitoring in the high mountains of Europe: the PACE project in its global context. *Permafrost and Periglacial Processes* 12(1): 3–11.

Hoelzle, M. & Haeberli, W. 1995. Simulating the effects of mean annual air temperature changes on permafrost distribution and glacier size. An example from the Upper Engadin, Swiss Alps. *Annals of Glaciology* 12: 400–405.

Hoelzle, M., Wegmann, M. & Krummenacher, B. 1999. Miniature temperature dataloggers for mapping and monitoring of permafrost in high mountain areas: First experience from the Swiss Alps. *Permafrost and Periglacial Processes* 10(2): 69–77.

Isaksen, K., Vonder Muehll, D., Gubler, H., Kohl, T. & Sollid, J.L. 2000. Ground surface-temperature reconstruction based on data from a deep borehole in permafrost at Jansonhaugen, Svalbard. *Annals of Glaciology* 31: 287–294.

Keller, F. & Gubler, H.U. 1993. Interaction between snow cover and high-mountain permafrost, Murtel/Corvatsch, Swiss Alps. In: *Proceedings of the 6th International Conference on Permafrost, Beijing*. 1: 332–337.

Kohl, T. 1999. Transient thermal effects below complex topographies. *Tectonophysics* 306: 311–324.

Lewkowicz, A.G. 2001. Temperature regime of a small sandstone tor, latitude 80°N, Ellesmere Island, Nunavut, Canada. *Permafrost and Periglacial Processes* 12(4): 351–366.

Lunardini, V.L. 1996. Climatic warming and the degeneration of warm permafost. *Permafrost and Periglacial Processes* 7(4): 311–320.

Matsuoka, N. & Sakai, H. 1999. Rockfall activity from an alpine cliff during thawing periods. *Geomorphology* 28: 309–328.

Matsuoka, N. 2001. Microgelivation versus macrogelivation: Towards bridging the gap between laboatory and field frost weathering. *Permafrost and Periglacial Processes* 12(3): 299–313.

Matsuoka, N., Hirakawa, K., Watanabe, T. & Moriwaki, K. 1997. Monitoring of periglacial slope processes in the Swiss Alps: the first two years of frost shattering, heave and creep. *Permafrost and Periglacial Processes* 8(2): 155–177.

Matsuoka, N., Hirakawa, K., Watanabe, T., Haeberli, W. & Keller, F. 1998. The role of diurnal, annual and millennial freeze-thaw cycles in controlling Alpine slope instability. *Proceedings of the 7th International Conference on Permafrost, Yellowknife, Canada 1998*. Collection Nordicana 57.

Noetzli, J., Hoelzle, M. & Haeberli, W. 2003, in press. Mountain permafrost and recent Alpine rock fall events: a GIS-based approach. *This issue.*

Wegmann, M. 1998. Frostdynamik in hochalpinen Felswänden am Beispiel der Region Jungfaujoch – Aletsch. *Mitteilungen der Versuchsanstalt für Wasserbau, Hydrologie und Glaziologie der ETH Zürich*, Switzerland.

Zhang, T., Barry, R.G. & Haeberli, W. 2001. Numerical simulations of the influence of the seasonal snow cover on the occurrence of permafrost at high latitudes. *Norsk Geographisk Tidsskrift – Norwegian Journal of Geography* 55(4): 261–266.

Publication 3:

Rock-wall temperatures in the Alps: modelling their topographic distribution and regional differences.

Citation:

Gruber, S., Hoelze, M. and Haeberli , W. (2004). Rock wall temperatures in the Alps: Modelling their Topographic Distribution and Regional Differences. Permafrost and Periglacial Processes, 15(3), 299-307.

Main findings:

- Spatial distribution patterns of rock-surface temperatures as well as their inter-annual variations are described.
- A quantitative surface energy-balance model was successfully validated using measurements of near-surface rock-wall temperatures.
- The inter-annual and diurnal variability of temperatures in the South is greater than in the North because two signal contribute (air temperature, solar radiation)
- The difference between Northern and Central Alps is greatest in southern aspects and at high elevation due the importance of short-wave radiation.
- Based on the energy-balance calculations, a model of reduced complexity can be designed to approximately map permafrost under most steep alpine rock surfaces.

PERMAFROST AND PERIGLACIAL PROCESSES
Permafrost and Periglac. Process. **15**: 299–307 (2004)
Published online in Wiley InterScience (www.interscience.wiley.com). DOI: 10.1002/ppp.501

Rock-wall Temperatures in the Alps: Modelling their Topographic Distribution and Regional Differences

Stephan Gruber, Martin Hoelzle and Wilfried Haeberli*

Department of Geography, Glaciology and Geomorphodynamics Group, University of Zurich, Switzerland

ABSTRACT

Rising temperatures or the complete thaw of permafrost in rock walls can affect their stability. Present as well as projected future atmospheric warming results in permafrost degradation and, as a consequence, makes knowledge of the spatial distribution and the temporal evolution of rock temperatures important. Rock-face near-surface temperatures have been measured over one year at 14 locations between 2500 and 4500 m a.s.l. in the Alps. Different slope aspects have been included in order to capture the maximum spatial differentiation of rock temperatures. These data were used to further develop and verify an energy-balance model that simulates daily surface temperatures over complex topography. Based on a 21-year (1982–2002) run of this model, spatial patterns of rock-face temperatures in the Swiss Alps are presented and discussed. This model provides a basis for the re-analysis of past rock-fall events with respect to permafrost degradation as well as for the simulation of future trends of rock temperatures. Furthermore, the spatial patterns of rock-wall temperatures provide a quantitative insight into the topography-related mechanisms affecting permafrost distribution in Alpine areas without local influence from snow cover or an active layer with a complex thermal offset.

KEY WORDS: rock temperatures; rock faces; Alps; mountain permafrost; energy balance; slope instability; rock fall

INTRODUCTION

Warming and thawing of permafrost can affect the stability of perennially frozen rock walls (Gruber *et al.*, 2004; Haeberli and Beniston, 1998). The thaw of ice-filled rock joints can open them to groundwater migration, raising water pressures (Haeberli *et al.*, 1997), and thus reduce the effective normal stresses. Davies *et al.* (2001) have shown that even the warming of ice in rock joints can result in reduced stability. Slopes that are stable when several degrees below freezing or when ice free could be destabilized in the temperature range between −1.5 and 0°C.

The transfer of these findings to the natural environment (cf. Nötzli *et al.*, 2003) requires knowledge about the spatial distribution of rock-wall temperatures and their evolution over time. Understanding and modelling of the processes that determine rock-face temperatures will also provide a means of assessing ranges of probable sub-surface temperatures caused by climate forcing and would provide a basis for assessing the impact of climatic change on rock-wall stability.

In comparison with debris-covered slopes, rock faces react quickly to climate change. This is due to the absence of a block layer (Harris, 1996; Harris and Pedersen, 1998; Mittaz *et al.*, 2000; Hoelzle *et al.*, 2001) and corresponding direct coupling of surface

* Correspondence to: Stephan Gruber, Department of Geography, Glaciology and Geomorphodynamics Group, University of Zurich, Winterthurerstrasse 190, CH 8057, Switzerland. E-mail: stgruber@geo.unizh.ch

Received 6 January 2004
Revised 29 June 2004
Accepted 29 June 2004

and sub-surface conditions, combined with a low water content and a small transfer of latent heat during melt.

This rapid reaction together with the effect of destabilization make rock fall due to permafrost degradation a likely and well perceivable impact of climate change in the near future (Gruber *et al.*, 2004). The influence that permafrost degradation in rock walls may have on human infrastructure and safety may be comparable to that of debris flows due to melt of perennially frozen debris slopes. Traditionally however, research on mountain permafrost has focussed almost exclusively on debris-covered slopes.

Although a wealth of rock-temperature measurements is available (see Gruber *et al.*, 2003, for a summary), only limited information on their spatial distribution can be extracted from them. Between the summers of 2001 and 2002 a measurement campaign (Gruber *et al.*, 2003) was carried out in order to investigate the spatial distribution and temporal evolution of near-surface temperatures in steep alpine rock faces.

This paper presents the results of this campaign as well as modelling results that extend the knowledge so gained beyond the measured years and locations. In particular this paper presents new results on

1. the distribution of rock-wall temperatures in the Alps
2. the inter-annual variability of temperatures
3. the processes that govern rock-face temperatures
4. process-based models of rock temperatures as a tool for research and engineering.

BACKGROUND AND STRATEGY

Rock Temperatures

Several researchers report rock surface or near-surface temperature measurements (e.g. Coutard and Francou, 1989; Hall, 1997; Matsuoka et al, 1997; Wegmann, 1998; Matsuoka and Sakai, 1999; Hall and André, 2001; Lewkowicz, 2001) but the question of their spatial distribution on a regional scale and in differing topographic conditions remains largely open. It is obvious that in rugged topography air temperature alone is a poor surrogate for rock surface temperatures. Net short-wave radiation is likely to be the major controlling factor causing the lateral variation of several degrees Celsius that can be deduced from previous research (Gruber *et al.*, 2003). Data recorded during Antarctic/Arctic winters by Hall (1997) and Lewkowicz (2001) demonstrate that, in the absence of solar radiation, rock-surface temperatures follow air temperature closely. Snow cover and mixed-media active layers are largely absent from near-vertical rock walls, making them a rather straightforward system characterized mainly by the influence of air temperature and short-wave solar radiation.

Temperature Variations with Time

The surface temperature in rock faces is subject to fluctuations over various time intervals: short term (e.g. moving clouds), diurnal (day–night cycles), annual (changing seasons) and inter-annual. The inter-annual variability in mean annual air temperature (MAAT) is of the order of 2–3°C for Swiss mountain stations and global radiation has fluctuated by about $\pm 5\%$ in recent decades (based on Aschwanden *et al.*, 1996). The combination of the two fluctuations can lead to an expected compound inter-annual signal having a range of up to 5°C. These signals are progressively dampened by heat diffusion with increasing depth in the rock.

Modelling Rock Temperatures

Rock faces are a comparatively straightforward system to model using energy-balance approaches such as PERMEBAL (Stocker-Mittaz *et al.*, 2002). The main sources of error are probably the extrapolation or parametrization of atmospheric variables in extreme topography and terrain geometry.

Hoelzle and Haeberli (1995) and Gruber and Hoelzle (2001) demonstrate successful statistical modelling of a ground temperature proxy that is subject to noise induced by snow cover and a mixed-media active layer. The absence of these sources of error makes statistical parametrization of rock-wall temperatures more likely to be successful than that on debris-covered slopes in more gentle terrain.

Research Strategy

A general distribution pattern of rock temperatures cannot be deduced from one or only a few years of measurements because rock temperatures are subject to large inter-annual fluctuations. Furthermore, the research goal is to relate the thermal response of rock surfaces to climatic change. Therefore, in this study, one year of measurements is used to improve and validate a process-based model of rock-face temperatures. This model is then used to simulate time series of rock temperatures over 21 years in order to deduce spatial patterns and temporal fluctuations.

The results from the process-based 21-year model experiment are then available as a basis for a

statistical model (not presented in this article) relating rock-wall permafrost distribution to simple variables such as slope/aspect/elevation or MAAT and potential direct short-wave radiation. In this way PERMEBAL experiments forced with a simulated future climate can be applied to a larger area and evaluated in a larger spatial context in future studies.

It has been demonstrated that rock-face temperatures mainly vary in response to air temperature (influenced by elevation) and short-wave radiation (influenced by slope aspect). The sampling strategy of the measurement campaign was therefore designed to include both factors.

MEASUREMENTS OF NEAR-SURFACE TEMPERATURES

In summer and autumn 2001, 21 data loggers were installed at elevations between 2000 and 4500 m a.s.l. Loggers were placed in the following areas: Gornergrat/Stockhorn, Monte Rosa and Kleinmatterhorn/Gandegg close to Zermatt, Birg/Schilthorn and Jungfraujoch in the Bernese Alps and Corvatsch/Furtschellas close to St. Moritz. For the recording of realistic daily surface temperatures, thermistors were placed at a depth of 10 cm, avoiding the difficult and error-prone direct measurement of rapidly fluctuating surface temperatures. Temperatures were logged every 2 hours. All measurement sites were roughly vertical and several metres above flat ground to ensure snow-free conditions. The research methodology and equipment is described in more detail by Gruber *et al.* (2003). 14 loggers yielded complete one-year time series from 15 October 2001 to 14 October 2002 upon recovery in autumn 2002. Table 1 summarizes their locations and site characteristics. Some of the time series were missing 1–5 days of the one-year interval and were completed by multiple regression analysis based on the three most correlated loggers in order to generate a consistent database of daily average temperatures for further processing. The temperature measured at the depth of 10 cm is considered a valid representation of the surface temperature on the basis of daily averages.

SIMULATING THE SURFACE ENERGY-BALANCE

The model PERMEBAL (Stocker-Mittaz *et al.*, 2002) has been extended and adapted for the simulation of rock temperatures in rugged topography. The model uses daily meteorological time series of air temperature, vapour pressure, air pressure, precipitation, wind speed, wind direction and global radiation from the operational Swiss meteorological network as input data. Based on these data, atmospheric variables are extrapolated over complex topography and the surface energy balance is simulated.

In the context of this article, only the one-dimensional version of the model that simulates one individual point is used. A two-dimensional version that calculates temperatures based on arrays representing the investigation area has also been developed.

Two different approaches are employed.

1. PEB: surface-only calculation, where the ground heat flux is set to a fixed value ($5.0\,W\,m^{-2}$) and the surface temperature is calculated based on long-wave emitted radiation as the sum of all calculated fluxes.

Table 1 Location and site characteristics of the 14 data loggers that recorded one-year time series.

ID No.	Location	Elevation [m]	Aspect [°]	Slope [°]	MAGST [°C]
70576	Klein Matterhorn	3850	170 (S)	86	−2.5
70611	Gandegg	3020	188 (S)	72	6.4
70623	Riffelhorn	2600	230 (SW)	77	5.5
70625	Klein Matterhorn	3845	50 (NE)	71	−2.9
70678	Eismeer	3150	100 (E)	87	1.5
70748	Jungfrau Ostgrat	3655	145 (NE)	70	1.2
96474	Mönchsgrat/Sphinx	3464	288 (W)	72	−4.1
109329	Schilthorn/Birg	2680	200 (S)	103	5.9
109381	Signalkuppe	4545	180 (S)	67	−4.5
109441	Corvatsch—Top	3290	15 (N)	62	−2.8
109478	Corvatsch—Mittel	2750	23 (N)	84	1.0
109482	Signalkuppe	4545	109 (E)	90	−5.4
109489	Schilthorn/Birg	2690	197 (S)	80	6.2
326947	Eigerwand	2860	325 (NW)	90	−0.4

2. PEB_HC: calculation with a ground heat-conduction scheme, where the ground heat flux is derived as the sum of all calculated fluxes. It serves as the upper boundary condition in a heat-conduction scheme.

The ground heat conduction is solved in a finite-difference Crank–Nicholson scheme. Latent heat is included as apparent heat capacity between -0.5 and 0.0°C assuming no movement of water.

For the calculation of the turbulent heat fluxes and emitted long-wave radiation (for PEB_HC), the surface temperature needs to be estimated. The models iterate part of the energy balance in order to converge the initial temperature estimate and the final result. For PEB the assumed and calculated surface temperature is iterated. For PEB_HC the estimated surface temperature and the temperature of the surface node of the heat conduction scheme are iterated. During a one-year run, only occasionally one or two days do not converge to better than 0.3°C within 30 iterations. Testing the model in several runs for all measured locations revealed that the surface roughness length $z_0 = 50$ mm that had been used in earlier versions of PERMEBAL was too high. A value of $z_0 = 0.3$ mm is assumed in this study. This lies well within the published range of 0.05–10 mm for soil, sand or snow (see, e.g., Oke, 1987).

MODEL VERIFICATION

All 14 locations with measured time series were simulated using both PERMEBAL approaches. Both approaches were tested in order to relate the benefit from the higher accuracy of the heat-conduction version (PEB_HC) to the much larger computational effort required.

In the verification run, only elevation, aspect and slope were adjusted to each logger site and the closest driving meteo station selected. Because measurements of surface and subsurface properties were not available parameters were set to one fixed value for all sites in order to prevent fitting of the result. The driving stations were Corvatsch (3315 m a.s.l.), Jungfraujoch (3580 m a.s.l.) and Zermatt (1638 m a.s.l.) (data source MeteoSwiss). Surface characteristics of rock were set to albedo = 0.2, emissivity = 0.96 and roughness length = 0.3 mm. The atmospheric lapse rate is taken as $-0.006\,\mathrm{K\,m^{-1}}$. For the heat-conduction scheme, the volumetric heat capacity of rock is assumed to be $1.8 \times 10^6\,\mathrm{J\,m^{-3}\,K^{-1}}$ and the thermal conductivity $2.2\,\mathrm{W\,K^{-1}\,m^{-1}}$ based on published values (Cermák and Rybach, 1982). A water content of 1% has been assumed. Due to strong topographic (Kohl, 1999) and transient (Harris *et al.*, 2003) effects it is not known whether the geothermal heat flux in complex topography is positive or negative. It is therefore assumed to be zero at the lower boundary of the heat-conduction scheme. The depth discretization is linear with a spacing of 10 cm and 150 elements. The second node is therefore located at a depth of 10 cm, like the measured temperatures.

Graphs for two neighbouring locations are provided to illustrate model performance (PEB_HC). PEB generally performs similarly to PEB_HC but has slightly stronger deviations. The locations represent two extreme cases in close proximity and roughly the same elevation: the north face of the Eiger with almost no direct radiation and a south-facing wall at Birg. Figure 1 shows a scatter plot of measured versus modelled temperature, Figure 2 plots measured and

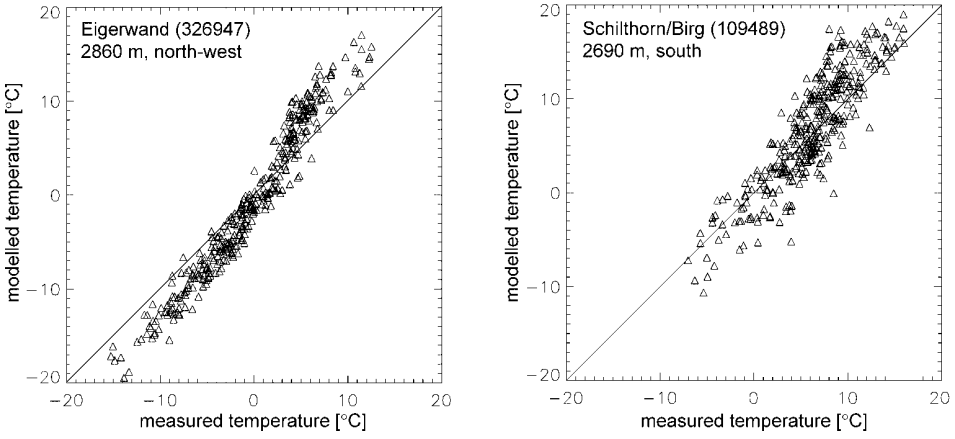

Figure 1 Measured versus modelled (PEB_HC) daily average near-surface (10 cm) temperatures [°C].

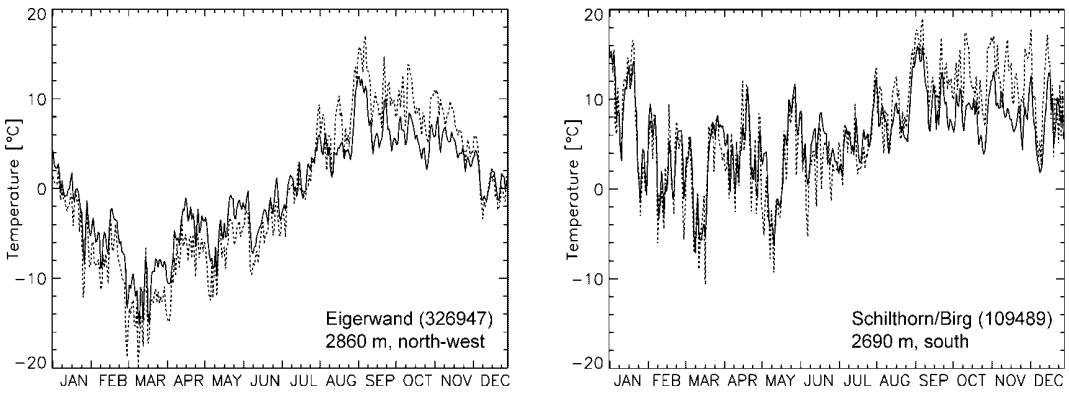

Figure 2 Measured (solid line) and modelled (PEB_HC, dashed line) mean daily near-surface (10 cm) temperatures at two locations.

modelled time series together and Figure 3 displays the difference between the two. Generally, mean annual temperatures and the temperature fluctuations are represented well. The south-facing site has a much greater variability because it receives a strong signal of short-wave radiation in addition to the long-wave signal related to air temperature. The amplitude of the day-to-day noise (Figure 3) on the north-facing rock wall is in the order of 2.5°C and about twice this amount on the south-facing slope. This is likely to be an effect of the parametrization of short-wave radiation and its spatial variability. The development of convective clouds, for instance, reduces surface temperatures through shading of direct radiation and is spatially and temporally highly variable. Additionally, an annual sinusoidal signal with an amplitude of about 2.5°C in the difference (measured PEB_HC) can be observed in Figure 3. At present, it is uncertain whether this is mainly related to the parametrization of long-wave radiation, turbulent fluxes, ground heat flux and subsurface thermal conditions or albedo and short-wave terrain-reflected radiation.

Table 2 summarizes the results of the model verification. It compares the daily measured values to the model runs using PEB and PEB_HC. A comparison with extrapolated air temperature is added in order to provide an intuitive reference against which to judge the accuracy achieved. From Table 2 and Figures 1–4, it is evident that temperature variability as well as model uncertainty are greater in locations with a high input in solar radiation.

The overall simulation of rock-wall temperatures with a mean coefficient of determination of 0.88 and a mean absolute difference in the mean annual ground surface temperature of 1.2°C is considered very encouraging. It should be kept in mind that surface temperatures accumulate the errors in the extrapolation and parametrization of all other variables and fluxes. The following sources contribute errors to the values discussed above:

- extrapolation over large distances (horizontal up to 14 km, vertical up to 2900 m)
- extrapolation in extreme terrain geometries

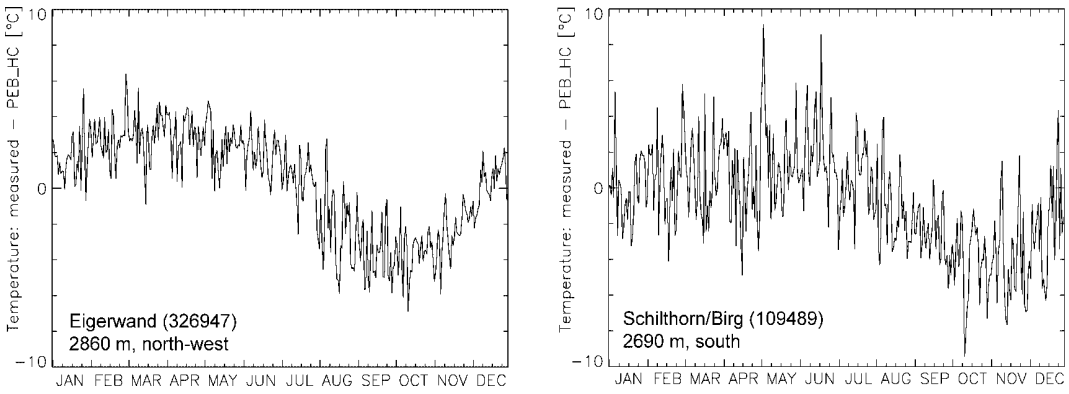

Figure 3 Residuals (measured–modelled) of daily average near-surface (10 cm) temperatures simulated using PEB_HC.

Table 2 Summary of the success of modelling daily surface temperatures. C_ refers to the coefficient of determination between the measured data and the model run. D_ refers to the mean annual difference between measured data and the model run. C_/D_AIR compares measured data with extrapolated air temperature. The means in the last line are mean coefficients of determination and mean absolute differences.

ID No.	C_PEB	D_PEB	C_PEB_HC	D_PEB_HC	C_AIR	D_AIR
70576	0.85	0.4	0.87	−0.1	0.85	6.4
70611	0.90	3.4	0.93	2.7	0.87	10.4
70623	0.87	0.6	0.88	0.2	0.89	7.0
70625	0.94	1.4	0.96	1.5	0.92	6.1
70678	0.79	0.0	0.87	−0.4	0.70	5.7
70748	0.82	0.8	0.88	−0.6	0.72	8.4
96474	0.88	−3.4	0.93	−3.8	0.83	1.9
109329	0.66	2.0	0.72	2.1	0.55	7.3
109381	0.70	1.1	0.73	−0.1	0.68	8.6
109441	0.93	−1.7	0.95	−0.9	0.82	1.9
109478	0.93	0.3	0.94	1.7	0.81	2.5
109482	0.84	2.4	0.86	2.0	0.87	7.7
109489	0.72	0.1	0.78	−0.7	0.62	7.6
326947	0.91	−0.6	0.95	0.3	0.80	2.1
Mean:	0.84	1.3	0.88	1.2	0.78	6.0

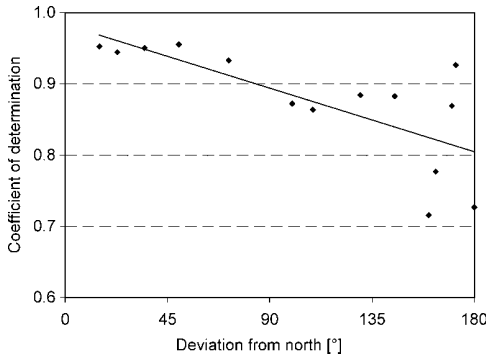

Figure 4 The coefficient of determination between the measured time series and that modelled using PEB_HC as a function of the deviation from north. This indicates the result of the growing influence of solar radiation on rock temperature.

- measurement errors at the meteorological stations
- deviation of the assumed and real surface and subsurface characteristics
- measurement errors in the rock-wall temperatures and the measurement of local aspect/slope
- limitations of the validity and completeness of the energy-balance model used.

As the actual energy balance in the measured rock face is not complicated by snow or coarse blocky layers but situated in terrain with extreme relief, this model evaluation is expected to reveal the maximum expected total error due to extrapolation of meteorologic variables and energy fluxes for more gentle, debris-covered surfaces.

The successful simulation of temperatures over a wide range of air temperature and radiation regimes establishes the validity of the model in the Alps. It is expected to yield results of equal reliability for other years using measured past time series of the Swiss meteorological network.

SPATIAL DISTRIBUTION OF SURFACE TEMPERATURES

One year of near-surface rock-temperature data is not sufficient to deduce permafrost distribution because of the large inter-annual fluctuations of air temperatures and global radiation. Therefore, rock-wall surface temperatures are modelled for the period 1982–2002 based on existing meteorological data from the stations Corvatsch and Jungfraujoch (data source: MeteoSwiss). As the Zermatt station is situated in a valley bottom and subject to corresponding local climatological effects it is not considered a valuable data source for this analysis. Corvatsch represents central-Alpine conditions with high radiation budgets and little clouding, whereas the data from Jungfraujoch is typical for the northern Alps, having comparably little direct solar irradiation and frequent clouding. For both areas, slopes of 50°, 70° and 90° steepness are modelled. Calculations are performed every 500 m at elevations between 2000 and 5000 m

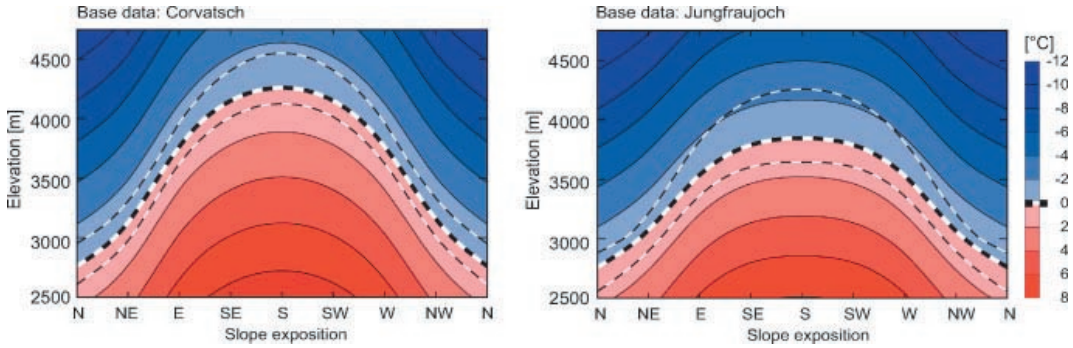

Plate 1 Mean simulated (PEB_HC) annual rock-wall surface temperature for 70° slope steepness and two locations, 1982–2002. The thick dashed line indicates the elevation of the mean 0°C isotherm during these 21 years. The thin dashed lines indicate the highest and lowest positions of the mean annual 0°C isotherm.

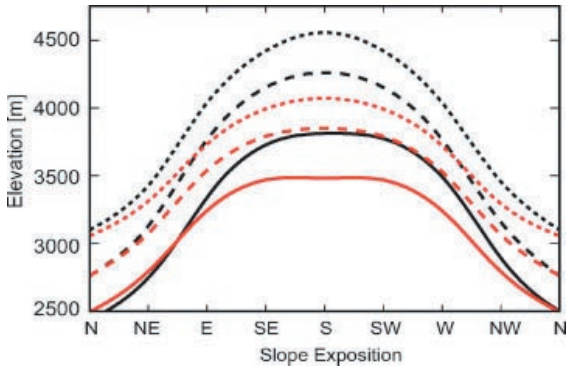

Plate 2 Mean elevation of the modelled (PEB_HC) 0°C isotherm for Corvatsch (black) and Jungfraujoch (red) and different slope angles: solid line, 90°; dashed line, 70°; dotted line, 50°.

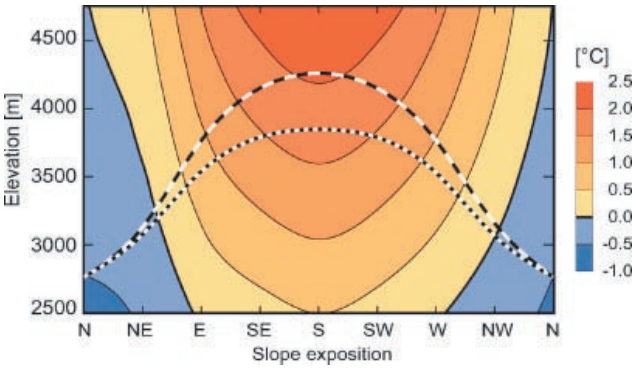

Plate 3 Difference in modelled (PEB_HC) mean annual surface temperature (1982–2002), Corvatsch–Jungfraujoch, for a slope angle of 70°. The dashed lines indicate the mean 0°C isotherm: long dashes, Corvatsch; short dashes, Jungfraujoch.

a.s.l. and for eight aspects (N, NE, E, . . . , NW). The same conditions as in the model verification were used. The depth discretization was 10 cm, having 200 nodes. The temperature profile at depth was initiated using the mean 1982 surface temperature followed by a two-year transient run with 1982 data before the 1982–2002 experiment to ensure realistic temperature distribution at depth.

Plate 1 shows the MAGT 1982–2002 for a slope steepness of 70°. The calculated temperatures have been averaged over the 21-year period and interpolated as a minimum curvature surface for better display. The thick dashed line indicates the elevation of the mean 0°C isotherm for the 21 years of this study. It approximates the limit of permafrost occurrence in rock walls as caused by the climatic conditions of that period. However, due to 20th century warming (Haeberli and Beniston, 1998; Beniston *et al.*, 1997; Diaz and Bradley, 1997) the actual lower limit of permafrost in rock walls is likely to be about 1.0°C or 150 m lower. This is due to possible remnants of inactive permafrost at greater depths within a rock face. Plate 2 shows the elevation of the modelled mean 0°C isotherm for both areas and other slope angles. Between slope angles of 90° and 50°, temperatures generally increase (and so the isotherm rises) with decreasing slope due to increased solar irradiation. The disturbance due to snow cover (Goodrich, 1982; Keller and Gubler, 1993; Zhang *et al.* 2001) that is not taken into account in this model increases at the same time, so the temperatures calculated for shallower slopes should be interpreted with care.

To illustrate the differentiation between the two locations, Plate 3 displays the difference between Corvatsch mean temperatures and Jungfraujoch mean temperatures modelled for a slope angle of 70°. Generally, the differences increase from north to south because they are related to short-wave radiation. The increase from lower towards higher elevations is caused by the growing importance of short-wave over long-wave radiation. Short-wave incoming radiation increases with elevation whereas long-wave incoming radiation decreases due to lower air temperature, air pressure, vapour pressure and other factors. The location of both 0°C isotherms is plotted in Plate 3 to underscore the aspect dependence of radiation-based differences in permafrost distribution.

Thin dashed lines in Plate 1 refer to the uppermost and lowermost mean annual 0°C isotherm between 1982 and 2002. These lines therefore separate three zones for this time interval: the zone of active permafrost (AP-zone; MAGST < 0 for all years); a transitional zone (T-zone; MAGST < 0 for some years) and the zone of seasonal frost (SF-zone; MAGST > 0 for all years). The vertical spread of these lines indicates the large inter-annual fluctuation of the MAGST and thus supports the combined approach of measurement and modelling used in this study.

CONCLUSION AND OUTLOOK

A combination of systematic rock-face near-surface temperature measurements and an energy-balance model has been employed to investigate rock-surface temperatures in the Swiss Alps. Spatial distribution patterns of rock-surface temperatures as well as ranges of their temporal fluctuation during 21 years have been revealed. The suitability of the energy-balance modelling approach in PEMEBAL for the simulation of ground temperatures in rugged terrain has been demonstrated.

Recently, scientific and public interest in the impact of climate change on the stability of perennially frozen slopes has increased and, thus, robust information on rock temperatures is required. In the Alps, the hot summer of 2003 resulted in increased depths of thaw and markedly increased rock-fall activity, especially on slopes exposed towards the north (Gruber *et al.*, 2004). This project lays the required basis for re-analysis of these events and for simulation of future scenarios and hazard zones.

The retreat of glaciers and the melt of ice faces change the temperature (and possibly also the hydrological) regime of many steep mountain-sides at an increasing speed. The tools developed here can assist the combined, quantitative assessment of ice/rock faces under transient conditions.

Large rock slopes usually have a complex structure comprising different slope angles, and as a consequence varying degrees of snow and debris cover. The near-vertical situation investigated in this paper and a talus slope or rock glacier can be regarded as two end-members of a continuum that characterizes most alpine rock walls. Further investigations of the distribution debris and snow cover in steep slopes and their effect on sub-surface temperatures are needed in order to understand and simulate temperatures realistically.

In 2003, the Swiss Permafrost Monitoring Network (PERMOS) initiated monitoring of rock-face temperatures routinely following the approach of this research programme. This will provide an opportunity for re-evaluation and further development of the model presented.

Based on the model put forward in this article, a more straightforward statistical model of rock temperatures is currently being designed and applied.

Northern slopes have the most abundant permafrost, and, at the same time the least spatial differentiation in rock temperature. This provides the opportunity to model a large proportion of existing rock-wall permafrost in Switzerland with relatively low computational effort and to estimate its total area.

ACKNOWLEDGEMENTS

The authors are grateful for the support given by the International Foundation High Altitude Research Stations Jungfraujoch and Gornergrat (HFSJG), the Corvatschbahnen cable car, the Gornergrat-Monte Rosa-Bahnen, the Matterhornbahnen and Burgergemeinde Zermatt. This project was funded by the Swiss National Science Foundation grant 'Analysis and Spatial Modelling of Permafrost Distribution in Cold-Mountain Areas by Integration of Advanced Remote Sensing Technology'. Project numbers 246979 and 21-63678.

REFERENCES

Aschwanden A, Beck M, Haeberli C, Haller G, Kiene M, Roesch A, Sie R, Stutz M. 1996. *Bereinigte Zeitreihen—Die Ergebnisse des Projekts KLIMA90*. Schweizerische Meteorologische Anstalt/MeteoSwiss: Zürich.

Beniston M, Diaz HF, Bradley RS. 1997. Climatic change at high elevation sites: an overview. *Climatic Change* **36**(3): 233–251.

Cermák V, Rybach L. 1982. Thermal conductivity and specific heat of minerals and rocks. In *Landolt–Börnstein Zahlenwerte and Funktionen aus Naturwissenschaften und Technik, Neue Serie, Physikalische Eigenschaften der Gesteine (V/1a)*, Angeneister G (ed.). Springer: Berlin; 305–343.

Coutard JP, Francou B. 1989. Rock temperature measurements in two Alpine environments: implications for frost shattering. *Arctic and Alpine Research* **8**(4): 399–416.

Davies MCR, Hamza O, Harris C. 2001. The effect of rise in mean annual temperature on the stability of rock slopes containing ice-filled discontinuities. *Permafrost and Periglacial Processes* **12**(1): 137–144.

Diaz HF, Bradley RS. 1997. Temperature variations during the last century at high elevation sites. *Climatic Change* **36**(3): 253–279.

Goodrich LE. 1982. The influence of snow cover on the ground thermal regime. *Canadian Geotechnical Journal* **19**: 421–432.

Gruber S, Hoelzle M. 2001. Statistical modelling of mountain permafrost distribution—local calibration and incorporation of remotely sensed data. *Permafrost and Periglacial Processes* **12**(1): 69–77.

Gruber S, Hoelzle M, Haeberli W. 2004. Permafrost thaw and destabilization of Alpine rock walls in the hot summer of 2003. *Geophysical Research Letters* **31**: doi:10.1029/2004GL020051.

Gruber S, Peter M, Hoelzle M, Woddhatch I, Haeberli W. 2003. Surface temperatures in steep Alpine rock faces—a strategy for regional-scale measurement and modelling. In *Proceedings of the Eighth International Conference on Permafrost 2003*. Swets & Zeitlinger: Zurich; 325–330.

Haeberli W, Beniston M. 1998. Climate change and its impacts on glaciers and permafrost in the Alps. *Ambio* **27**(4): 258–265.

Haeberli W, Wegmann M, Vonder Mühll D. 1997. Slope stability problems related to glacier shrinkage and permafrost degradation in the Alps. *Eclogae Geologicae Helvetiae* **90**: 407–414.

Hall K. 1997. Rock temperatures and implications for cold region weathering—I: new data from Viking Valley, Alexander Island, Antarctica. *Permafrost and Periglacial Processes* **8**: 69–90.

Hall K, André MF. 2001. New insights into rock weathering from high-frequency rock temperature data: an Antarctic study of weathering by thermal stress. *Geomorphology* **41**: 23–35.

Harris C, Vonder Mühll D, Isaksen K, Haeberli W, Sollid JL, King L, Holmlund P, Dramis F, Guglielmin M, Palacios D. 2003. Warming permafrost in European mountains. *Global and Planetary Change* **39**(3–4): 215–225.

Harris SA. 1996. Lower mean annual ground temperature beneath a block stream in the Kunlun Pass, Qinghai Province, China. In *Proceedings Fifth Chinese Permafrost Conference, Lanzhou*; 227–237.

Harris SA, Pedersen DE. 1998. Thermal regimes beneath coarse blocky material. *Permafrost and Periglacial Processes* **9**: 107–120.

Hoelzle M, Haeberli W. 1995. Simulating the effects of mean annual air temperature changes on permafrost distribution and glacier size: an example from the Upper Engadin, Swiss Alps. *Annals of Glaciology* **12**: 400–405.

Hoelzle M, Mittaz C, Etzelmüller B, Haeberli W. 2001. Surface energy fluxes and distribution models of permafrost in high mountain areas: an overview of current developments. *Permafrost and Periglacial Processes* **12**(1): 53–68.

Keller F, Gubler HU. 1993. Interaction between snow cover and high-mountain permafrost, Murtèl/Corvatsch, Swiss Alps. In *Proceedings of the Sixth International Conference on Permafrost, Beijing*, Vol. 1. South China University of Technology Press: Beijing; 332–337.

Kohl T. 1999. Transient thermal effects below complex topographies. *Tectonophysics* **306**: 311–324.

Lewkowicz AG. 2001. Temperature regime of a small sandstone tor, latitude 80 °N, Ellesmere Island, Nunavut, Canada. *Permafrost and Periglacial Processes* **12**(4): 351–366.

Matsuoka N, Hirakawa K, Watanabe T, Moriwaki K. 1997. Monitoring of periglacial slope processes in the Swiss Alps: the first two years of frost shattering, heave and creep. *Permafrost and Periglacial Processes* **8**(2): 155–177.

Matsuoka N, Sakai H. 1999. Rockfall activity from an alpine cliff during thawing periods. *Geomorphology* **28**: 309–328.

Mittaz C, Hoelzle M, Haeberli W. 2000. First results and interpretation of energy-flux measurements over Alpine permafrost. *Annals of Glaciology* **31**: 275–280.

Nötzli J, Hoelzle M, Haeberli W. 2003. Mountain permafrost and recent Alpine rock fall events: a GIS-based approach. In *Proceedings of the Eighth International Conference on Permafrost 2003, Zurich*. Swets & Zeitlinger: Zurich; 827–832.

Oke TR. 1987. *Boundary Layer Climates*, 2nd edn. Routledge: London.

Stocker-Mittaz C, Hoelzle M, Haeberli W. 2002. Modelling alpine permafrost distribution based on energy-balance data: a first step. *Permafrost and Periglacial Processes* **13**(4): 271–282.

Wegmann M. 1998. Frostdynamik in hochalpinen Felswänden am Beispiel der Region Jungfaujoch—Aletsch. *Mitteilungen der Versuchsanstalt für Wasserbau, Hydrologie und Glaziologie der ETH Zürich*, Switzerland.

Zhang T, Barry RG, Haeberli W. 2001. Numerical simulations of the influence of the seasonal snow cover on the occurence of permafrost at high latitudes. *Norsk Geografisk Tidskrift* **55**: 261–266.

Publication 4:

Interpretation of geothermal profiles perturbed by topography: the Alpine permafrost boreholes at Stockhorn Plateau, Switzerland

Citation:

Gruber, S., King, L., Kohl, T., Herz, T., Haeberli , W. and Hoelzle, M. (2004). Interpretation of geothermal profiles perturbed by topography: the Alpine permafrost boreholes at Stockhorn Plateau, Switzerland. Permafrost and Periglacial Processes, 15(4), 349-357.

Main findings:

- T(z) profiles from permafrost boreholes in complex topography are strongly modified by variable surface conditions as well as topography.
- Mean temperatures as well as gradients and T(z) profile curvature can vary strongly depending on the borehole location (within tens of meters horizontal) even in steady state.
- Negative temperature gradients are possible in steady state.
- Temperature histories from T(z) profiles in mountains can only be inverted successfully using special techniques for 3-dimensional conditions.
- The noise introduced to the profile by topography and variable surface conditions is likely in the same magnitude or greater than atmospheric warming during the 20th century. Derived temperature histories need to be interpreted with care.

PERMAFROST AND PERIGLACIAL PROCESSES
Permafrost and Periglac. Process. **15**: 349–357 (2004)
Published online in Wiley InterScience (www.interscience.wiley.com). DOI: 10.1002/ppp.503

Interpretation of Geothermal Profiles Perturbed by Topography: the Alpine Permafrost Boreholes at Stockhorn Plateau, Switzerland

Stephan Gruber,[1]* *Lorenz King,*[2] *Thomas Kohl,*[3] *Thomas Herz,*[2] *Wilfried Haeberli*[1] *and Martin Hoelzle*[1]

[1] Glaciology and Geomorphodynamics Group, Department of Geography, University of Zurich, Switzerland
[2] Institute for Geography, Justus-Liebig-University, Giessen, Germany
[3] Institute of Geophysics, ETH Zurich, Switzerland

ABSTRACT

The temperature regime of alpine permafrost is altered by the generally warmer atmospheric temperatures of recent decades. Eight boreholes, with depths between 100 and 130 m, have recently been drilled in European mountain permafrost as part of the Permafrost and Climate in Europe (PACE) project. They have been equipped with temperature sensors in order to better understand and quantify the effect of climate change on permafrost temperatures. Their interpretation with respect to signals of surface temperature histories is complicated by topographic effects. An apparent warming signal is present in all of the PACE boreholes but quantification of this effect in mountainous terrain remains difficult. The influence of topography and spatially-variable surface temperatures on temperature-depth profiles is demonstrated with measurements from the Stockhorn borehole and a simple model. A conceptual framework for the interpretation of topographically-disturbed temperature-depth profiles and the modelling of temperature histories based on these data is proposed. Copyright © 2004 John Wiley & Sons, Ltd.

KEY WORDS: mountain permafrost; borehole temperatures; climate change; ground surface temperature history; geothermal monitoring

INTRODUCTION

Two boreholes in perennially frozen bedrock have been drilled at Stockhorn Plateau in the southern Swiss Alps above Zermatt (Valais) within the framework of the European Union (EU)-funded project 'Permafrost and Climate in Europe (PACE): climate change, mountain permafrost degradation and geotechnical hazard'. They are part of the north-south (N-S) transect comprising eight drill sites, extending from the Mediterranean Spanish Sierra Nevada at 37° N, through several sites in the Alps, southern Norway and northern Sweden to polar latitudes in the Svalbard Archipelago at 78° N (cf. Harris *et al.*, 2001). The boreholes have been instrumented with a thermistor chain and with an automatic weather station.

Bedrock temperature-depth profiles (T(z)-profiles) in permafrost provide the basis for: (1) monitoring of ground temperatures and quantification of concurrent changes; (2) investigation and modelling of energy exchange and transfer processes in the shallow subsurface; and (3) modelling past climatic changes based on histories of the ground temperature regime that can be inferred from the T(z)-profiles. For several decades, T(z)-profiles from the arctic have been used to monitor and model changes in ground temperatures and climatic conditions (e.g. Lachenbruch and Marshall, 1986; Lachenbruch *et al.*, 1988; Osterkamp, 2003). This includes research on three-dimensional

* Correspondence to: Stephan Gruber, Glaciology and Geomorphodynamics Group, Department of Geography, University of Zurich, Winterthurerstrasse 190, CH-8057 Zurich, Switzerland. E-mail: stgruber@geo.unizh.ch

Received 25 November 2003
Revised 10 April 2004
Accepted 1 June 2004

effects below relatively flat topography such as the influence of lakes, buildings or the ocean on temperature fields at depth (Gold and Lachenbruch, 1973).

Temperature histories derived by inversion modelling based on T(z)-profiles are affected by several sources of error. These include: (1) advective heat transfer by fluid flow in bedrock, (2) changes in surface conditions (e.g. deforestation, changes in land use), (3) spatially-variable surface temperatures, (4) effects of latent heat, (5) topography, and (6) heterogeneities and anisotropy of the subsurface material properties.

In alpine permafrost, the effects of fluid flow and changes in surface conditions can be neglected. However, spatially-variable surface temperatures and topography (Kohl, 1999; cf. also Sergueev *et al.*, 2003) have a profound effect on the temperature distribution at depth, violating the common assumption of one-dimensional heat transfer. As a consequence, care must be taken in the interpretation of T(z)-profiles below rugged topography. The modelling of temperature histories based on geothermal data requires two- or three-dimensional inversion techniques in order to separate the transient signal from that induced by spatially-variable surface temperatures and topography. This ability to compensate topographic effects provides the possibility to extract information on the past climate in many mountain ranges of the world where available instrumental records are sparse and short, and at the same time, climatic changes are expected to be most pronounced (Barry, 1990; Diaz and Bradley, 1997; Haeberli and Beniston, 1998).

Results of the PACE network of instrumented boreholes contribute to the Global Terrestrial Observing System (GTOS) of the Global Climate Observing System (GCOS) as outlined by Cihlar *et al.* (1997).

The present paper characterizes the two boreholes at Stockhorn and provides a discussion of a full year's temperature data with emphasis on the clearly-visible effect of topography on the temperature profile. A conceptual framework for the interpretation of permafrost geothermal data below complex topography is also proposed.

THE FIELD SITE

The two drillholes are located on the Stockhorn Plateau (45°59′12″N, 7°49′27″E) above Zermatt, Valais, Swiss Alps at 3410 m a.s.l. (Figure 1). At the study site, the east-west (E-W) running mountain crest between Gornergrat and Stockhorn widens to a small plateau that is gently inclined to the south. It separates the steep glacier-covered north face of this crest from a non-glaciated southern face. Bedrock is part of the

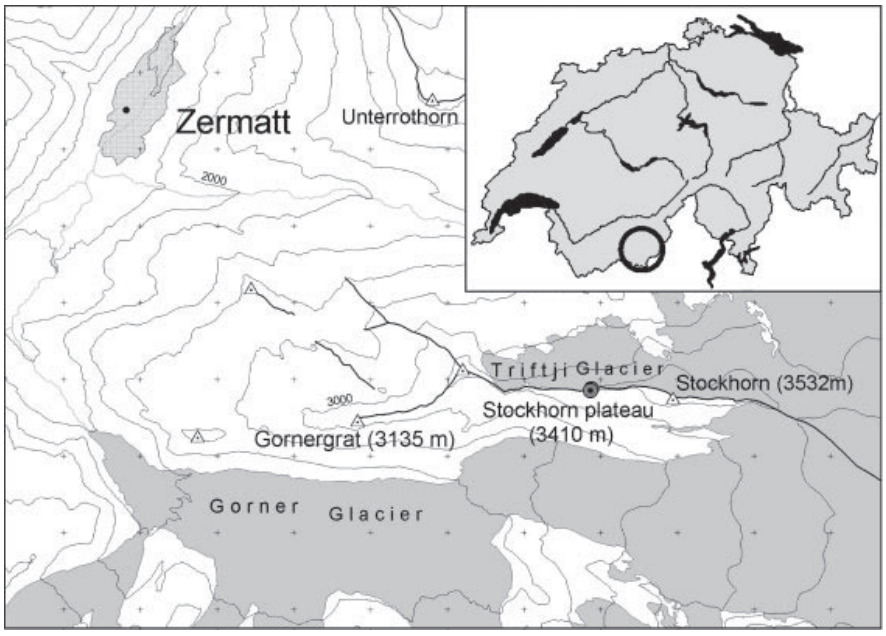

Figure 1 Overview map of the Zermatt area. The circle in the insert map shows the location of the project area within Switzerland.

palaeozoic crystalline Monte Rosa nappe and consists of Albit-Muskovit schist. Patterned ground has developed in the thin debris cover of the drill site area. Vegetation consists of isolated specimens of *Gentiana verna* and *Ranunculus glacialis* and boulders are only rarely covered with epipetric lichens, indicating that perennial snow patches might have been much larger in former times.

The Stockhorn-Gornergrat crest is surrounded by mountain ranges that exceed altitudes of 4000 m. This causes a local climate characterized by reduced cloud cover and high solar radiation. The annual precipitation in the Zermatt valley is relatively low and can be estimated to be 1500 mm at Stockhorn based on King (1990). A mean annual air temperature between −5 and −6°C is estimated for the drill site for 1961–1990 (based on Begert *et al.*, 2003; King, 1990). The top station of the Stockhorn funicular is in close proximity to the boreholes and facilitates easy access.

EQUIPMENT AND MEASUREMENT PROCEDURES

Borehole Drilling and Preparations

The two boreholes were drilled in July 2000 by a research team from Giessen University together with a private company. The 100.7 m 'deep hole' was located almost on top of the crest, whereas the 31 m 'shallow hole' is 28 m to the south, near the edge of the plateau (Figure 2). A 2-inch (50.8 mm) PVC-casing was inserted into the holes and the space between the PVC-tube and the bedrock was filled with concrete. For the uppermost 3 m a steel lining was used through the active layer for safety reasons. The top of the deep hole was secured with a metal protective cover screwed onto bedrock. A metal pipe with a lid has been inserted 40 cm into the ground at the top of the shallow hole and protrudes about 30 cm from the ground. Several days or weeks after the installation of the drill holes, concrete perforated the PVC-casing of the deep borehole and caused a blockage at 33 m depth. The obstacle was removed in December 2000, but material filled-up the lowest 2 m of the borehole due to these operations and the thermistor chain could subsequently be lowered to only 98.5 m in June 2001.

Thermistor Chains and Data Logging

Two thermistor chains with lengths of 100 m and 17 m, respectively, were manufactured with YSI 44006 NTC thermistors following PACE standards (cf. Harris *et al.*, 2001). Their relative accuracy is ± 0.02°C (further technical specifications in Isaksen *et al.*, 2001). Both thermistor strings were connected to a CR10X datalogger. Measurement intervals are 6 h (00, 06, 12 and 18 h) in the shallow borehole and for the upper 5m of the deep borehole. Thermistors below 5 m in the deep hole are recorded once a day. Data are regularly recorded since June 2001.

Climate Station

In June 2002 a meteorological station was installed next to the deep borehole. Data are recorded every 6 h

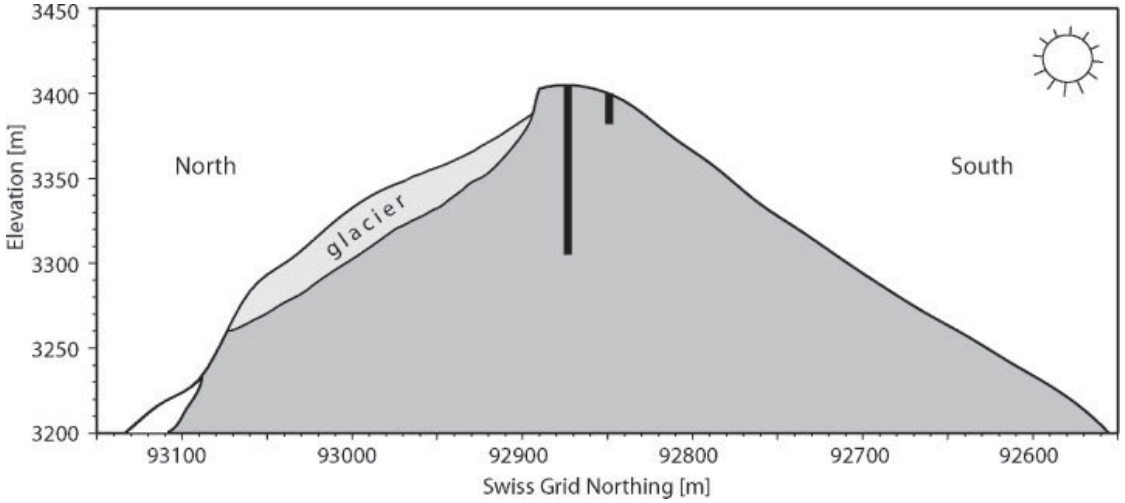

Figure 2 North-south transect through the Stockhorn ridge. Horizontal and vertical dimensions as well as thermistor chain position and depths are plotted to the same scale.

together with the borehole temperatures. The measured variables are: short-wave radiation (up- and down, 0.3–3 μm), long-wave radiation (up- and down, 5–50 μm), air temperature, relative humidity, wind direction, wind speed and snow cover height. These measurements allow investigations of the energy transfer processes at the surface and in the active layer. These processes 'translate' climatic signals into ground temperatures.

TEMPERATURE DATA 2001/2002

Thermal Profiles

A full year of data from 1 October 2001 to 30 September 2002 has been used for analysis and all statistics presented here refer to that period. Figure 3 shows a graph of the temperature profile of the deep borehole and its gradients.

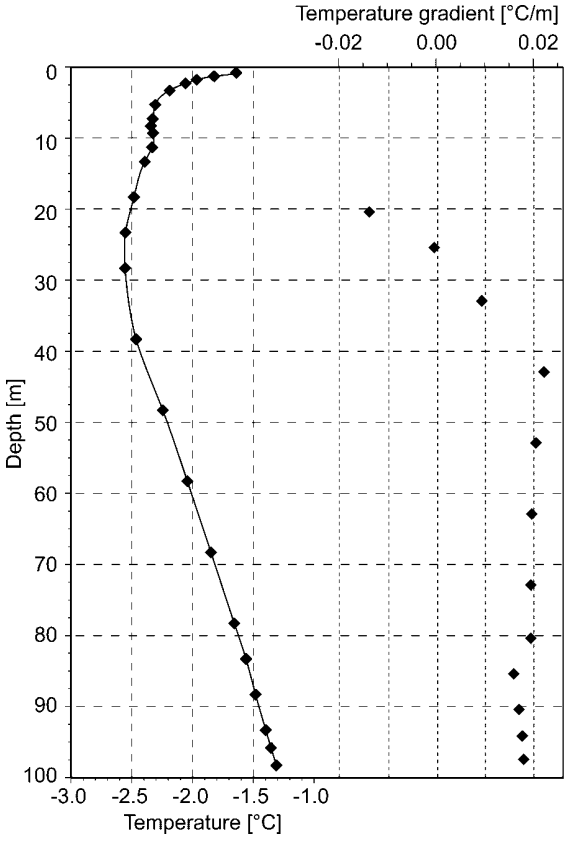

Figure 3 Temperature profile and gradient in the 100 m deep borehole on Stockhorn, Switzerland. Diamonds indicate measured mean annual temperatures (October 2001 to September 2002) and gradients calculated between them. The continuous line is a spline interpolation of the temperatures values.

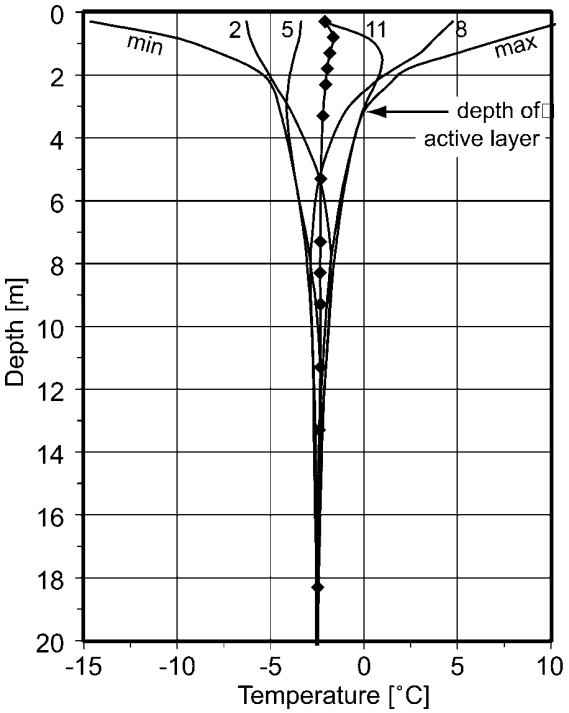

Figure 4 Temperatures and temperature envelope for the top 20 m of the 100 m deep borehole. Diamonds indicate the annual mean. Daily curves for 8 November 2001 (11), 8 February 2002 (2), 8 May 2002 (5), and 8 August 2002 (8) are shown.

The depth of zero annual amplitude (ZAA), where the annual temperature wave is attenuated to <0.1°C, is located at about 17.7 m in the deep hole. The mean annual ground temperature ($MAGT_{ZAA}$) is determined at this depth to be -2.5°C. Downward extrapolation of the gradient between 84 and 98 m suggests the permafrost thickness to be about 170–180 m. The uppermost 20 m of the profile in Figure 4 show the active layer thickness to be 3.1 m. Plate 1 displays temperature variations for some shallow sensors in the deep borehole. Note the long period of almost constant temperatures just below 0°C of the 3.3 m sensor. This so-called 'zero-curtain effect' is caused by transfer of latent heat during freezing and thawing of water contained in the rock or soil. All sensors in the active layer except the one at 0.3 m recorded a zero-curtain in autumn but not in spring, suggesting slow water removal by sublimation and transfer of water vapour along the temperature gradient below the snow. At the beginning of May, the sensors between 1.3 m and 3.3 m were almost isothermal at about -3.5°C

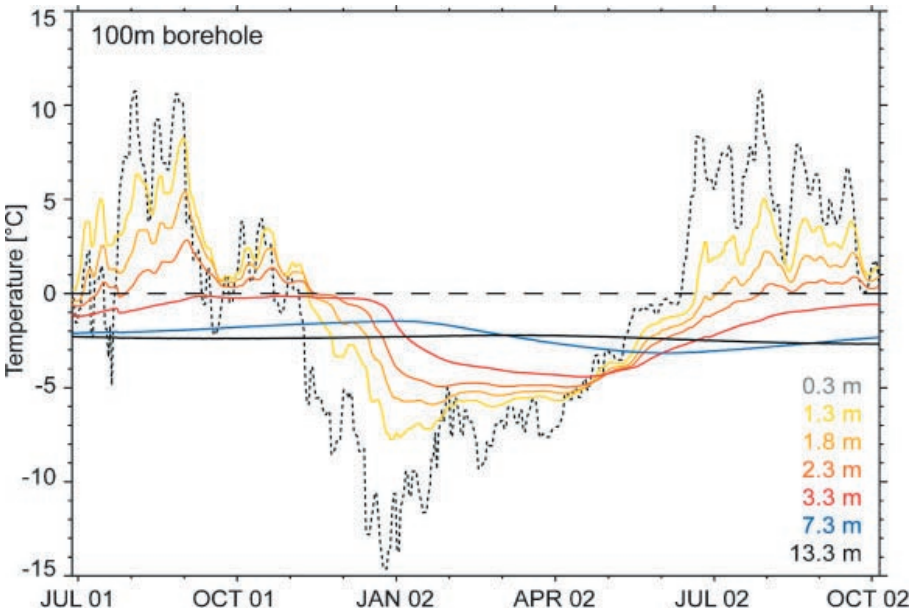

Plate 1 Daily temperature curves for shallow sensors of the 100 m deep borehole. Nearly isothermal conditions of the top 3.3 m in May 2002 indicate the BTS effect.

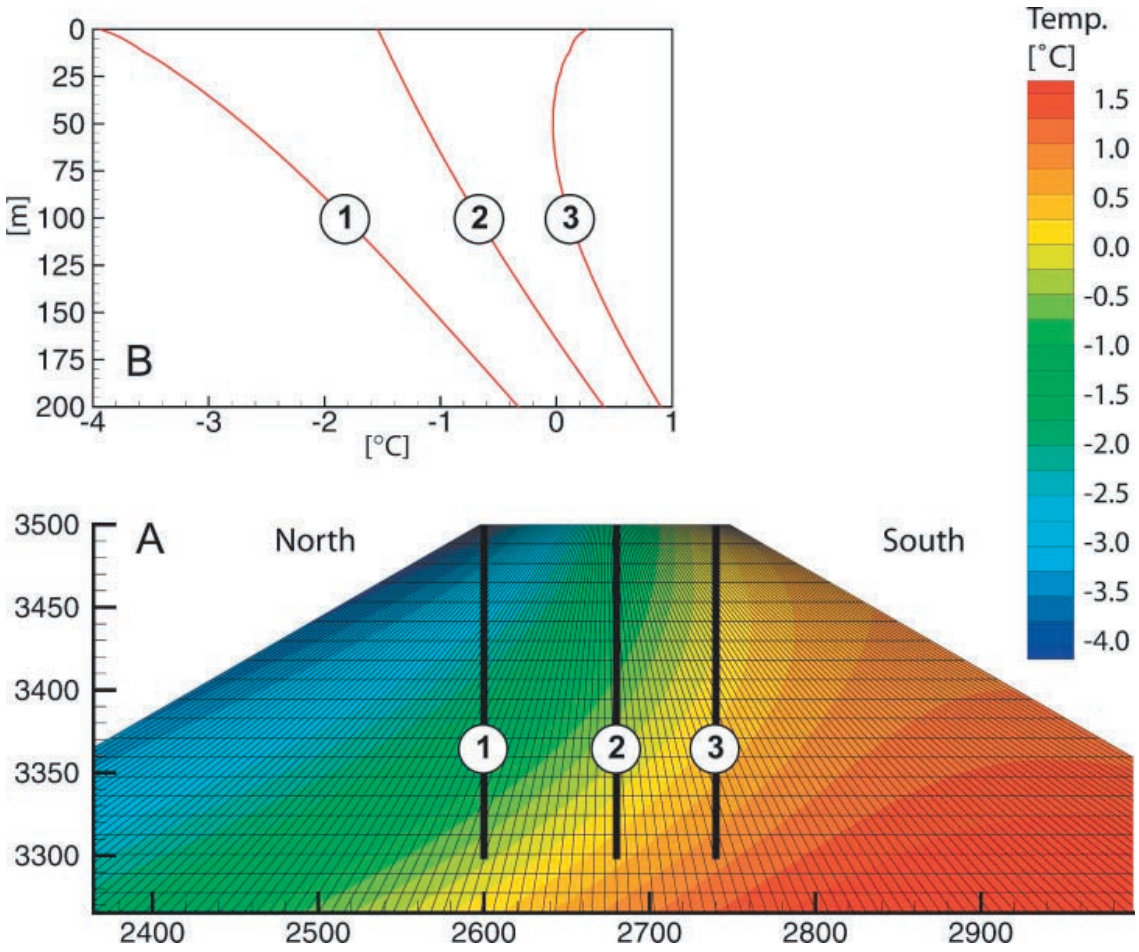

Plate 2 (A) Steady-state temperature distribution in a simplified geometry representing Stockhorn. (B) T(z) profiles extracted from the calculated temperature field for the hypothetical boreholes shown by vertical thick lines in A.

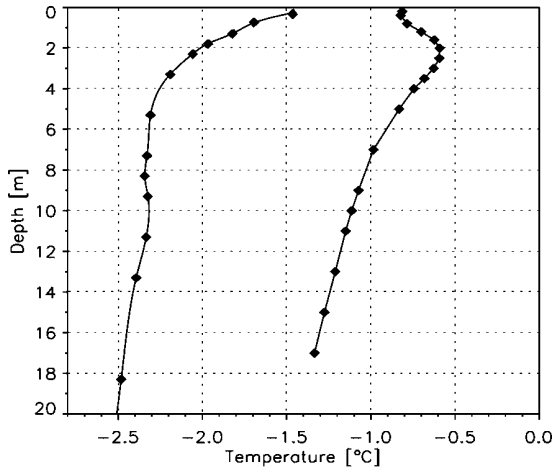

Figure 5 Mean temperature profiles of the two Stockhorn boreholes. The horizontal distance between holes is about 28 m. Left profile: deep hole; right profile: shallow hole.

suggesting insulation by a thick snow cover. This effect is also known from the bottom temperature of the snow (BTS) method (Haeberli, 1973). The mean temperatures between the surface and about 5 m depth in both profiles showed peculiar features (Figure 5). In the deep hole this was a strong warm-side deviation above 5 m. The shallow hole had the warmest mean temperature at around 2.5 m depth with decreasing temperatures above and below. These features may be caused by two reasons. (1) Borehole equipment: the protrusion of the protective covers through or into the winter snow cover effectively removes heat from the ground directly at the boreholes. In summer, the metal covers may actually warm the ground. The steel liner used in the upper 3 m of the boreholes also modifies the heat conduction at the top of the boreholes. At shallow depths, this perturbation can contribute strongly to the measured signal and cause a positive or negative mean temperature deviation. (2) Transient effects: the short time period of 1 year over which the temperature average has been calculated makes the possible influence of short term transient effects in the upper part of the profile large.

Climate Signals and Topographic Effects

The uppermost 30–40 m of the T(z)-profile in the deep hole (Figure 3) exhibit a pronounced warm-side deviation from a straight line that can be fitted to the temperatures of the lowermost sensors. At first sight this suggests a warming of 0.5 to 1.0°C at the ground surface during the last decades based on the upward extrapolation of deeper gradients. However, the evidence presented in this section suggests that great care has to be taken in the interpretation of geothermal data in complex topography. While the warm-side deviation of the upper part of the T(z) profile likely reflects warming, the quantification of this effect remains difficult and it may be both over- or underestimated without consideration of topographic effects.

Table 1 Comparison of the two temperature profiles. The gradients are calculated between 18.3 m and 3.3 m and 17 m and 3.5 m respectively.

	Deep hole 100 m	Shallow hole 30 m
ZAA	17.7 m	16.0 m
ALT	3.1 m	3.5 m
$MAGT_{ZAA}$	−2.5°C	−1.3°C
TTOP	−2.2°C	−0.7°C
Gradient	−0.019°C/m	−0.048°C/m
BTS	−3.5°C	−2.0°C

ALT refers to active-layer thickness and the BTS is estimated from the near-isothermal period of the topmost sensors. Other abbreviations defined in the text.

A cross-section through the top of Stockhorn is shown in Figure 2. Horizontal and vertical axes as well as the position, distance and depth of the boreholes are all shown at the same scale. Despite their horizontal distance of 28 m only, the temperature profiles (Figure 5) of the deep and the shallow borehole have distinct differences as summarized in Table 1. From these differences it is evident that the position of the borehole on the Stockhorn plateau has a major influence on its temperatures and temperature gradients at depth.

TWO DIMENSIONAL MODELLING

Modelling of rock temperatures below mountainous topography and variable surface temperatures helps to explore and visualize their effect on temperature profiles. To achieve this, the finite element (FE) program FRACTure (Kohl and Hopkirk, 1995) was used for forward modelling of rock temperatures in steady-state and with simplified boundary conditions. One of the features of this code is the integration of complex topography and surface conditions into a robust and well-tested numerical code.

Estimation of Boundary Conditions

A mean annual air temperature (MAAT) of −6°C at 3500 m a.s.l. and an environmental lapse rate of −0.0055°C/m is assumed (cf. King, 1990). This

temperature is modified by the input of solar radiation, active-layer processes and snow cover. The variation of near-surface temperatures with elevation is mostly due to the lapse rate of air temperature, whereas the N-S difference between ground temperatures is largely caused by differences in solar irradiation. Therefore, steep terrain exhibits larger lateral variation in temperatures than flat terrain. In addition, a thick and homogeneous snow pack that smoothes out lateral variations is not likely to form on steep slopes. Three sources of information are available for the estimation of the N-S variation of ground temperatures on Stockhorn: (1) the BTS can be regarded as a crude proxy of MAGT in the upper metres (the model described by Gruber and Hoelzle, 2001 predicts a N-S difference of about 3.5°C for the drill site); (2) measurements of rock temperatures in steep walls indicate 5–8°C difference between N and S (Gruber *et al.*, 2003); and (3) the measured difference in mean temperature at the top of permafrost (TTOP) between the two holes is about 1.5°C.

Considering the general slope steepness mostly between 33° and 42° for Stockhorn, the N-S difference in ground surface temperatures will be greater than that predicted by the BTS model (calibrated in more gentle terrain) but less than that measured in rock walls. The difference between northern and southern slopes was assumed therefore to be 4.5°C with −4°C in the northern and +0.5°C in the southern slope. This is in agreement with the measured difference of about 1.5°C in TTOP/MAGT between deep and the shallow boreholes and approximately reproduces the measured TTOP temperatures (Table 1). The glacier on the northern slope was neglected.

Model Run

The N-S transect through the E-W trending Stockhorn ridge shown in Figure 2 was approximated by a trapezium (Plate 2A) having a width of 150 m at the top, 30° steep flanks and an altitudinal range of 2000 to 3500 m. Below that, a rectangle down to −1000 m with a lower boundary condition heat flux of $80\,\mathrm{mW\,m^{-2}}$ and no heat transfer across the sides was generated. The boundary condition for the surface temperature of the mountain was given at the upper angles of the trapeze to be −4°C on the northern side and +0.5°C on the southern side. The temperature at the two lower angles was +4.25°C and +8.75°C, respectively. After generation of the FE mesh, boundary conditions for the surface elements were derived by linear interpolation between the angles of the trapezium. In the diffusive steady-state thermal energy equation the thermal conductivity is the only petrophysical parameter of importance. It was set to $3.0\,\mathrm{W\,K^{-1}\,m^{-1}}$ and directional isotropy was assumed.

Model Results

In Plate 2A the model result is displayed. The bent isotherms illustrate that there is a strong lateral heat flux from S to N. In Plate 2B, three temperature profiles retrieved from the model are shown. Although only 150 m apart in total, they all differ strongly in temperature and temperature gradients. Depending on the positioning of the borehole, the MAGT at a certain depth in the model can differ by several degrees. With standard assumptions on one-dimensionality, different degrees of transient warming or cooling could be misinterpreted. These differences in temperatures and temperature gradients predicted by the model can also be observed in the measured data (Figure 5). However, the model (Plate 2B, profile 1 or 2) did not reproduce the strong warming observed in the upper part of the measured profile (Figure 3).

INTERPRETING GEOTHERMAL DATA IN MOUNTAIN TOPOGRAPHY

The differences between the thermal profiles of the deep and the shallow holes (Figure 5 and Table 1), as well as the similarity of the measurements and the model underscore the importance of jointly treating topographic and transient effects when interpreting T(z) data measured in complex topography. Accurate knowledge of the spatial distribution of ground temperatures is needed for this treatment of topographic effects. In this context, the term ground surface temperature (GST), as used in the geothermal community is equivalent to the mean TTOP below which energy transfer is dominated by conduction. Above the top of permafrost the active layer together with seasonal snow cover represent a complex system that translates climatic variables into ground temperatures at depth. The active-layer depth, however, changes spatially and between years and the concept of TTOP is restricted to permafrost areas only. It is therefore more practical to use the MAGT at a certain depth, e.g. $MAGT_5$ at 5 m, as an equivalent of the term GST. This depth should be greater than the maximum active-layer thickness that is expected for most of the area under investigation.

Calculating $MAGT_X$ Histories

The derivation of estimates about $MAGT_X$ histories generally involves two problems: (a) to find a valid

physical model describing the subsurface heat flux and (b) to obtain a unique and stable $MAGT_X$ result from the T(z) data, based on that model. The physical model for mountain permafrost can be assumed to have negligible influence of fluid flow and to be influenced by topographic multi-dimensionality as well as spatially-variable $MAGT_X$.

For the inversion of $MAGT_X$ histories from T(z) data, Wang (1992) provides an overview of several approaches developed for one-dimensional cases. These approaches may be used only in cases with negligible topographic disturbance. In mountain topography, the information contained in a T(z) log is a complex superposition of spatially-variable temperature signals below a surface that has a distinctly different geometry than that assumed in the one-dimensional case. As a consequence, a fully three-dimensional, transient model is needed in the process of $MAGT_X$ estimation. This requires the parameterization of the spatial $MAGT_X$ boundary condition together with a function describing its behaviour in time. It is evident that this implies great uncertainties and involves a large number of assumptions. Therefore, only very robust approaches for $MAGT_X$ inversion should be used. Furthermore, the treatment of latent heat is of importance for transient models in warm permafrost (cf. Wegmann *et al.*, 1998).

For the estimation of $MAGT_X$ histories in topographically complex situations, Kohl and Gruber (2003) describe an inversion scheme based on the FE-forward code FRACTure and the computer program UCODE. In combination, UCODE and FRACTure perform inverse modelling, posed as a parameter-estimation problem, by calculating parameter values that minimize a weighted least-squares objective function using non-linear regression. With this tool complex multi-dimensional inversion studies can be theoretically accomplished and first results for a two-dimensional case study are reported by Kohl and Gruber (2003). However, numerical instability and non-uniqueness represent well-known problems in inverse modelling and obtaining useful results can become more difficult for highly heterogeneous conditions.

Interpreting $MAGT_X$ Histories

Histories of $MAGT_X$ inverted from T(z) profiles are a valuable indicator of the past evolution of the ground thermal regime. However, the $MAGT_X$ is distinctly different from the real surface or air temperatures (cf. Lachenbruch *et al.*, 1988). The buffer layer between the atmosphere and the top of alpine permafrost (including active layer and snow cover) is characterized by complex and spatially-variable processes of heat transfer. The quantitative understanding of these processes is still limited. Therefore, the deduction of climatic changes from the obtained $MAGT_X$ history is subject to large uncertainties and not straightforward. In particular, the seasonal snow cover in winter influences ground temperatures depending on timing, structure, duration and thickness (cf. Zhang *et al.*, 1996, 2001; Goodrich, 1982). Because the snow cover is highly variable in space (wind drift, avalanches, solar radiation) and time (inter-annual characteristics) only limited quantitative data on its role are available. Overall, it is a noisy parameter that is estimated to have a warming affect on ground temperatures of 1 to 4.5°C for the Alps (cf. Hoelzle *et al.*, 2003; Keller, 1994; Vonder Muehll *et al.*, 1998; Imhof *et al.*, 2000). The effect of changing snow characteristics may outweigh or compensate the effect of changing air temperatures in some instances.

DISCUSSION AND CONCLUSION

The presented measurements on Stockhorn demonstrate that the T(z) profile is heavily disturbed by topography. This effect could be reproduced in a simple model experiment demonstrating the coexistence of both positive (temperature increasing with depth) and negative near-surface geothermal gradients even in steady state. The value of geothermal monitoring in mountains is not affected by topographic effects, but for the interpretation of transient signals contained in the T(z) profile it is a major obstacle. A warming signal can be inferred from the data (along with all other PACE boreholes in more gentle topography), but its quantification remains difficult. The required separation of topographic and transient effects from geothermal profiles of alpine permafrost has two prerequisites: (1) an accurate description of the spatial field of $MAGT_X$ and (2) suitable modelling tools for three-dimensional inversion of T(z) profiles.

Research on the interpretation of geothermal data from the PACE network of permafrost boreholes is expected to promote the ability to handle three-dimensional effects. Improved guidelines for the selection and instrumentation of mountain permafrost drill sites are likely to evolve.

ACKNOWLEDGEMENTS

Funds for the drill holes and the measuring equipment came from the European commission (EU-project PACE, ENV4-CT97-0492). Generous logistic support

was provided by the railway companies Brig-Visp-Zermatt-Bahnen and the Gornergrat-Monte Rosa-Bahnen. The personnel of these companies and of other institutions such as the Kleinmatterhornbahnen and the Burgergemeinde Zermatt readily gave advice and support at innumerable times. Several students and friends helped with enthusiasm during field work, often under very unfavourable weather conditions. Thanks to all of them. The authors received valuable comments from two anonymous reviewers.

REFERENCES

Barry RG. 1990. Development changes in mountain climate and glacio-hydrological responses. *Mountain Research and Development* **10**(2): 161–170.

Begert M, Seiz G, Schlegel T, Musa M, Baudraz G. 2003. Homogenisierung von Klimamessreihen der Schweiz und Bestimmung der Normwerte 1961–1990, Schlussbericht des Projekts NORM 90. MeteoSchweiz, Zürich, Schweiz Veröffentlichungen 67.

Cihlar J, Barry TG, Ortega GE, Haeberli W, Kuma K, Landwehr JM, Norse D, Running S, Scholes R, Solomon AM, Zhao S. 1997. GCOS/GTOS plan for terrestrial climate-related observation. GCOS 32, version 2.0, WMO/TD-796, UNEP/DEIA/TR, 97-7.

Diaz HF, Bradley RS. 1997. Temperature variations during the last century at high elevation sites. *Climatic Change* **36**(3): 253–279.

Gold LW, Lachenbruch AH. 1973. Thermal conditions in permafrost—a review of North American literature. Permafrost: The North American Contribution to the Second International Conference, National Academy of Sciences, Washington D.C., Publication 2115, 3–23.

Goodrich LE. 1982. The influence of snow cover on the ground thermal regime. *Canadian Geotechnical Journal* **19**: 421–432.

Gruber S, Hoelzle M. 2001. Statistical modelling of mountain permafrost distribution—local calibration and incorporation of remotely sensed data. *Permafrost and Periglacial Processes* **12**(1): 69–77.

Gruber S, Peter M, Hoelzle M, Woddhatch I, Haeberli W. 2003. Surface temperatures in steep Alpine rock faces—a strategy for regional-scale measurement and modelling. In *8th International Conference on Permafrost, Proceedings*, Phillips M, Springman S, Arenson L (eds). Swets & Zeitlinger: Lisse, Zürich; 325–330.

Haeberli W. 1973. Die basis- temperatur der winterlichen Schneedecke als möglicher Indikator für die Verbreitung von permafrost. *Zeitschrift für Gletscherkunde und Glazialgeologie* **9**(1–2): 221–227.

Haeberli W, Beniston M. 1998. Climate change and its impacts on glaciers and permafrost in the Alps. *Ambio* **27**(4): 258–265.

Harris C, Haeberli W, Vonder Muehll D, King L. 2001. Permafrost monitoring in the high mountains of Europe: the PACE Project in its global context. *Permafrost and Periglacial Processes* **12**(1): 3–11.

Hoelzle M, Haeberli W, Stocker-Mittaz C. 2003. Miniature ground temperature data logger measurements 2000–2002 in the Murtel-Corvatsch area; Eastern Sviss Alps. In *8th International Conference on Permafrost, Proceedings*, Phillips M, Springman S, Arenson L (eds). Swets & Zeitlinger: Lisse, Zürich; 419–424.

Imhof M, Pierrehumbert G, Haeberli W, Kienholz H. 2000. Permafrost investigation in the Schilthorn massif, Bernese Alps, Switzerland. *Permafrost and Periglacial Processes* **11**: 189–206.

Isaksen K, Holmlund P, Sollid JL, Harris C. 2001. Three deep alpine-permafrost boreholes in Svalbard and Scandinavia. *Permafrost and Periglacial Processes* **12**(1): 13–25.

Keller F. 1994. Interaktionen zwischen Schnee und Permafrost- Eine Grundlagenstudie im Oberengadin. *Mitteilungen der Versuchsanstalt für Wasserbau, Hydrologie und Glaziologie der ETH Zürich*, 127.

King L. 1990. Soil and rock temperatures in discontinuous permafrost: Gornergrat and Unterrothorn, Wallis, Swiss Alps. *Permafrost and Periglacial Processes* **1**: 177–188.

Kohl T. 1999. Transient thermal effects below complex topographies. *Tectonophysics* **306**: 311–324.

Kohl T, Gruber S. 2003. Evidence of paleotemperature signals in mountain permafrost areas. *Extended abstract volume, 8th International Conference on Permafrost 2003, Zurich, Switzerland*.

Kohl T, Hopkirk RJ. 1995. 'FRACTure' a simulation code for forced fluid flow and transport in fractured porous rock. *Geothermics* **24**(3): 345–359.

Lachenbruch AH, Marshall BV. 1986. Changing climate: geothermal evidence from permafrost in the Alaskan Arctic. *Science* **234**: 689–696.

Lachenbruch AH, Cladouhos TT, Saltus RW. 1988. Permafrost temperature and the changing climate. In *Permafrost, Fifth International Conference on Permafrost*, vol. 3, Senneset K (ed.). Tapir Publishers: Trondheim, Norway; 9–17.

Osterkamp TE. 2003. Establishing long-term permafrost observatories for active-layer and permafrost investigations in Alaska: 1977–2002. *Permafrost and Periglacial Processes* **14**(4): 331–342.

Sergueev D, Tipenko G, Romanovsky V, Romanovskii N. 2003. Mountain permafrost thickness evolution under the influence of long-term climate fluctuations (results from numerical simulation). In *8th International Conference on Permafrost, Proceedings*, Phillips M, Springman S, Arenson L (eds). Swets & Zeitlinger: Lisse, Zürich; 1017–1021.

Vonder Mühll D, Stucki T, Haeberli W. 1998. Borehole temperatures in alpine permafrost: a ten years series. *Proceedings, Seventh International Conference on Permafrost*, June 23–27, 1998, Yellowknife, Canada.

Centre d'études nordiques, Université Laval, Nordicama 57, 1085–1096.
Wang K. 1992. Estimation of ground surface temperatures from borehole data. *Journal of Geophysical Research* **97**: 2095–2106.
Wegmann M, Gudmundsson GH, Haeberli W. 1998. Permafrost changes in rock walls and the retreat of Alpine glaciers: a thermal modelling approach. *Permafrost and Periglacial Processes* **9**: 23–33.
Zhang T, Osterkamp TE, Stamnes K. 1996. Influence of the depth hoar layer of the seasonal snow cover on the ground thermal regime. *Water Resources Research* **32**(7): 2075–2086.
Zhang T, Barry RG, Haeberli W. 2001. Numerical simulations of the influence of the seasonal snow cover on the occurence of permafrost at high latitudes. *Norsk Geografisk Tidskrift* **55**: 261–266.

Publication 5:

Imaging spectrometry in high-alpine topography: the derivation of accurate broadband albedo

Citation:

Gruber, S., D. Schläpfer, and M. Hoelzle. 2003. Imaging spectrometry in high-alpine topography: the derivation of accurate broadband albedo. Pages 196-205 in M. Habermeyer, editor. 3rd Intl. Workshop on Imaging Spectroscopy. EARSeL, Herrsching, Germany.

Main findings:

- Airborne imaging spectrometer data in rugged topography can be ortho-rectified to pixel accuracy using the parametric geocoding software PARGE.
- After topographic-atmospheric corrections using ATCOR strong BRDF effects are visible in the resulting image (HDRF-hemispherical-directional reflectance factors) and need to be corrected for the derivation of ground properties such as albedo.
- A kernel-based BRDF model can be fitted to a group of pixels from only one image line using local illumination, viewing and relative azimuth angles determined with respect to the local surface normal.
- Angular anisotropy of a surface results in actual differences for the surface energy balance. A different albedo for north- and south-facing slopes can result from identical surfaces.

Erratum:

The coefficients of determination (R^2) stated in Section 9.2 “BRDF-model variations: shape versus brightness” in fact refer to coefficients of correlation (R).

Imaging Spectrometry in High-Alpine Topography: The Derivation of Accurate Broadband Albedo•

Stephan Gruber[a] , Daniel Schläpfer[b] and Martin Hoelzle[a]

[a] Glaciology and Geomorphodynamics Group, Department of Geography, University of Zurich, Winterthurerstr. 190, CH-8057 Zurich, Switzerland, email: stgruber@geo.unizh.ch
[b] Remote Sensing Laboratories, Department of Geography, University of Zurich, Winterthurerstr. 190, CH-8057 Zurich, Switzerland

ABSTRACT

Three flight lines over high-alpine terrain have been recorded with the imaging spectrometer DAIS7915 in August 2002. The aim of this campaign was the derivation of broadband albedo to support distributed energy-balance modelling. The data was successfully ortho-rectified and a vicarious calibration as well as topographic-atmospheric correction were performed. To enable the derivation and investigation of black-sky and white-sky albedo, two-parameter kernel-based BRDF models were fitted to subsets. Coupling of these BRDF-models with the energy-balance code PERMEBAL suggests a significant influence of angular anisotropy on net radiation in complex topography. Comparison of modeled and measured time series of albedo show a good representation of its temporal evolution, but a large offset between the ground measurements and the BRDF model inversions is present.

Keywords: Albedo, BRDF, mountains, block surface, imaging spectrometry, energy-balance modeling

1 INTRODUCTION

Albedo is defined as the reflected fraction of incident radiation. It is therefore one of the most important factors that influence the ground surface energy-balance. For models of boundary layer processes and atmosphere-ground interactions it is one of the most sensitive surface characteristics to be measured or parameterized. This paper describes the derivation of broadband short-wave albedo from DAIS7915 hyperspectral imagery over complex alpine terrain together with corresponding sensitivity studies. As this work is aimed at the provision of data to a specific model, a short description of that model together with its purpose is provided.

PERMEBAL [1],[2] is a model of atmosphere-cryospere interaction in high-mountain regions developed at the University of Zurich in recent years. Due to the enhanced magnitude of global climatic change in mountain systems [3],[4] and its expected influence on natural hazards [5] the development of corresponding models is presently receiving growing attention. PERMEBAL simulates daily vertical energy-balances for each cell of a two-dimensional grid, based on spatial data on surface characteristics and daily meteorological time series. The model typically operates on cell sizes of 10-50m. The build-up as well as the melting of the winter snow cover are successfully simulated [6]. During summer, snow-free conditions and high solar elevation result in strong energy input into the ground. Then, snow-free albedo (a spatially variable surface characteristic) greatly affects short-wave net radiation. It is therefore desirable to investigate and describe spatial data fields of summer albedo.

A verification campaign and sensitivity analyses with PERMEBAL show that the current level of absolute accuracy is better than ±1 °C for mean annual surface temperatures in steep rock walls of different expositions. Modeled and measured daily time series at 14 locations are correlated to 60-90%. A deviation of ±1 °C corresponds to an absolute error in albedo of ±0.05-0.08 (or 25-35% relative) for areas of medium insolation, assuming an otherwise perfect model. However, these errors contain both the effect of an estimated uniform albedo at each point and the errors inherent in the model algorithms. The absolute accuracy in the final albedo product therefore should be better than ±0.05.

The aim of this study is the derivation of a spatial data field of snow-free albedo and estimate its errors. The effect that the solar incidence-angle dependence of albedo has on net radiation in complex topography needs to be investigated at this level of accuracy. Furthermore, this campaign will provide first experience with preprocessing and correction of imaging spectrometer data in complex terrain.

• Presented at the 3rd EARSeL Workshop on Imaging Spectroscopy, Oberpfaffenhofen, May 13-16 2003

2 BACKGROUND AND METHODS

The reflective behavior of most natural surfaces is variable both spectrally and angularly, i.e. as a function of illumination and measurement geometry. This surface behavior is mathematically described by the bidirectional reflectance distribution function (BRDF) [7] for each wavelength. Spectral albedo or bihemispherical reflectance (following the naming conventions put forward in [8]) in one waveband also depends on the angular distribution of incident radiation due to the angular anisotropy in most BRDFs. Broadband albedo is furthermore influenced by the spectral characteristic of incident light due to the spectral integration of narrowband albedos.

Several BRDF models have been developed to describe the behavior of the bidirectional reflectance in appropriate and simple mathematical terms. A review is provided by [9]. Using several measurements under varying illumination and viewing geometries, appropriate models may be selected and their parameters fitted. Subsequently, these models describe the reflectance for angles that have not been measured. In kernel-based models [10]-[12], the BRDF is expanded into a linear sum of terms (the so-called kernels), characterizing different scattering modes. The model parameters are the weights assigned to each kernel in the linear sum. The derivation of albedo from a kernel-based model characterizing the BRDF of a target is described in detail by [10]. The two extreme cases of completely diffuse and isotropic illumination (white-sky albedo) and completely direct illumination (black-sky albedo) are differentiated. Black-sky albedo is the directional-hemispherical integral of the BRDF model and therefore a function of the solar incidence angle. White-sky albedo is the bihemispherical integral of the BRDF model and a constant for a given wavelength. Natural illumination conditions are always intermediate values between these two cases, assuming the diffuse fraction of illumination to be isotropic. Finally, broadband albedo is derived by integration of spectral albedos over the desired waveband, weighted by the illuminating spectral solar flux.

For meteorological applications, albedo usually refers to the waveband between about 300 and 2500nm wavelength, covering most of the average solar irradiation at ground level. Other definitions ranging up to 3000 or 5000nm exist. Wavelengths shorter than 300nm are effectively absorbed by ozone. Beyond 2500nm, solar irradiance is minimal and largely absorbed by atmospheric water. Short-wave albedo is determined by dividing the measurements of two pyranometers, one for the downwelling and one for the upwelling radiative flux. Each measures over the solid angle 2π (a full hemisphere). The glass domes over the sensors are usually opaque to radiation outside the 300-3000nm band.

3 FIELD SITE

The Corvatsch area is situated in the south-east of Switzerland, close to the town of St. Moritz at latitude: 46° 26´ and longitude: 9° 50´. The area lies between 1800 and 3700m a.s.l and is characterized by steep slopes, and high mountain features such as glaciers and extensive block fields in the periglacial zone. The area has been one of the prime sites for the investigation of permafrost and periglacial processes during the last 30 years [13] and research here benefits from a wealth of base data as well as easy access by cable car.

4 MEASUREMENTS

On 14 August 2002, three flight lines (Table 1) were recorded with the imaging spectrometer DAIS7915 [14] under perfectly cloudless sky. Areas above 3000m a.s.l. were snow-covered due to recent snow fall. A DGPS base station has been operated for the post-processing of the aircraft path. A Reagan Solar Radiometer was used to support characterization of the atmosphere and a GER 1500 spectro-radiometer was used to collect field spectra during the overpass.

Table 1. Details of DAIS7915 flight lines acquired on 14 August 2002 over Corvatsch, Switzerland.

	Time UTC	Image lines	Scan frequency	Flight elevation	Flight heading	Solar elevation	Solar azimuth	Clouds	Cast shadow
Line 1	10:05	1865	11.5Hz	6040m	358°	53.7°	146.1°	none	0.8%
Line 2	09:52	2094	13.0Hz	6040m	358°	52.2°	140.9°	none	1.4%
Line 3	10:20	2370	14.5Hz	6040m	358°	54.9°	151.4°	none	0.6%

Two targets of 30*30m were characterized by more than 200 measurements each using an ASD FieldSpec Pro Fr spectro-radiometer, several days before the overpass. Finding homogenous areas of that size is extremely difficult in the periglacial zone. An almost horizontal moraine surface and a scree slope with a slope angle of about

30° were selected. Both targets had virtually no vegetation cover and are expected not to have changed their reflective behavior between the field measurement and the data flight. For the moraine target this assumption has been verified with the GER1500 measurement during the overpass.

Since 1997, a meteorological station is recording up- and downwelling short-wave radiation on the rock glacier Murtèl using two Kipp & Zonen CM3 pyranometers. Their spectral range is 300-3000 nm and the accuracy for daily totals of either sensor is reported by the manufacturer to be ±10%. The combined uncertainty in the albedo is believed to be better than ±10% because the usual accuracy of these sensors is known to be better than the value stated by the manufacturer.

5 PREPROCESSING

5.1 Geometric Correction

The DAIS7915 imagery has been geometrically corrected using the software packacge PARGE [15]. Ground control points (GCP) were taken from digital maps and orthophotos. The digital elevation model with a final pixel size of 10m has been generated photogrammetically. The PARGE quality control parameters listed in Table 2 indicate the successful achievement of pixel-accuracy. In complex topography this carries special significance as illumination and viewing geometries as well as surface characteristics are laterally extremely variable.

Table 2. Quality control parameters of PARGE processing indicate pixel-accuracy. INS: inertial navigation system.

	No of GCPs	Offset INS attitude		Offset DGPS flight path	
		RMS (roll)	RMS (pitch)	RMS (X)	RMS (Y)
Line 1	39	4.47 m	4.27 m	4.53 m	4.30 m
Line 2	25	4.54 m	4.70 m	4.63 m	4.41 m
Line 3	18	3.26 m	4.04 m	3.43 m	4.14 m

Almost each final pixel contained a real measurement due to the large across-track over-sampling of DAIS7915. The final image cube was generated by assigning nearest measurements to each pixel. This resulted in many imaging spectrometer measurements being lost, while preserving original, measured spectra.

5.2 Radiometric Quality

In order to verify the quality of the recorded imagery, a quality assessment based on visual inspection and image statistics was performed using the radiance values of the laboratory-calibrated image cube. In all three flight lines striping is visible for the bands 41-45 and 59-72, which are all part of spectrometer 3. In bands 1-19, about 5% of all pixels are saturated due to fresh snow exceeding the sensors dynamic range. Negative radiance values are caused by errors in the sensor or by inadequate calibration and are thus indicative of problematic channels. Most bands of the spectrometer 3 (SWIR-2) have between 10 and 45% negative pixels (Figure 2). The fluctuations in negative pixel abundance per band are small (2-7%) between flight lines, suggesting a rather stable cause of error. Only bands 52,53,55 and 56 always have less than 5% of negative values.

Noise can be estimated from homogeneous targets in the image cube and thus an order of magnitude for the signal to noise ratio (SNR) of each band can be established to support data quality control. A target of deep water was selected on lake Silvaplana assuming it to be spectrally flat at the ground instantaneous field of view (GIFOV) of around 10m. The noise was calculated as the standard deviation of the signal minus its 3x3 boxcar average for 25,000 pixels. Using a region of 165,000 pixels, the mean and standard deviation of the expected signal range for rock surfaces and alpine meadows has been determined, excluding very low values of water bodies and very high or saturated values for snow. The thus calculated SNR (Figure 1) represents a rather high estimate, as noise levels from water likely underestimate true noise levels in brighter targets. Nevertheless, a comparison of individual channels is facilitated.

Combining the above evidence, only the reflective channels 1-36, 38 and 39 are of satisfactory quality. However, for supporting the derivation of broadband albedo, the four best SWIR-2 channels 52, 53, 55 and 56 are used as well, adding up to a total of 42 used bands.

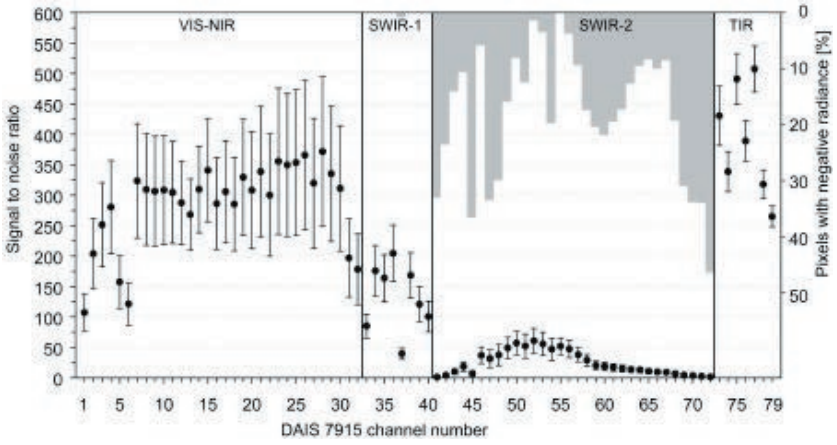

Figure 1. Image-based signal-to-noise ratio and the percentage of negative pixels (gray columns, right axis). The bad performance of the SWIR-2 spectrometer is evident.

5.3 Atmospheric and Topographic Correction, Vicarious Calibration

Atmospheric-topographic correction has been performed using the software package ATCOR4 [16]. A standard atmosphere with rural aerosol type and water vapor content of 10g/cm² (sea level to space) and 80km visibility have been employed. The resulting reflectance values are nadir-corrected hemispherical-directional reflectance factors (HDRF, cf. [8]), assuming Lambertian behavior.

Comparison of these HDRF spectra to ground spectro-radiometric measurements and library clear-water spectra revealed unacceptably large errors in the laboratory calibration of DAIS7915. A vicarious two-point calibration has been performed using the bright moraine and the deep clear water of lake Silvaplana as targets.

6 ALBEDO RETRIEVAL

6.1 Fitting of BRDF Kernels

For the fitting of kernel-based BRDF models, the solar incidence angle (θ_0), the view angle (θ_S) and the relative azimuth angle (ϕ') need to be known. In complex mountain topography, these vary considerably over short distances. The angles θ_0 and θ_S are determined between the surface normal and the vectors to the sun and the sensor, respectively. The relative azimuth is the angle between the projection of the vectors to the sun/sensor onto the plane perpendicular to the surface normal. This relies on the assumption, that for our area of interest the angular properties of a tilted surface remain the same as for the horizontal case. For e.g. forest, this assumption would not be valid as trees grow vertically on a steep slope and not normal to it. BRDF model fits are calculated using the algorithms and code described by [9] based on AMBRALS (Algorithm for Modis Bidirectional Reflectance Anisotropy of the Land Surface) developed by [12] for the MODIS BRDF and albedo product [10].

Fitting of a BRDF model to each pixel or very few pixels is not feasible since only one or two observations are available for each pixel and the geometry will be affected by noise that is always present in digital elevation model derivatives in complex topography. Therefore, adequate subsets of the image are used for the derivation of a BRDF model. This model then represents the mean reflectance and the mean BRDF shape for the chosen subset. This model can be used for a) investigating the role of angular anisotropy in complex terrain and b) defining the BRDF model for every pixel of the subset using a multiplicative correction. This correction however relies on two hypotheses that need to be tested: 1) the BRDF model adequately characterises each pixel of the subset and 2) the shape of the BRDF does not change significantly within the chosen subset.

For lines 1 and 2, masks for a) alpine meadows; b) vegetation-free blocks and moraines and c) the rock glacier Murtèl were derived. The small Murtèl mask was generated manually, while the others were based on a spectral angle mapper classification. Several kernels and kernel combinations were tested on the data (spectral HDRFs and the angles θ_0, θ_S and ϕ' for each pixel) sampled within these masks. The three-parameter model comprising an isotropic, a volume-scattering, and a geometrically-scattering kernel generally performed badly resulting in mostly negative weights for the geometric kernel. A two-parameter model was chosen. In almost all cases, the combination

between isotropic and RossThick [11],[12] kernels performed best. Especially on block fields it is surprising to see the volume scattering kernel outperform the geometric one.

Each model fit results in two coefficients per band together with a value for R^2 for the fit per band. The R^2 value contains both the error in the model fit in terms of its shape as well as the error due to brightness variations within the class.

6.2 Derivation of Spectral Albedo from BRDF Kernel Models

Following the approach described by [10], spectral black-sky and white-sky albedos can be obtained using the pre-computed directional-hemispherical and bihemispherical kernel integrals, the derived model coefficients and the solar incidence angle.

6.3 Narrowband to Broadband Conversion

The derivation of broadband albedo involves the weighted integration of narrowband albedos. The weights for each band are proportional to the irradiant energy in the waveband represented by that measurement. The weights as well as the result of this integration are therefore a function of the spectral characteristics of the illumination. The method used for interpolation between measured bands and extrapolation outside the measured wavelengths influences the result significantly. Especially the extrapolation assumptions for blue and UV light are very sensitive and can affect the broadband albedo in the range of ±5-10%. In our approach, the extrapolation into the UV range is achieved by a multiplying the spectral albedo of the shortest wavelength by 0.8.

The irradiance spectra shown in Figure 2 were simulated using MODTRAN 4.0 [17]. As black-sky and white-sky albedo mark two extreme cases of illumination conditions, the weights for their integration from spectral albedos are also determined separately, assuming that with increasing diffuse radiation also the spectral characteristics change. The weights for direct illumination are determined from a clear-sky spectrum with a solar zenith angle of 30° and the weights for diffuse illumination from a spectrum assuming a position surrounded by a stratus cloud.

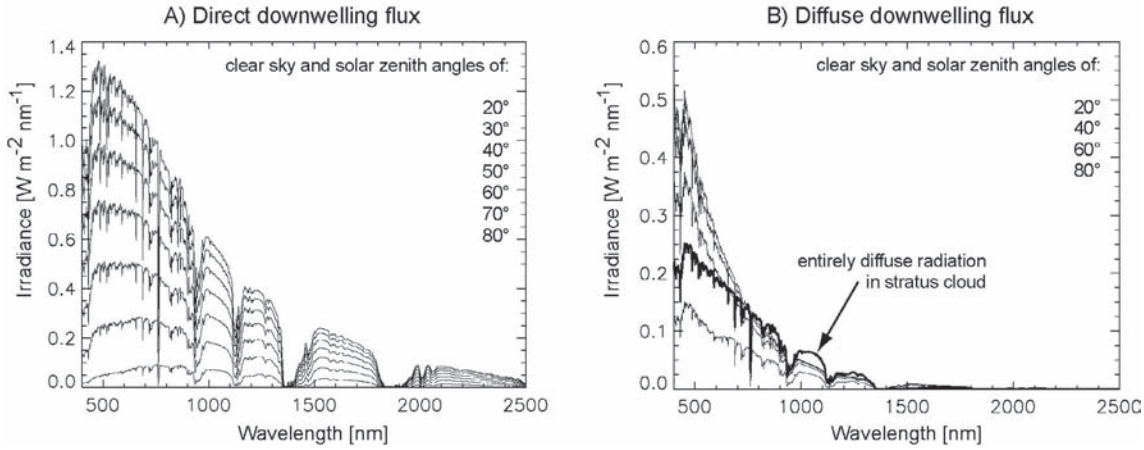

Figure 2. Spectra of the downwelling short-wave flux. A) direct radiation; B) diffuse radiation.

7 SENSITIVITY ANALYSIS FOR BRDF-MODEL DERIVED ALBEDO IN STEEP TOPOGRAPHY

Now that mean BRFD models have been derived based on subsets, these models can be used to investigate the influence of angular anisotropy on net radiation in steep terrain. The question is: how big is the difference in effective albedo between a northern slope (generally large solar incidence angles, large proportion of diffuse illumination) and a southern slope, given exactly the same surface characteristics? The magnitude of this difference in relation to the targeted accuracy determines whether a constant value for albedo suffices or albedo needs to be parameterised by an angular model.

Based on hourly standard meteorological data on global radiation from the station Corvatsch made by the Swiss Meteorological Service, the radiation regime for different slopes was parameterised for 1999 using the algorithms

implemented in PERMEBAL. The algorithm proposed by [18] and verified in the test area by [2] is used to parameterise the ratio of direct and diffuse radiation. Calculating the solar illumination geometry and sky-view factors as described in [2], hourly total short-wave insolation is parameterised for slopes of 0°, 10°, 20°, 30°, 40° and 50°, north-facing and south-facing. The calculated parameters are: solar incidence angle (in relation to surface normal), diffuse radiation and direct radiation. Table 3 summarizes the model results.

Table 3. Mean annual percentage of direct short-wave downwelling radiation (% direct) and annual mean of daily short-wave downwelling radiation totals (sw-down [W/m²]) for the modeled slopes.

slope	**50° N**	**40° N**	**30° N**	**20° N**	**10° N**	**0°**	**10° S**	**20° S**	**30° S**	**40° S**	**50° S**
% direct	42.9	43.1	43.3	42.5	44.1	47.2	49.4	50.9	53.1	53.7	53.5
sw down	160.6	162	163.6	165.5	169	170.8	186.5	198.6	206.6	210.4	209.4

Black-sky albedo was calculated for every hour and slope angle based on the BRDF models for the rock glacier Murtèl as well as alpine meadows and the modeled solar incidence angle. The percentage of direct and diffuse radiation determines the weights for black and white-sky albedo in the calculation of hourly net radiation. The so derived one-year time series were compared by defining the mean annual BRDF-derived albedo as: the total annual short-wave upwelling radiation over the total annual short-wave downwelling radiation. This is a radiation-weighted averaging of albedo which also reflects the net effect on the surface energy balance. Figure 3 illustrates the deviation of this effective mean annual BRDF-derived albedo from the white-sky albedo that is a possible constant substitute for it (solid lines). Dashed lines are calculated only from 15 July to 15 September, assuming a snow cover during winter. In order to demonstrate that the observed anisotropy does not originate from different weights used for the diffuse and direct spectral integration, one model run was performed with equal spectral integration weights for diffuse and direct radiation (blocks, equal weights).

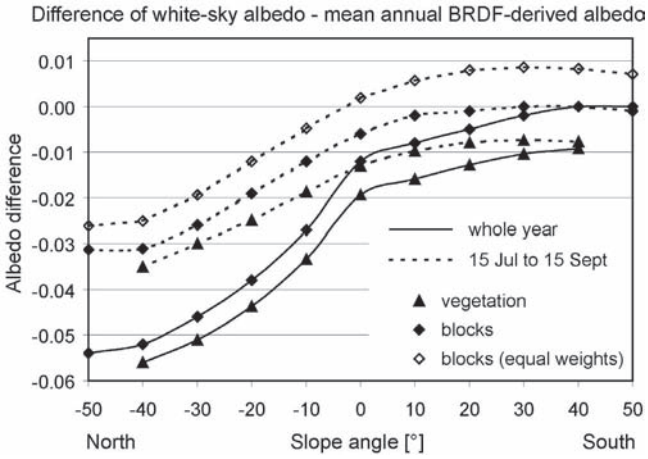

Figure 3. Difference of white-sky albedo and mean annual BRDF-derived albedo for different slope angles. Negative angles indicate northern slopes, positive angles southern slopes. See text for further details.

This illustrates, that an absolute error of up to -0.05 (25% relative error) in albedo has to be taken into account when neglecting its angular anisotropy. This indicates, that BRDF effects may significantly influence the ground - surface radiation balance.

8 IMAGE CORRECTION

The derivation of albedo for each image pixel (or for subsets) requires a correction procedure that applies the BRDF model inversion to each measurement; cf. [9] for detailed treatment of this problem. The basic assumption is the adequate representation of the real angular behaviour of each image (global or subset) pixel by the kernel-based model. Two applications are investigated here: 1) multiplicative BRDF-normalization 2) scaling of black- and white-sky albedo to measured image HDRF values.

The multiplicative correction factor is obtained by dividing the kernel-model result for the chosen geometry (desired θ_0, θ_S=0 and ϕ'=0) by the model result for the geometry of the imaging spectrometer measurement. The multiplication of the measured HDRF with this factor will perform a BRDF-normalization of the image. The corrected image shows the expected nadir HDRF for every pixel if the image was recorded in flat topography.

After the derivation of black- and white-sky albedo from the BRDF model, these need to be scaled to the observed HDRF values if albedo per pixel is desired without sufficient angular measurements in one pixel. The underlying assumption is a linear scaling of the BRDF-model integrals. The correction factor is determined by division of the measured HDRF by the value predicted by the kernel-model. Black and white-sky albedo can be scaled using this factor.

9 VALIDATION

9.1 Comparison of flight lines 1 and 2

Figure 4 provides a visual impression of the pre-processed imagery as well as of the results of the BRDF-normalization and the albedo retrieval. Band 20 of lines 1 and 2 was combined into a checkerboard mosaic.

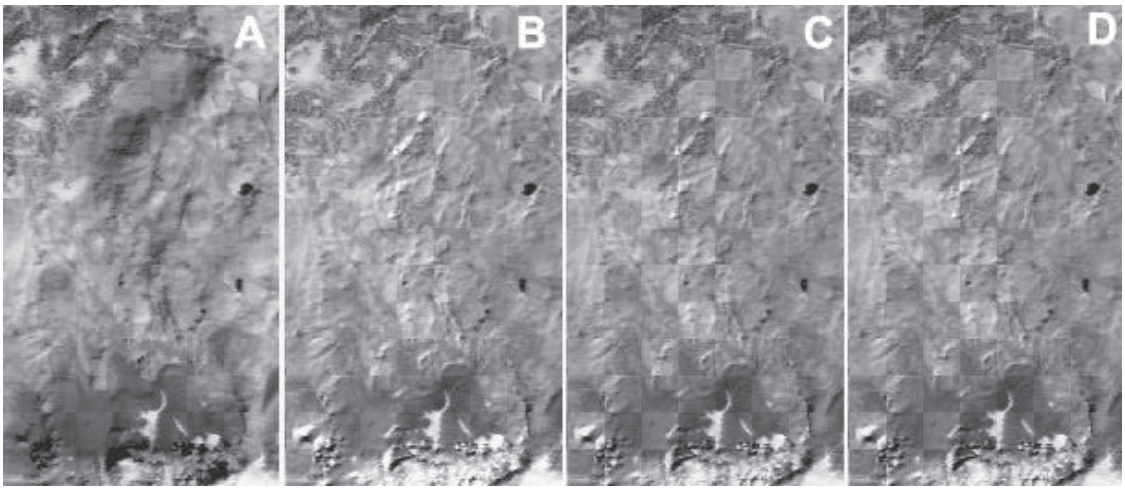

Figure 4. Visual comparison of lines 1 and 2 in a checkerboard mosaic of band 20. A) geometrically corrected data; B) result of topographic-atmospheric correction using ATCOR4; C) BRDF-normalized image and D) white-sky albedo

The successful correction of dark low-illumination areas during topographic-atmospheric processing as well as a reduction of the bright BRDF-effects by the BRDF-normalization are discernible in Figure 4. However, it is also visible that the checkerboard pattern becomes more prominent with increasing processing level and the extraction of higher-value data products. This visualizes the degree of misrepresentation of reality in the models used. Ideally, the images should become more alike during processing which is aimed at retrieving surface characteristics. Table 4 provides a preliminary comparison between lines 1 and 2 at different processing stages.

Table 4. Comparison of lines 1 and 2 at different processing levels and for subsets of blocky surfaces and alpine meadows. B-norm: BRDF-normalized, albedo: white-sky albedo

	Coefficient of correlation between images				**Relative difference between image means**		
Subset	**geo**	**atmo**	**nadir**	**albedo**	**atmo**	**B-norm**	**albedo**
Blocks	0.95	0.87	0.79	0.79	15.0%	20.7%	21.5%
Vegetation	0.93	0.84	0.71	0.75	10.8%	12.2%	12.6%

9.2 BRDF-model variations: shape versus brightness

The scaling of albedo derived from the inversion of BRDF models relies on an adequate representation of the BRDF of individual pixels by the model derived from an image subset. To test the hypothesis of shape constancy, random samples of 200 pixels were taken from the used subsets and a BRDF model fitted. The result of 200 of such experiments were aggregated to provide an idea of the subset-internal variation in BRDF shape. The R^2 describes the goodness of fit for the model. The means, standard deviations, minima and maxima for all 200 random experiments are calculated. The same statistics are provided for the shape of the model, defined by the ratio of the weights in the two kernel model. The total model brightness is given by the sum of both kernel weights. To relate the error in shape to an error in the inversion result, the white-sky integral is calculated from the kernel model using weights that represent the whole range of encountered shapes, while preserving its brightness. This approximates the shape-related error in white-sky albedo. The above parameters are shown for each used band in Figure 5.

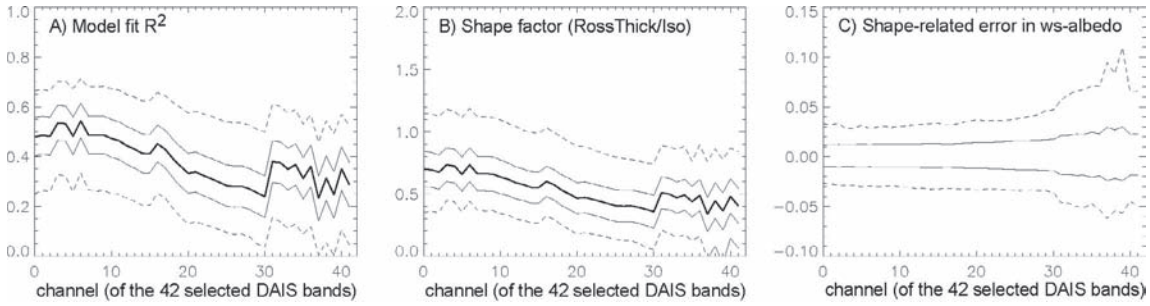

Figure 5. The variation of BRDF model shape within a subset of blocky surfaces in line 1 and its consequence on the derived white-sky albedo. Values are determined from 200 model inversion of 200 random samples each. Thick line: mean values; thin line: mean ± 1 Stdev; dotted line: min/max values. The shape-related error in white-sky albedo is given in absolute terms.

Table 5 provides an overview of the means over all bands for the parameters shown in Figure 5. Lines 1 and 2 were investigated using data taken from subsets representing blocky surfaces and alpine meadows. The error in white-sky albedo is given in relative terms.

Table 5. Indication of the variation of BRDF model shape within different subsets and its consequence on the derived white-sky albedo. Values are determined from 200 model inversion of 200 random samples each.

	No of Points	Model fit R^2	Standard deviation of R^2	Shape factor	Relative st. deviation of shape	White sky relative error
Line1_block	13821	0.384	± 0.080	0.534	23.6%	6.2%
Line2_block	20195	0.168	± 0.088	0.297	62.9%	11.7%
Line1_veg	54808	0.348	± 0.074	0.698	25.2%	7.4%
Line2_veg	35388	0.273	± 0.085	0.537	37.1%	9.4%

9.3 Comparison of modelled and measured broadband albedo

A BRDF model has been fitted for the rock glacier Murtèl independently for lines 1 and 2 based on a subset of 280 pixels as described in section 6. Inversion of this model was used to derive hourly albedo for a northern slope of 10° as described in section 7. This enables the comparison of a modeled and measured time series of albedo at the meteo station on Murtèl. For the snow-free period from 15 July to 15 September 1999, the measured albedo is 0.164; line 1 results in 0.197 and line 2 in 0.230. The differences in mean albedo are +0.03 (+20.2%) for line1 and +0.07 (+40.7%) for line 2. The difference between lines is 15.7% The calculated albedo was not scaled to the meteo station pixel to avoid the influence of noise. The subset used for the model generation has a standard deviation of ± 7% in the image corrected albedo. Despite this offset between modelled and observed albedo, the temporal evolution of albedo is represented well (Figure 6).

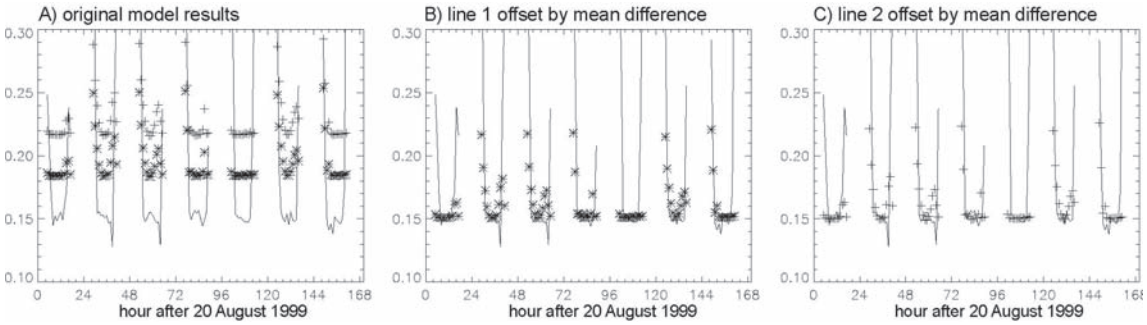

Figure 6. Comparison of measured broad-band albedo (line) with BRDF-model derived albedo for line 1 (x) and line 2 (+). A absolute values; B+C) simulated values offset by mean difference to illustrate successful modeling of temporal albedo changes

10 DISCUSSION OF ERRORS

In section 9 large differences between the means of subsets of lines 1 and 2 were shown. These differences are no lessened but amplified in the process of atmospheric and BRDF correction. It is assumed, that at least in part this is a problem of sensor stability.

In Section 7, it has been demonstrated, that the approximation of albedo by a constant (e.g. white-sky albedo) can result in an underestimation of albedo by 15-25% for steep slopes. The shape-related error in white-sky albedo here is in the order of 6-12%. Therefore it appears feasible to fit and invert a BRDF model and subsequently scale i to each image pixel.

The relative difference between image means presented in section 9.1 can be used as an indication of the standard deviation in the final albedo product being 13-22%. This would indicate, that the accuracy requirements defined for use in the model PERMEBAL are just met.

The large offset between modelled and measured albedo shown in 9.3 is striking. Even more so, because the difference between albedo derived from line 2 and measured albedo is largest, despite the fact, that vicarious calibration has been performed on line 2. Part of this deviation may be explained by the errors for the pyranometers and by the extreme heterogeneity of Murtèl Rock glacier. Nevertheless, an albedo of 0.23 appears to be rather large and open questions about the reason for his offset remain.

11 CONCLUSION

To the knowledge of the authors, this campaign has been the first time to employ airborne imaging spectrometry over such complex terrain. The successful geometric correction has been demonstrated. The complex topography results in a much larger range and much larger variability of sun-target-sensor geometries. As a consequence correction of the effects of atmospheric interaction, varying illumination and angular anisotropy is much more important than in gently sloping terrain, if the quantitative extraction of surface characteristics is desired. At the same time, this correction is greatly affected by noise in the digital elevation data that is used for correction. The fundamental problem of adequate representation of surfaces and the generation of its derivatives is amplified by errors introduced by inaccurate spatial co-registration.

It was demonstrated, that kernel-based BRDF models could successfully be fitted on subscenes and the information so gained applied for the derivation of albedo for each pixel.

Coupling of an image-derived BRDF model with the radiation module of the energy-balance program PERMEBAL revealed, that angular anisotropy has a significant influence on the ground surface energy balance

ACKNOWLEDGMENTS

This project has been carried-out in the Swiss National Foundation project "Analysis and spatial modeling of permafrost distribution in cold-mountain areas by integration of advanced remote sensing". Further support has been provided by the EU-program HySens. Dr. Andreas Kaeaeb kindly provided the digital elevation model used Many thanks to Gabriela Schaepman-Strub and especially Dr. Stefan Dangel for their help and discussions on the

treatment of angular anisotropy. The authors also whish to thank Dr Rolf Richter and Stefanie Holzwarth of the German Aerospace Center (DLR) for their cooperation and help throughout this study.

REFERENCES

[1] STOCKER-MITTAZ, C., HOELZLE, M., AND HAEBERLI, W. 2002: Modelling Alpine permafrost distribution based on energy-balance data: a first step. *Permafrost and Periglacial Processes 13*, pp 271-282.
[2] MITTAZ, C., HOELZLE, M., AND HAEBERLI, W. 2000: First results and interpretation of energy flux measurements of Alpine permafrost. *Annals of Glaciology 31*, pp 275-280.
[3] WANNER, H., GYALISTRAS, D., LUTERBACHER, J., RICKLI, R., SALVISBERG, E. & SCHMUTZ, C. 2000: Klimawandel im Schweizer Alpenraum. *Final Report of the Swiss National Research Program 31*, vdf, Hochschulverlag AG, ETH Zürich, 296 pp.
[4] OHMURA, A., BENISTON, M., ROTACH, M., TSCHUCK, P., WILD, M. AND MARINUCCI, M. 1996: Simulation of Climate Trends over the Alpine Region. *Final Report of the Swiss National Research Program 31*, vdf, Hochschulverlag AG, ETH Zürich, 285 pp
[5] HAEBERLI, W., KÄÄB, A., HOELZLE, M., BÖSCH, H., FUNK, M., VONDER MÜHLL, D. AND KELLER, F. 1999: Eisschwund und Naturkatastrophen im Hochgebirge. *Final Report of the Swiss National Research Program 31*, vdf Hochschulverlag an der ETH Zürich. 190 pp.
[6] MITTAZ, C., IMHOF, M., HOELZLE, M., AND HAEBERLI, W. 2002: Snowmelt evolution mapping using an energy balance approach over alpine terrain. *Arctic, Antarctic and Alpine Research 34(3)*, pp 274-281.
[7] NICODEMUS, F.E., RICHMOND, J.C., HSIA, J.J., GINSBERG, I.W. AND LIMPERIS, T. 1977: Geometrical Considerations and Nomenclature for Reflectance, U.S. Department of Commerce, National Bureau of Standards.
[8] MARTONCHIK, J.V., BRUEGGE, C.J. AND STRAHLER, A.H. 2000: A review of reflectance nomenclature used in remote sensing. *Remote Sensing Reviews*, Vol. 19, pp. 9-20.
[9] BEISL U. 2001: Correction of Bidirectional Effects in Imaging Spectrometer Data. PhD Thesis, *Remote Sensing Series* 37, RSL, University of Zurich, pp. 189.
[10] LUCHT, W., C.B. SCHAAF, AND A.H. STRAHLER. 2000: An Algorithm for the retrieval of albedo from space using semiempirical BRDF models. *IEEE Trans. Geosci. Remote Sens*., 38, 977-998.
[11] ROUJEAN, J-L., M. LEROY, AND P-Y. DESHAMPS. 1992: A bidirectional reflectance model of the earth's surface for the correction of remote sensing data. *J. Geophys. Res*., 97(D18), pp 20455-20468.
[12] WANNER, W., LI, X., & STRAHLER, A. 1995: On the derivation of kernels for kernel-driven models of bidirectional reflectance. *J. Geophys. Res*, 100(D10), pp 21077-21089.
[13] HOELZLE, M., VONDER MÜHLL, D. AND HAEBERLI, W. 2002: Thirty years of permafrost research in the Corvatsch-Furtschellas area, Eastern Swiss Alps: a review. *Norwegian Journal of Geography*. 56(2), 137-145.
[14] STROBL, P., NIELSEN, A., LEHMANN, F., RICHTER, R. AND MUELLER, A. 1996: DAIS System Performance, First results from the 1995 Evaluation Campaigns. *Proc. 2nd International Airborne Remote Sensing Conference and Exhibition, San Francisco*, Vol. II, pp. 325-334.
[15] SCHLÄPFER, D. AND RICHTER, R. 2002: Geo-atmospheric Processing of Airborne Imaging Spectrometry Data Part 1: Parametric Orthorectification. *International Journal of Remote Sensing,* 23, pp. 2609-2630.
[16] RICHTER R. AND SCHLÄPFER D. 2002: Geo-atmospheric Processing of Airborne Imaging Spectrometry Data Part 2: atmospheric/topographic correction. *International Journal of Remote Sensing*, 23, pp. 2631-2649.
[17] BERK, A., BERNSTEIN, L.S., ANDERSON, G.P., ACHARYA, P.K., ROBERTSON, D.C., CHETWYND, J.H. AND ADLER-GOLDEN S.M. 1998: MODTRAN Cloud and Multiple Scattering Upgrades with Application to AVIRIS. *Remote Sens. Environ*. 65, pp. 367-375.
[18] COLLAR-PEREIRA, M. AND RABL, A. 1979. The average distribution of solar radiation correlations between diffuse and hemispherical and between daily and hourly insolation values. *Solar Energy 22*, pp 155-164.

Publication 6:

Estimating BRDF and albedo of coarse debris surfaces from hyperspectral imagery in rugged topography using single flight lines

Citation:

Gruber, S., Dangel, S., Schläpfer, D. and Itten, K. 2004, to be submitted. Estimating BRDF and albedo of coarse debris from hyperspectral imagery in rugged topography using single flight lines.

Main findings:

- A kernel-based BRDF model could be fitted to HDRFs from single flight lines over complex topography explaining 4-7% of the observed variance, always yielding non-negative kernel weights.
- Broadband albedo could be derived with an approximate accuracy of ±16%.
- Approximation of angularly-dependent albedo with the constant white-sky albedo results in an error below ±5% for most coarse blocky surfaces in the test area.
- The correction of BRDF effects is needed for the derivation of albedo but the inclusion of an angular parameterization scheme for albedo into the energy-balance model is of minor importance.
- The overall uncertainty of ±16% in the albedo product corresponds to an error in simulated temperature of less than ±0.2 °C for most topographic situations.

Estimating BRDF and albedo of coarse debris surfaces from hyperspectral imagery in rugged topography using single flight-lines

Stephan Gruber, Stefan Dangel, Daniel Schläpfer, Klaus Itten

ABSTRACT

The derivation of albedo from remote sensing data in rugged terrain requires the correction of the effects of the atmosphere, variable illumination and angularly anisotropic reflectance. DAIS7915 imagery was used to fit kernel-based BRDF models in high-mountain topography using single flight lines alone. These BRDF models could be applied to the original image in order to obtain albedo values for each pixel. Comparison of two overlapping lines as well as illumination angles are used to assess the model performance. A BRDF model has been included into the radiation module of a surface energy-balance model in order to investigate the importance of angular anisotropy of albedo in rugged terrain. The accuracy of the overall process is estimated to be about ±16% for albedo retrieval whereas the approximation of the angularly-dependent black-sky albedo by white-sky albedo causes an error of less than ±5%.

INTRODUCTION

Albedo is defined as the reflected fraction of incident radiation. It is one of the most important factors that influence the ground surface energy-balance. For models of boundary layer processes and atmosphere-ground interactions it is an important and sensitive surface property to be measured or parameterized.

Engineering problems and natural hazards arising from the thaw of permafrost (Haeberli and Beniston 1998, Harris et al. 2003, Gruber et al. 2004a) in mountain areas have lead to the development and application of synoptic energy-balance models (Stocker-Mittaz et al. 2002, Gruber et al. 2004b) for the transient simulation of ground temperatures in complex topography. Geometric effects on illumination as well as the duration of snow cover (Mittaz et al. 2002) are presently parameterized in these models. During summer, however, when the energy input into the ground and its spatial variation are largest the albedo is unknown.

In mountain landscapes the spatial variability of surface characteristics is high. At the same time, the derivation of albedo from remote sensing data is complicated by the effects of variable and extreme illumination geometries as well as by angularly anisotropic reflectance (cf. Schaaf et al. 1994, Combal and Isaka 2002). This paper describes the derivation of BRDF model parameters and spatial data fields of broadband short-wave albedo from single flight lines of DAIS7915 hyperspectral imagery over complex alpine terrain aimed at the use in spatial energy-balance models. Furthermore, the errors inherent in the derivation of albedo and the approximation of actual (angularly anisotropic) albedo by a constant value (e.g. white-sky albedo) are roughly quantified and compared to the sensitivity of the energy-balance model.

BACKGROUND AND METHODS

The reflective behavior of most natural surfaces is variable both spectrally and angularly, i.e. as a function of illumination and measurement geometry. This surface behavior is mathematically described by the bidirectional reflectance distribution function (BRDF) (Nicodemus et al. 1977) for each wavelength. The albedo or bihemispherical reflectance (For a review on nomenclature see: Martonchik et al. 2000) in one waveband therefore also depends on the angular distribution of incident radiation. Broadband albedo is furthermore influenced by the spectral characteristics of incident light due to the spectral integration of narrowband albedos.

The derivation of albedo from remote sensing data in complex topography requires a topographic-/geo-atmospheric correction in order to remove the effects of variable illumination and to obtain ground reflectance. In this process, however, it becomes evident that angular effects are quite strong and the reflectances that are calculated under the assumption of Lambertian behavior reflect changes in geometry rather than changes in surface characteristics. This leads to two conclusions: 1) a BRDF correction is necessary for the derivation of albedo; and 2) the angular anisotropy of albedo is likely important for the surface energy-balance in mountain topography and, therefore, knowledge of the BRDF is required.

While multiple flight lines are desirable in order to have multiple measurements and measurement-geometries for each pixel these are often not available. Having only a single flight line, only one observation is available for each pixel and, as a consequence, information on the BRDF can only be derived from a group of pixels belonging to the same surface type. This model then represents the mean reflectance and the mean BRDF shape for the chosen subset and can be applied to every pixel. This process however relies on the hypothesis that the BRDF model adequately characterizes each pixel it is applied to (i.e. the shape of the BRDF does not change significantly within the chosen subset).

A large number of BRDF models have been developed to describe the behavior of the bidirectional reflectance in appropriate and simple mathematical terms (Beisl 2001). Using several measurements under varying illumination and viewing geometries, appropriate models may be selected and their parameters fitted. Subsequently, these models are used as a substitute for the reflectance for angles that have not been measured. In kernel-based models (Roujean et al. 1992, Wanner et al. 1995, Lucht et al. 2000), the BRDF is expanded into a linear sum of terms (the so-called kernels), characterizing different scattering modes. The model parameters are the weights assigned to each kernel in the linear sum. The derivation of albedo from a kernel-based model characterizing the BRDF of a target is described in detail by Lucht and co-workers (2000). The two extreme cases of completely diffuse and isotropic illumination (white-sky albedo) and completely direct illumination (black-sky albedo) are differentiated. Black-sky albedo is the directional-hemispherical integral of the BRDF model and therefore a function of the solar incidence angle. White-sky albedo is the bihemispherical integral of the BRDF and a constant for a given wavelength. It is an intrinsic surface property. Natural illumination conditions are always bracketed by these two cases, assuming the diffuse fraction of illumination to be isotropic. Finally, broadband albedo is derived by integration of narrowband albedos (Narrow- to broadband conversion; NTB) over the desired waveband, weighted by the illuminating spectral solar flux.

For meteorological applications, albedo usually refers to the waveband between about 300 and 2500 nm wavelength, covering most of the average solar irradiation at ground level. Other definitions ranging up to 3000 or 5000 nm exist. Wavelengths shorter than 300 nm are effectively absorbed by ozone. Beyond 2500 nm, solar irradiance is minimal and largely absorbed by atmospheric water. In near-ground measurements, short-wave albedo is determined by dividing the measurements of two pyranometers, one for the downwelling and one for the upwelling radiative flux. Each measures over the solid angle 2π (a full hemisphere). The glass domes over the sensors are usually opaque to radiation outside the 300-3000 nm band.

MEASUREMENTS

Field site

The test site is situated in the Corvatsch area in the south-east of Switzerland, close to the town of St. Moritz (46° 26´ N 9° 50´E). The area lies between 1800 and 3700 m a.s.l and is characterized by steep slopes, alpine meadows and high mountain features such as glaciers and extensive block fields without vegetation.

Hyperspectral imagery

On 14 August 2002, the two flight lines (Table 1) used here were recorded (Gruber et al. 2003) with the imaging spectrometer DAIS7915 (Chang et al. 1993) under perfectly cloudless sky during the HySens 2002 campaign. A hyperspectral instrument was preferred over multispectral sensors due to the importance of spectral coverage for the derivation of broad-band albedo and, due to the generally better calibration of hyperspectral sensors. Areas above 3000 m a.s.l. were snow-covered due to recent snow fall during the overpass.

PREPROCESSING

Geo-atmospheric correction

The DAIS7915 imagery has been geometrically corrected using the software package PARGE (Schläpfer and Richter 2002) and pixel-accuracy has been achieved. In complex topography this carries special significance as illumination and viewing geometries are laterally extremely variable. Almost each final pixel contained a real measurement due to the large across-track over-sampling of DAIS7915. The final image cube was generated by assigning nearest measurements to each pixel. This resulted in many imaging spectrometer measurements being lost, while preserving original, measured spectra. Atmospheric-topographic correction has been performed using the software package ATCOR4 (Richter and Schläpfer 2002). A standard atmosphere with rural aerosol type and water vapor content of 10 g/cm^2 (sea level to space) and 80 km visibility have been employed. The resulting reflectance values are nadir-corrected approximations of hemispherical-directional reflectance factors (HDRF, cf. (Martonchik et al. 2000)).

Radiometric quality and vicarious calibration

A quality assessment based on visual inspection and image statistics was performed using the radiance values of the laboratory-calibrated image cube. Data were checked

for striping, saturation and an image-based signal-to-noise ratio has been derived using a lake as a homogeneous target for noise level estimation (for details see: Gruber et al. 2003). Combining all information, only the reflective channels 1-36, 38 and 39 are of satisfactory quality. However, for supporting the derivation of broadband albedo, the four best SWIR-2 channels 52, 53, 55 and 56 are used as well, adding up to a total of 42 used bands. Comparison of the HDRF spectra derived by topo-atmospheric correction with ground spectro-radiometric measurements and library clear-water spectra revealed errors in the laboratory calibration of DAIS7915 and a vicarious two-point calibration has been performed.

Viewing and illumination angles

For the fitting of kernel-based BRDF models, the illumination angle (φ_i), the viewing angle (φ_v) and the relative azimuth angle (Ψ, assuming surface properties to be rotationally symmetric) need to be known. In mountain topography, these vary considerably over short distances as they must be determined with respect to a tilted surface (Figure 1). The angles φ_i and φ_v are determined between the surface normal ($\vec{n}$) and the unit vectors to the sun ($\vec{i}$) and to the sensor ($\vec{v}$), respectively:

$$\varphi_i = \arccos\left(\vec{n} \cdot \vec{i}\right) \tag{1}$$

$$\varphi_v = \arccos\left(\vec{n} \cdot \vec{v}\right) \tag{2}$$

$\vec{i}$ (constant) and $\vec{n}$ (over a DEM) are calculated (Corripio 2003) and $\vec{v}$ is taken from the scan angle file produced during PARGE (Schläpfer and Richter 2002) ortho-rectification. A local orthogonal X,Y,Z system in which values increase towards the south and east and the XY plane is tangential to the earth surface is used. The relative azimuth angle (Ψ) for the tilted surface is the angle between the projection of the vectors to the sun/sensor onto the tilted surface (Figure 1):

$$\Psi = \arccos\left(\vec{v}' \cdot \vec{i}'\right) \tag{3}$$

$$\vec{i}' = \vec{i} \times \vec{n} \tag{4}$$

$$\vec{v}' = \vec{v} \times \vec{n} \tag{5}$$

Surface class masks

For the fitting of BRDF models only suitable pixels are selected: A mask has been computed to identify excluded areas that have: a) cast shadow; b) high local illumination angle that would result in an unfavorable signal-to-noise ratio; c) high local viewing angle; d) snow cover; or e) are a water surface. Cast shadow has been computed from the DEM (Corripio 2003). The local viewing and illumination angles were considered to be unfavorable below a cosine of 0.2. Snow cover is expected to have a normalized difference snow index (NDSI) greater than 0.1. The NDSI (Hall et al. 1995, Hall et al. 2002) has been adapted for DAIS using bands 4 (551 nm) and 34 (1570 nm). Clear water could be identified as pixel having a HDRF below 0.1 in all reflective bands. Additionally, areas with a surface slope of less than 0.5° based on the DEM were considered water in order to include turbid glacial lakes. Vegetation cover has been parameterized using OSAVI (Rondeaux et al. 1996) adapted for DAIS using bands 11

(675 nm) and 18 (798 nm). Pixels with an OSAVI < 0.1 are considered free of vegetation and pixels with 0.35 < OSAVI < 0.6 are considered alpine meadows.

ALBEDO RETRIEVAL

Derivation of BRFD kernels

Fitting a BRDF kernel model in complex topography using the tilted local viewing and illumination geometry (Figure 1) relies on the assumption, that for the surface cover type of interest the angular properties of a tilted surface remain the same as for the horizontal case with respect to the surface normal. For e.g. forest, this assumption would not be valid as trees grow vertically on a steep slope and not normal to it (cf. Schaaf et al. 1994, Combal et al. 2000, Combal and Isaka 2002).

BRDF model fits are calculated using the algorithms and code described by (Beisl 2001) based on AMBRALS (Algorithm for Modis Bidirectional Reflectance Anisotropy of the Land Surface) developed by (Wanner et al. 1995) for the MODIS BRDF and albedo product (Lucht et al. 2000).

For flight lines 1 and 2, surface class masks for debris surfaces free of vegetation were applied to select suitable pixels, only. Several kernels and kernel combinations were tested on the data (spectral HDRFs and the angles φ_i, φ_v and Ψ for each pixel) sampled within these subsets. The three-parameter model used in MODIS (Lucht et al. 2000) comprising an isotropic, a volume-scattering, and a geometrically-scattering kernel generally performed badly resulting in mostly negative weights for the geometric kernel. A two-parameter model was chosen after several tests. In almost all cases, the combination between isotropic and RossThick (Roujean et al. 1992, Wanner et al. 1995) kernels performed best (see Table 2). Especially on block fields it is surprising to see the volume scattering kernel outperform the geometric one.

Each model fit results in two coefficients per band (narrow wavebands being denoted by Λ) together with a value for R^2 for the fit per band. The first coefficient is the weight of the isotropic kernel (f_{iso}) and the second on the weight of the RossThick kernel ($f_{RossThick}$). The BRDF is then defined by:

$$R(\varphi_i,\varphi_v,\Psi,\Lambda) = f_{iso}(\Lambda) + f_{RossThick}(\Lambda)K_{RossThick}(\varphi_i,\varphi_v,\Psi) \quad (8)$$

Derivation of narrowband albedo from BRDF kernel models

Following the approach described by (Lucht et al. 2000), spectral black-sky and white-sky albedos can be obtained using the pre-computed directional-hemispherical and bihemispherical kernel integrals, the derived model coefficients and the solar incidence angle. The spectral white sky (α_{ws}) and black sky albedo (α_{bs}) is then given by:

$$\alpha_{ws} = f_{iso}(\Lambda) + f_{RossThick}(\Lambda) \times 0.189184 \quad (9)$$

$$\alpha_{bs}(\varphi_i, \Lambda) = f_{iso}(\Lambda) + f_{RossThick}(\Lambda) \times (-0.007574 - 0.070987 \times \varphi_i^{\,2} + 0.307588 \times \varphi_i^{\,3}) \quad (10)$$

Narrow- to broadband conversion

The derivation of broadband albedo (α) involves the weighted integration of narrowband albedos (α_i). Narrowband albedo can refer to black- or white-sky albedo or to a combination of both derived using specific illumination and atmospheric conditions. The

weights (c_i) for each band are proportional to the irradiant energy in the waveband represented by that measurement.

$$\alpha = \sum_i c_i \alpha_i \tag{11}$$

The weights as well as the result of this integration are therefore a function of the spectral characteristics of the illumination. Even for hyperspectral sensors the spectral coverage of the broadband incoming solar radiation is neither complete nor continuous. It is assumed, that the narrow band (i) closest to a certain wavelength is the best estimate of the spectral albedo (α_λ) at that wavelength. Each narrowband albedo α_i is used for wavelengths bound by:

$$\lambda\min_i = \frac{\lambda_i + \lambda_{i-1}}{2}; \quad \lambda\max_i = \frac{\lambda_i + \lambda_{i+1}}{2} \tag{12}$$

The first band i=1 and last band i=n are used as the best approximation of α_λ at wavelengths shorter and longer than actually measured. The weights for NTB conversion are derived by:

$$c_i = \int_{\lambda\min_i}^{\lambda\max_i} \frac{S\downarrow_\lambda}{S\downarrow} \tag{13}$$

where $S\downarrow_\lambda$ is the spectral incoming and $S\downarrow$ is the total (of the irradiant spectral range considered) short-wave solar radiative flux.

The method used for the derivation of c_i influences the result significantly. Especially the extrapolation assumptions for blue and UV light are very sensitive and can affect the broadband albedo in the range of ±5-10%. Furthermore, the first and last band as well as spectral bands adjacent to atmospheric windows receive a relatively high weight making the broadband albedo more sensitive to noise in these bands than in others.

Irradiance spectra were simulated using MODTRAN 4 (Berk et al. 1998). As black-sky and white-sky albedo mark two extreme cases of illumination conditions, the weights for their integration from spectral albedos are also determined separately, assuming that with increasing diffuse radiation also the spectral characteristics change. The weights for direct illumination are determined from a clear-sky spectrum with a solar zenith angle of 30° and the weights for diffuse illumination from a spectrum assuming a position surrounded by a stratus cloud.

IMAGE CORRECTION

The derivation of albedo for each image pixel (or for subsets) requires a correction procedure that applies the BRDF model inversion to each pixel (cf. Beisl 2001 for a detailed treatment of this problem). The basic assumption is the adequate representation of the real angular behavior of each corrected pixel by the kernel-based model derived from a group of pixels. Two applications are investigated here: 1) multiplicative BRDF-normalization; and 2) scaling of black- and white-sky albedo using image HDRF values.

The multiplicative geometry correction factor (MGCF) is obtained by dividing the kernel-model result for the chosen geometry by the model result for the geometry of the imaging spectrometer measurement.

$$MGCF_{nadir} = \frac{R(\varphi_{solar\,zenith},0,0,\Lambda)}{R(\varphi_i,\varphi_v,\Psi,\Lambda)} \quad (14)$$

The multiplication of the measured HDRF with this factor will perform a BRDF-normalization of the image. The corrected image shows the expected nadir HDRF for every pixel if the image was recorded in flat topography.

After the derivation of black- and white-sky albedo from the BRDF model, these need to be scaled to the observed HDRF values if albedo per pixel is desired without sufficient angular measurements in one pixel. The underlying assumption is a linear scaling of the BRDF-model integrals. The linear image scaling factor (LISF) is determined by division of the measured HDRF by the value predicted by the kernel-model. Black and white-sky albedo derived from groups of pixels can be scaled back to each measurement using this factor.

$$LISF = \frac{HDRF(\varphi_i,\varphi_v,\Psi,\Lambda)}{R(\varphi_i,\varphi_v,\Psi,\Lambda)} \quad (15)$$

RESULTS AND VERIFICATION

Model fit

Table 2 lists the results of the kernel-based BRDF model fits performed for both flight lines. 4-7% (using the average over all bands) of the observed variance in measured HDRF values can be explained by the fitted kernel models.

BRDF model stability

The scaling of albedo derived from the inversion of BRDF models relies on an adequate representation of the BRDF shape of individual pixels by the model derived from an image subset. Due to the process of multiplicative scaling, the actual kernel weights are not important for image correction but only their ratio needs to be known.

To test the assumption of shape constancy (i.e. how well the global BRDF model represent all the pixels in the subset), random samples of 200 pixels were taken from the used subsets and a BRDF model was fitted. The result of 200 of such experiments were aggregated to provide an idea of the subset-internal variation in BRDF shape. The R^2 describes the goodness of fit for the model. The means, standard deviations, minima and maxima for all 200 random experiments are calculated. The same statistics are provided for the shape of the model, defined by the ratio of the weights (RossThick/Iso) in the two kernel model. The above parameters are shown for each used band in Figure 2. Table 3 provides an overview of the means over all bands for both flight lines. Although the coefficient of determination for the fitted models is rather low it can be seen that the inversion results are similar for all random model fits to data subsets. No negative kernel weights occur.

Comparing flight lines and illumination-dependence

White-sky albedo is the highest-order data product to be compared because it is a surface characteristic and should be independent of illumination geometry. We assume an independence of the distribution of surface characteristics from topographic position for the surface type classes debris and meadow. For the consecutive processing

steps/products "geo" (ortho-rectified at-sensor radiance), "HDRF" (topo-atmospherically corrected) and "α_{ws}" (white-sky albedo) the correlation with illumination decreases clearly (Table 4) as it would be expected from a successful removal of topographic and BRDF effects. At the same time, the correlation between both flight lines decreases although an increase should theoretically be expected. Because both flight lines were recorded in very similar illumination and viewing conditions, the correlation is rather high. During processing, the correlation gets less for higher order products due to the introduction of noise though imperfect corrections of e.g. atmospheric and angular effects. Equally, the relative difference between the mean values in both lines also increase for the higher order data products. The reduction of correlation with the illumination angle could also be due to random noise introduced by a model that has no validity. We tested this by adding an amount of random noise to the HDRF pixels that degrades the correlation of both flight lines to that of the white-sky albedo. This lowers the dependence on the illumination angle only insignificantly as compared to the values of white-sky albedo, thus the hypothesis of pure noise content in the model can be refuted.

Sensitivity of the derived albedo on angular anisotropy

The angular anisotropy of the derived albedo can now be further investigated by including the angular parameterization of albedo into the short-wave radiation module of the model PERMEBAL (Stocker-Mittaz et al. 2002). In complex mountain terrain the solar incidence angle is highly variable and, as a consequence, the black-sky albedo is variable, too. We define the mean daily black-sky albedo as a cosine(φ_i)-weighted average of instantaneous black-sky albedo:

$$\alpha_{bs-day} = \frac{\sum_{sunrise}^{sunset} \alpha_{bs} \cos(\varphi_i)}{\sum_{sunrise}^{sunset} \cos(\varphi_i)} \tag{16}$$

Figure 3 shows the frequency distribution of the difference between the angularly anisotropic black-sky albedo and the constant white-sky albedo for the winter solstice, summer solstice and the equinoxes. For these three days black-sky albedo was parameterized from insolation geometry (Corripio 2003) over steep mountain terrain in 50 time steps. Areas above 2300m and with a slope angle < 37° were used which roughly corresponds to the conditions where coarse debris covers are found. Between 180,000 and 220,000 cells were use for each days histogram statistics. The smaller number of cells in winter is due to all-day self- or cast shadow which precludes the calculation of black-sky albedo. During summer when solar radiation input is greatest, the effect of the angular anisotropy in black-sky albedo is below ±10% for nearly the entire area, below ±10% for over 80% of the area. Towards the equinoxes and the winter up to 40% of the area have deviations over +10% from the white-sky albedo. However, during winter and in areas of low illumination angles the presence of a snow cover largely obliterates this effect in cold-mountain areas. Furthermore, roughly half the downwelling short-wave solar radiation at the test site is diffuse reducing the influence of the angular anisotropy on albedo by about half. The likely total error in neglecting the angular anisotropy of albedo is for these reasons assumed to be below 5% for nearly all coarse debris surfaces occurring in the project area.

Sensitivity of the simulated surface temperature to albedo

A PERMEBAL model sensitivity run using 17 classes of albedo (0.05-0.45) randomly distributed over 200x200 cells has been compared to a base run with an albedo of 0.25. All other surface parameters were kept constant, the snow cover was turned of and the run was performed over one year. Figure 4 shows the deviation of the mean annual simulated surface temperature from the base run for different albedo values. Deviations of ±20% in albedo result mostly in less than ±0.2 °C difference in the result.

DISCUSSION AND CONCLUSION

A successful technique for the fitting of kernel-based BRDF models using individual flight lines in complex topography has been described. Together with multiplicative correction and linear image scaling this allows for the semi-quantitative correction of BRDF effects in imagery as well as for the derivation of albedo.

Useful results were obtained using a 2-parameter isotropic-RossThick model but many open questions remain. Is the rather weak model fit due to the generally noisy DAIS7915 data and additional noise introduced by the error-prone topo-atmospheric correction in complex topography or would a different kernel provide better results? Almost 20 different kernels were tested and it is surprising to see a volume-scattering kernel perform best on a surface that constitutes a geometric problem. Larger backward and smaller forward scattering should be expected. Is the difference in image means (Table 4) between lines 1 and 2 due to instability of the sensor calibration or a consequence of inappropriate treatment of BRDF effects?

Even though the models explain only 4-7% of the observed variance the fitting results yield stable and non-negative values. The successful removal of inter-correlation with illumination further underscores the usefulness of the model. The relative difference of 16% between the mean values of white-sky albedo from both lines is taken as a first estimate of the uncertainty involved. Comparison with the AWS data results in similar numbers.

Including a BRDF-scheme into the radiation module of the surface energy-balance model PERMEBAL the effect of angular anisotropy could be investigated. The error due to approximation of angularly-dependent albedo with the constant white-sky albedo is below ±5% for most of the test area.

Comparing the overall uncertainty of ±16% with the mostly less than ±5% when using only white-sky albedo we can conclude that the methods presented in the paper are needed for the correction of BRDF effects and the derivation of albedo but the inclusion of a BRDF model in existing energy-balance models is of minor importance.

The overall uncertainty of ±16% corresponds to an error in simulated temperature of less than ±0.2 °C for most situations based on a simple sensitivity study with PERMEBAL. The usefulness of albedo as a model input needs to be judged by comparison of this figure with other sources of error for the task at hand.

ACKNOWLEDGEMENTS

This project has been carried-out in the Swiss National Foundation project "Analysis and spatial modeling of permafrost distribution in cold-mountain areas by integration of

advanced remote sensing". Further support has been provided by the EU-program HySens. Dr Rolf Richter of the German Aerospace Center (DLR) provided valuable discussion and help throughout this study.

REFERENCES

Beisl, U. 2001. Correction of Bidirectional Effects in Imaging Spectrometer Data. Pages pp. 188 *in* Remote Sensing Series. RSL, Zürich.

Berk, A., L. S. Bernstein, G. P. Anderson, P. K. Acharya, D. C. Robertson, J. H. Chetwynd, and S. M. Adler-Golden. 1998. MODTRAN Cloud and Multiple Scattering Upgrades with Application to AVIRIS. *Remote Sensing of Environment* (65):367-375.

Chang, S.-H., M. J. Westfield, F. Lehmann, D. Oertel, and R. Richter. 1993. 79-Channel Airborne Imaging Spectrometer. *Im. Spec. of the Terr. Env.* (SPIE Vol. 1937):164-172.

Combal, B., and H. Isaka. 2002. The effect of small topographic variation on reflectance. *IEEE Trans. on Geosc. and R. S.* (40(3)):663-670.

Combal, B., H. Isaka, and C. Trotter. 2000. Extending a turbid medium BRDF model to allow sloping terrain with a vertical plant stand. *IEEE Transactions on Geoscience and Remote Sensing* (38):798-810.

Corripio, J. G. 2003. Vectorial algebra algorithms for calculating terrain parameters from DEMs and solar radiation modelling in mountainous terrain. *International Journal of Geographical Information Science* (17):1-23.

Gruber, S., M. Hoelzle, and W. Haeberli. 2004a. Permafrost thaw and destabilization of Alpine rock walls in the hot summer of 2003. *Geophys. Res. Lett.* (31.

Gruber, S., M. Hoelzle, and W. Haeberli. 2004b. Rock wall temperatures in the Alps: Modelling their Topographic Distribution and Regional Differences. *Permafrost and Periglacial Processes* (15):299-307.

Gruber, S., D. Schläpfer, and M. Hoelzle. 2003. Imaging spectrometry in high-alpine topography: the derivation of accurate broadband albedo. Pages 196-205 *in* M. Habermeyer, editor. 3rd Intl. Workshop on Imaging Spectroscopy. EARSeL, Herrsching, Germany.

Haeberli, W., and M. Beniston. 1998. Climate change and its impacts on glaciers and permafrost in the Alps. Pages 258-265 *in* A. Rapp and E. Kessler, editors. AMBIO - A Journal of the Human Environment. The Royal Swedish Academy of Sciences.

Hall, D. K., G. A. Riggs, and V. V. Salomonson. 1995. Development of Methods for Mapping Global Snow Cover Using Moderate Resolution Imaging Spectroradiometer Data. *Remote Sens. Environ.* (Vol. 54):pp. 127-140.

Hall, D. K., G. A. Riggs, V. V. Salomonson, N. E. DiGirolamo, and K. J. Bayr. 2002. MODIS snow-cover products. *Remote Sensing of Environment* (83):181-194.

Harris, C., D. Vonder Mühll, K. Isaksen, W. Haeberli, J. L. Sollid, L. King, P. Holmlund, F. Dramis, M. Guglielmin, and D. Palacios. 2003. Warming permafrost in European mountains. *Global and Planetary Change* (39):215-225.

Lucht, W., C. B. Schaaf, and A. H. Strahler. 2000. An algorithm for the retrieval of albedo from space using semiempirical BRDF models. *IEEE Transactions on Geoscience and Remote Sensing* (38):977-998.

Martonchik, J. V., C. J. Bruegge, and A. H. Strahler. 2000. A Review of Reflectance Nomenclature Used in Remote Sensing. *Remote Sensing Reviews* (19):9-20.

Mittaz, C., M. Imhof, M. Hoelzle, and W. Haeberli. 2002. Snowmelt evolution mapping using an energy balance approach over an alpine terrain. *Arctic, Antarctic and Alpine Research* (34):264-281.

Nicodemus, F. E., J. C. Richmond, I. W. Ginsberg, and T. Limperis. 1977. Geometrical Considerations and Nomenclature for Reflectance. Pages 52 *in*. National Bureau of Standards, US. Department of Commerce.

Richter, R., and D. Schläpfer. 2002. Geo-atmospheric processing of airborne imaging spectrometry data. Part 2: Atmospheric/Topographic Correction. *International Journal of Remote Sensing* (23(13)):2631-2649.

Rondeaux, G., M. Steven, and F. Baret. 1996. Optimization of soil-adjusted vegetation indices. *Remote Sensing of Environment* (55):95-107.

Roujean, J. L., M. Leroy, and P. Y. Deschamps. 1992. A Bidirectional Reflectance Model of the Earths Surface for the Correction of Remote-Sensing Data. *Journal of Geophysical Research-Atmospheres* (97):20455-20468.

Schaaf, C. B., X. W. Li, and A. H. Strahler. 1994. Topographic Effects on Bidirectional and Hemispherical Reflectances Calculated with a Geometric-Optical Canopy Model. *IEEE Transactions on Geoscience and Remote Sensing* (32):1186-1193.

Schläpfer, D., and R. Richter. 2002. Geo-atmospheric processing of airborne imaging spectrometry data. Part 1: Parametric Ortho-Rectification Process. *International Journal of Remote Sensing* (23(13)):2609-2630.

Stocker-Mittaz, C., M. Hoelzle, and W. Haeberli. 2002. Permafrost distribution modeling based on energy-balance data: a first step. *Permafrost and Periglacial Processes* (13):271-282.

Wanner, W., X. Li, and A. H. Strahler. 1995. On the Derivation of Kernels for Kernel-Driven Models of Bidirectional Reflectance. *Journal of Geophysical Research-Atmospheres* (100):21077-21089.

TABLES

Table 1. Details of DAIS7915 flight lines acquired on 14 August 2002 over Corvatsch, Switzerland.

	Time UTC	Image lines	Scan frequency	Flight elevation	Flight heading	Solar elevation	Solar azimuth	Clouds	Cast shadow
Line 1	10:05	1865	11.5Hz	6040m	358°	53.7°	146.1°	none	0.8%
Line 2	09:52	2094	13.0Hz	6040m	358°	52.2°	140.9°	none	1.4%

Table 2. Results of fitting Iso/RossThick 2-parameter BRDF kernel model to image subsets. R^2, f_{iso} and $f_{RossThick}$ are mean values over all wavelengths; minimum and maximum values in brackets.

	pixels	R^2	f_{iso}	$f_{RossThick}$
Line 1	13,071	0.066 (0.010-0.165)	0.21 (0.16-0.30)	0.08 (0.04-0.11)
Line 2	13,699	0.044 (0.011-0.110)	0.24 (0.20-0.33)	0.09 (0.04-0.20)

Table 3. Model fit and shape factor as derived from 200 simulations using 200 random samples, each. Values are averaged over all 42 used DAIS7915 bands.

	Model fit R^2	Shape factor
Line 1	0.070 ±0.033	0.385 ±0.116
Line 2	0.050 ±0.030	0.383 ±0.141

Table 4. Comparison between flight lines and between processed data and illumination angle using band 9 as an example. Geo: geometrically-corrected data; HDRF: topo-atmospherically corrected data; α_{ws}: white-sky albedo; illu: cosine of illumination angle; Δ: difference between subset means (normalized by mean).

	geo	**HDRF**	**α_{ws}**
Line 1/illu R^2	0.130	0.018	0.00014
Line 2/illu R^2	0.286	0.179	0.086
Line 1/2 R^2	0.917	0.784	0.655
Line 1/2 Δ	9.9 %	14.0 %	16.0 %

FIGURES

Figure 1. Vectors and angles defining the BRDF for horizontal and inclined surfaces. φ_i φ_v are equivalent to the view and illumination zenith angles in the horizontal case but not for sloping surfaces.

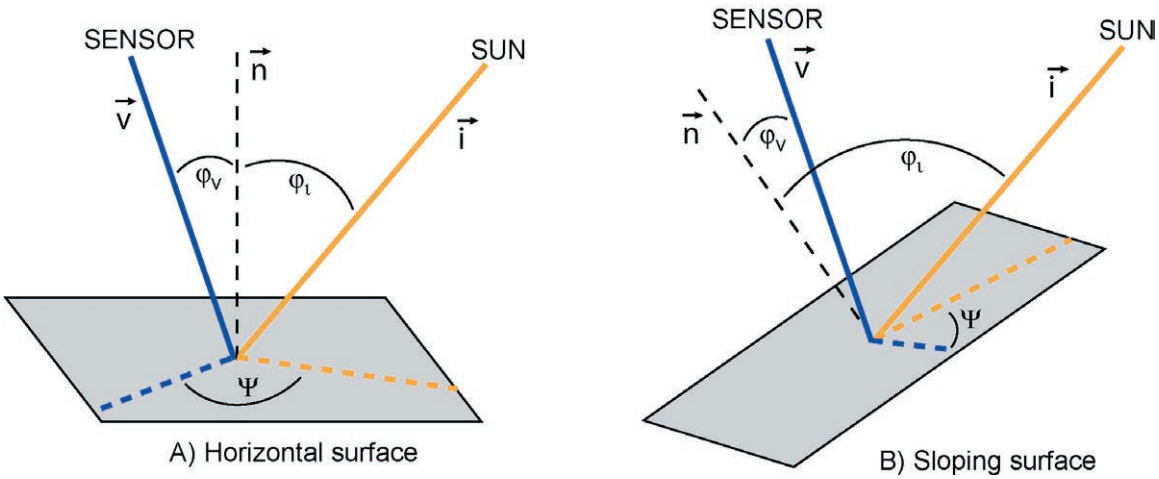

Figure 2. Variations in BRDF model fit and model shape factor for debris surfaces in line 1. Values were determined from 200 model inversions using 200 random samples each. Thick lines: mean values; thin lines: ±1 standard deviation.; dotted lines: min/max values.

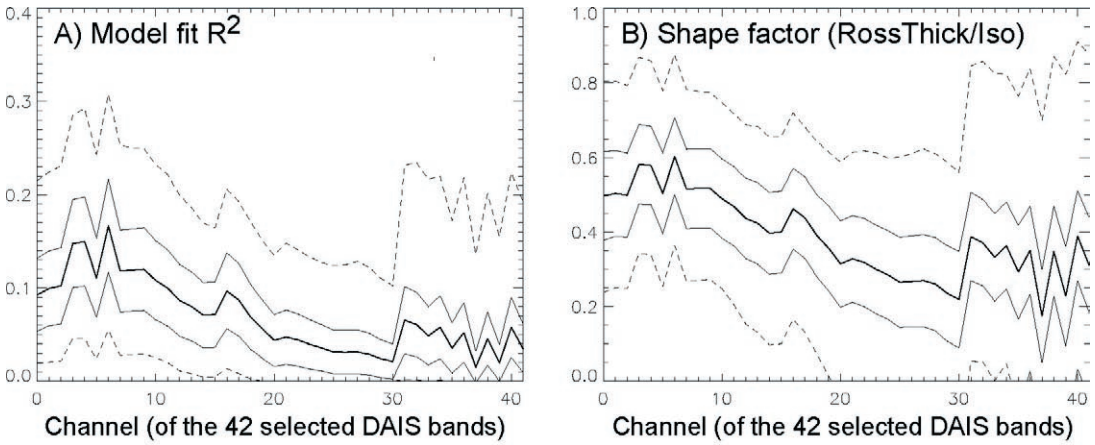

Figure 3. Cumulative histograms for the mean daily difference between black-sky and constant white-sky albedo expressed as a relative error. Derived from a model run on 600x600 cells.

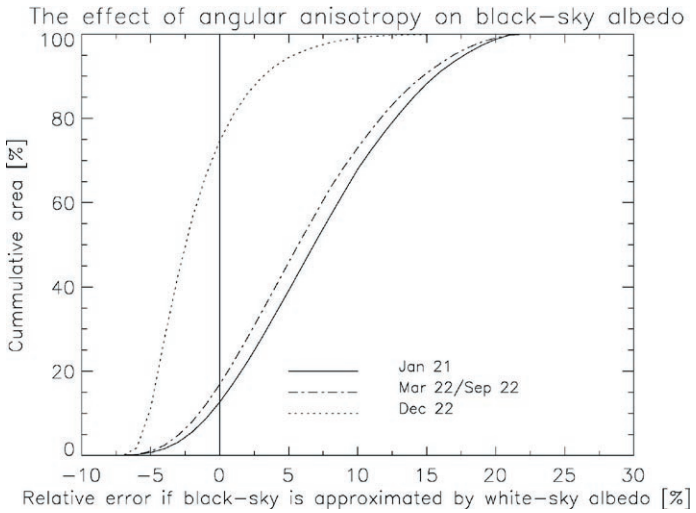

Figure 4. Sensitivity of simulated mean annual surface temperatures in complex terrain on albedo variations. Based on model run using 17 albedo classes randomly distributed over 200x200 cells in the test area.

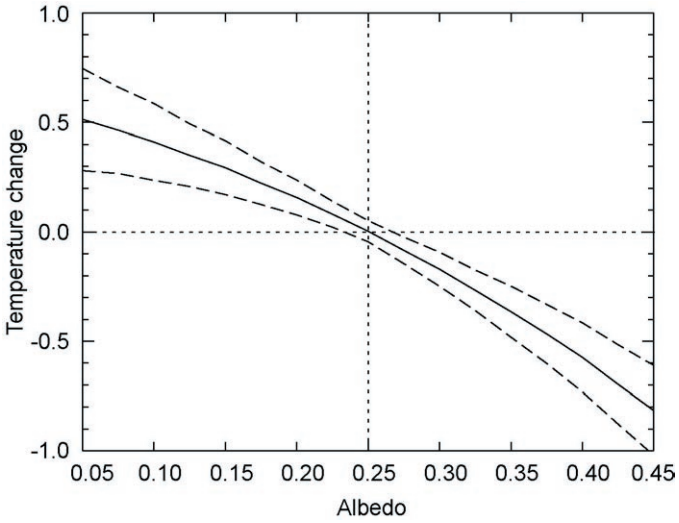

Part C: Appendix

Publications by Stephan Gruber

Peer-reviewed journals

Gruber, S., Hoelzle, M. and Haeberli, W. (2004). Permafrost thaw and destabilization of alpine rock walls in the hot summer of 2003. *Geophysical Research Letters,* 31, L13504.

Gruber, S., Hoelzle, M. and Haeberli, W. (2004). Rock-wall wall temperatures in the Alps: modelling their topographic distribution and regional differences. *Permafrost and Periglacial Processes,* 15(3), 299-307.

Gruber, S., King, L., Kohl, T., Herz, T., Haeberli, W. and Hoelzle, M. (2004, in press). Interpretation of geothermal profiles perturbed by topography: the Alpine permafrost boreholes at Stockhorn Plateau, Switzerland. *Permafrost and Periglacial Processes*, 15(4).

Hengl, T., Gruber, S. and Shrestha, D. P. (2004) Reduction of errors in digital terrain parameters used in soil-landscape modelling. *International Journal of Applied Earth Observation and Geoinformation,* 5, 97-112.

Gruber, S. and Hoelzle, M. (2001): Statistical modelling of mountain permafrost distribution – local calibration and incorporation of remotely sensed data. *Permafrost and Periglacial Processes*, 12(1), 69-77.

Tanarro, L. M., Hoelzle, M., García, A., Ramos, M., Gruber, S., Gómez, A. Piquer, M. and Palacios, D. (2001). Permafrost distribution modelling in the mountains of the Mediterranean: Corral del Veleta, Sierra Nevada, Spain. *Norsk Geografisk Tidsskrift-Norwegian Journal of Geography*, 55, 253-260.

Conference papers

Gruber, S., Peter, M., Hoelzle, M., Woddhatch, I. & Haeberli, W. (2003) Surface temperatures in steep Alpine rock faces - a strategy for regional-scale measurement and modelling. In: *Proceedings of the 8th International Conference on Permafrost 2003, Zurich, Switzerland*.

Gruber, S., Schläpfer, D. and Hoelzle, M. (2003) Imaging spectrometry in high-alpine topography: the derivation of accurate broadband albedo. *Proceedings of the the 3rd EARSeL Workshop on Imaging Spectroscopy*, Oberpfaffenhofen, May 13-16 2003

Schläpfer, D., Koetz, B, Gruber S. and Morsdorf, F. (2003) The influence of DEM characteristics on preprocessing of DAIS/ROSIS data in high altitude Alpine terrain. *Proceedings of the the 3rd EARSeL Workshop on Imaging Spectroscopy*, Oberpfaffenhofen, May 13-16 2003

Extended Abstracts

Gruber, S., Schläpfer, D. and Hoelzle, M. (2003) Ground albedo derived from DAIS 7915 hyperspectral imagery for energy balance modeling in high-Alpine topography. *Extended abstract volume*, *8th International Conference on Permafrost 2003, Zurich, Switzerland*.

Heiner, S., Gruber, S. and Meier, E. (2003) The spatial extend and characteristics of block fields in Alpine areas: evaluation of aerial photography, LIDAR and SAR as data sources. *Extended abstract volume, 8th International Conference on Permafrost 2003, Zurich, Switzerland*.

Kohl, T. and Gruber, S. (2003) Evidence of paleotemperature signals in mountain permafrost areas. *Extended abstract volume, 8th International Conference on Permafrost 2003, Zurich, Switzerland*.

King, L., Hof, R., Herz, T and Gruber, S. (2003) Long-term monitoring of borehole temperatures and permafrost-related data for climate change research and natural hazard management: examples from the Mattertal, Swiss Alps. Extended abstract volume, *8th International Conference on Permafrost 2003, Zurich, Switzerland*.

Hof, R., King, L., Herz, T and Gruber, S. (2003) Influence of human activities and climatic change on permafrost at construction sites in Zermatt, Swiss Alps. Extended abstract volume, *8th International Conference on Permafrost 2003, Zurich, Switzerland*.

Other Conference Presentations

Ramos, M., Vieira, G., Garcia, J.A., Hoelzle, M. and Gruber S. (2004) Permafrost and active layer monitoring and modelling in livingston and deception islands (South Shetlands, Antarctic) – permamodel. XXVIII SCAR Open Science Conference, Bremen, Germany, 27/28 July, 2004

Caine, N, Clow D., Janke, J., Losleben, M, Williams, M. and Gruber, S. (2004) The importance of seasonally frozen ground (SFG) in mountain environments to hydrological, ecological, and geomorphic systems. *Mountain Climate Science Symposium*, Lake Tahoe, California/USA, 25 May 2004.

Gruber, S. and Hoelzle, M. (2004) Surface temperatures in rock faces: measurements and models. *EGU 1st General Assembly*. Nice, France, 25 - 30 April 2004

Gruber, S. and Hoelzle, M. (2004) The energy-balance model PERMEBAL: Measurement and calibration approach, new features. *EGU 1st General Assembly*. Nice, France, 25 - 30 April 2004

Brenning, A., Gruber, S. and Hoelzle, M. (2004) Statistical charateristics of BTS data: implications for measurement campaigns and permafrost modelling. *EGU 1st General Assembly*. Nice, France, 25 - 30 April 2004

Gredig, B., Gruber, S. and Hoelzle, M. (2004) Glaciological investigations at a possible low-altitute ice archive in lower Engadin area, Eastern Swiss Alps. *EGU 1st General Assembly*. Nice, France, 25 - 30 April 2004

Haeberli, W., Paul, F., Gruber, S., Hoelzle, M., Kaeaeb, A, Machguth, H., Noetzli, J. and Rothenbühler, C. (2004) Effects of the extreme summer 2003 on glaciers and permafrost in the Alps - first impressions and estimations. *EGU 1st General Assembly*. Nice, France, 25 - 30 April 2004

Gruber, S., Hoelzle, M. and Haeberli, W. (2004) Temperature variation (spatial, temporal, at depth) in steep rock slopes and its relation to thermally-induced slope instability. *EGU 1st General Assembly*. Nice, France, 25 - 30 April 2004

Noetzli, J., Gruber, S., Hoelzle, M.; and Haeberli, W. (2004) Modelling of permafrost distribution for the re-analysis of 2003 rock falls in steep rock faces of the Swiss Alps. *EGU 1st General Assembly*. Nice, France, 25 - 30 April 2004.

Harris, C., Vonder Mühll , D., Haeberli, W., Isaksen , K., King, L.; Holmlund , P., Gruber , S., Kohl , T., Guglielmin , M. (2003) Evidence for secular warming of European mountain permafrost (solicited). *EGS-AGU-EUG Joint Assembly*. Nice, France, 06 - 11 April 2003

Gruber, S.; Hoelzle, M.; Haeberli, W. (2003) Distributed process-based models of mountain permafrost: the importance of accurate spatial input and calibration data. *EGS-AGU-EUG Joint Assembly*. Nice, France, 06 - 11 April 2003

Kohl, T. and Gruber, T. (2003) Assessing ground surface temperature changes in mountainous permafrost areas. *IUGG General Assembly*, June 2003, Sapporo, Japan.

Gruber, S., Haeberli, W. and Noetzli, J. (2002) The thermal regime of steep Alpine rock faces. *AGU Fall Meeting*, San Francisco.

Harris, C., Haeberli, W., Gruber, S. and Kohl, T. (2002) European mountain permafrost: geothermal change and associated geomorphological impacts. *AGU Fall Meeting*, San Francisco.

Gruber, S., Hoelzle, M. and Mittaz, C. (2001) Cryosphere model development: Permafrost and ground temperatures. Oral presentation, meeting of the IGS Nordic Branch, Rovaniemi, Finland, 2001

Curriculum vitae

Stephan Gruber
Date and place of birth: 01.10.1973, Siegburg, Germany
Nationality: German

Primary and secondary school, Germany 1980 – 1993

AGARD, Paris, France 1991
Two-week work placement in a civilian NATO research agency.

Private Travels, USA/Canda 1993
Six months.

Justus-Liebig-University, Giessen, Germany 1994 – 2000
Masters of science in physical geography (included geology, soil science, botany).
Thesis on permafrost and slope instability in Switzerland as part of the EU-project PACE.

Saracen Minerals Limited, Solomon Islands 1995 – 1996
Three months work placement and contract work in a feasibility study for a gold mine.

Arctic Centre / University of Lapland, Finland 1996 – 1997
Diploma in Arctic Studies. 2-semester international course.

Gold Ridge Mining Limited, Solomon Islands 1997
Three months contracting in the definition of an environmental program for a gold mine.

ITC, Enschede, The Netherlands 1998 – 1999
14 months course: Environmental Systems Monitoring and Analysis at the International Institute for Aerospace Survey and Earth Sciences (ITC).

Munich Reinsurance, Germany 1999 – 2000
Four months trainee in the natural hazard group of Munich RE.

University of Heidelberg, Germany 2000
Five months employment as research assistant within the EU-project ALPCLIM.

University of Zurich, Switzerland 2000 – 2004
Student at the Department of Geography. Since 2001 PhD student in the project: „Analysis and Spatial Modelling of Permafrost Distribution in Cold-Mountain Areas by Integration of Advanced Remote Sensing Technology“ funded by the Swiss National Science Foundation.

University Courses on Svalbard, Norway 2002
Five week postgraduate course: Glacial and Periglacial Processes

National Snow and Ice Data Centre, Boulder, USA 2004
Two months research in the group of Dr. Tingjun Zhang.

Acknowledgements

This dissertation has been made possible by a grant from the Swiss National Science Foundation (projects 246979 and 21-63678). Further support in connection with the imaging spectrometer DAIS7915 was available from the EC-project HySens. Valuable and always friendly assistance during field work was given by the Corvatschbahnen, the Gornergrat-Monte Rosa-Bahnen, the International Foundation High Altitude Research Stations Jungfraujoch and Gornergrat (HFSJG), the Schilthornbahn AG and the Jungfraubahnen.

Wilfried Haeberli and Martin Hoelzle were my main supervisors and superiors in my employment. I can hardly imagine having better motivation, support and conditions to work and to enjoy work elsewhere. Dani Schläpfer was an always-patient supervisor and I am grateful for his critical and constructive assistance that helped me in more than just the remote sensing part of this dissertation.

The people of our group have not only contributed to this dissertation through discussions, field work and other things but especially made my everyday life in Zürich very enjoyable. I am very happy ahout the work, coffee breaks and free time that I have shared with Sabina Dürrenberger, Eileen Eckmeier, Regula Frauenfelder, Karen Hammes, Susanne Hanson, Alex Heim, Christian Huggel, Andi Kääb, Horst Machguth, Jeannette Nötzli, Frank Paul, Christine Rothenbühler, Nadine Salzmann, Catherine Stocker-Mittaz, Ivan Woodhatch, Michel Zemp, Sonja Zgraggen-Oswald.

For their help, support or advice I am also indebted to: Thomas Kohl, Ross Purves, Javier Corripio, Tingjun Zhang, Lorenz King, Felix Keller, Daniel Vonder Mühll, Erich Meier, Stefanie Holzwarth, Rolf Richter, Stefan Dangel, Ketil Isaksen and Reynald Delaloye.

Many people have helped in field campaigns during this dissertation. I would like to thank: Ralph Böhlert, Claudio Busarello, Constantin Döring, Berni Gredig, Igor Iwaschur, Benjamin Kötz, Felix Morsdorf, Sandy Ubl, Karen Hammes, Andreas Hasler, Stephan Heiner, Thomas Herz, Constanze Hofstötter, Stefan Kapeller, Christina Maffra (& Marco), Monika Oswald, Marco Peter, Simone Phillipi, Christoph Popp, Nina Schmidig-Riesen, Oliver Schuhmacher, André Seiler, Robin Straub, Monika Weber and Adrian Zgraggen.

I am grateful to my family who has always been supportive and motivating - in the context of this dissertation and also with other crazy ideas and plans: Gisela Gruber and Dieter Belling, Gerhard Gruber and Heidi Schmidt as well as Monika and Keith Wood. Especially my father, sister and brother in law have helped me more than once by correcting the English and commenting the content and structure of the various documents I had to write during the last years. Julia Peth and Sven Kaufmann have stayed close friends during the more than 10 years that I have been moving between different cities and countries. Thats great.